MICROSTRESS DISTRIBUTIONS IN SINGLE CRYSTALS

by

HAMOUDA GHONEM

A thesis submitted to the Faculty of Graduate Studies and Research in partial fulfillment of the requirements for the Degree of Master of Engineering

Department of Mechanical Engineering
McGill University
Montreal, Canada

February, 1976

MICROSTRESS DISTRIBUTIONS IN SINGLE CRYSTALS

H. Ghonem

ABSTRACT

A method to determine the microstress distributions in crystals is presented in this thesis. The dislocation segments embedded inside a single crystal are considered the main mechanism for obtaining the necessary knowledge to describe the microstress distribution in this crystal system. Utilizing a line-tension model, a modified expression to describe the stress field acting on a dislocation line in terms of its geometrical parameters is obtained. In this analytical derivation, the increase in energy due to interactions between a particular dislocation line and an infinite number of surrounded dislocations is considered.

An experimental study utilizing an x-ray Lang Scanning technique has been carried out to obtain the dislocation distribution pattern in a Silicon single crystal. From the geometrical parameters measured from the experimentally obtained pattern, the stress field acting on each individual dislocation, in this pattern, is calculated. This leads to the description of the stress distributions inside a single crystal via the analytic expressions of the present study.

SOMMAIRE

Cette thèse développe une méthode d'évaluer les distributions de micro-contrainte à l'intérieur d'un cristal. On considère que les segments de dislocation à l'intérieur d'un seul cristal contiennent toute l'information nécessaire pour en déduire la distribution de micro-contrainte du système cristallin . En utilisant un modèle de tension linéaire, on obtient ainsi une nouvelle expression analytique pour décrire le champs de contrainte imposé sur une ligne de dislocation en fonction de ses paramètres géométriques. Cette expression induit l'énergie additionnelle due aux intéractions entre une ligne de dislocation et un nombre infini de dislocations voisines.

Cette thèse présente aussi une étude expérimentale qui se sert de la méthode de balayage de rayons x de Lang afin d'obtenir la distribution des dislocations à l'intérieur d'un seul cristal de silicium. Les paramètres géométriques mesurés au laboratoire permettent ainsi de calculer le champs de contrainte imposé sur chaque dislocation individuelle. Ce dernier calcul est enfin utilisé avec les expressions analytiques developpées dans la thèse pour obtenir les distributions de contrainte à l'intérieur d'un seul cristal.

ACKNOWLEDGEMENT

The author wishes to express his sincere gratitude to his research supervisor, Professor J.W. Provan, without whose guidance and encouragement the completion of the present work would not have been possible. The author wishes to express his deep appreciation to Professor D.R. Axelrad for his help and useful discussions on several occasions during the course of this work. The author wishes also to acknowledge the help of Dr. S. Basu and Mr. G. Thouret.

The author wishes to express his sincere thanks to Mr. B. Piwczyk and Dr. R.R. Robinson for giving him the opportunity to complete the experimental course of this study in the X-Ray Diffraction Lab of Bell-Northern Research in Ottawa. Mr. Piwczyk gave every cooperation to the author and the success of the joint venture is largely due to his willingness to give of his valuable time and experience.

Sincere thanks are due to Mr. Paul Thibault for preparing the French version of the abstract and to Ms. Sandi Diamond for typing this thesis.

This project was supported by a National Research Council of Canada grant no. A 7525. This financial help is gratefully acknowledged.

TABLE OF CONTENTS

LIST OF NOTATIONS

A	Area surrounded by a dislocation loop
$\underset{\sim}{b}$	Burgers vector of a dislocation segment
δD	Distance between two components of the X-ray diffracted beam.
d_{hkl}	Interplanar spacing.
$E(n)$	Total dislocation energy per unit length.
E_s	Dislocation self energy per unit length
ΔE	Dislocation energy increase caused by the bow out mechanism
e	Exponential function
e_3	A third sensor in a nonorthogonal coordinate system and is perpendicular to another two sensors ξ_1 and ξ_2
$\underset{\sim}{f}(n)$	Force per unit length on the dislocation line
$\underset{\sim}{g}_{hkl}$	Reciprocal lattice vector
$\underset{\sim}{k}_H$	X-ray diffracted wave vector
$\underset{\sim}{k}_o$	X-ray wave vacuum vector
$\underset{\sim}{k}_{o\alpha}$ and $\underset{\sim}{k}_{o\beta}$	Components of X-ray wave vector in the incident and diffracted beam direction
L	Dislocation segment length
L_1 and L_2	X-ray collimated slits
m	Total dislocation lengths interact with a particular dislocation segment, $m \to \infty$
n	Order of X-ray reflection, it may take values: 1,2,3---

r and r'	Distances between two dislocation loops and an arbitrary origin
R	The difference between r and r'
$\delta r(n)$	Virtual change to an arbitrary point on the dislocation line and causes, for a point (X,Y) a displacement $(\delta X(n), \delta Y(n))$
S	Arc length along the dislocation segment
t	Unit vector tangent to a dislocation line at a point n
T_{ij}	Tensor equal to $\frac{\partial R}{\partial X_i \partial X_j}$
V	Vertical resolution of a dislocation image
W	X-ray focal spot width
W_E^d	Work done on a dislocation line due to its self energy
Z	Horizontal resolution of a dislocation image
α	A dislocation core parameter
Γ_{ij}	A second order orientation tensor
δ_{ij}	Kronecker delta
n	A parameter chosen along a dislocation segment and it increases in the positive sense of the dislocation
λ	Wave length of the X-ray beam
μ	The shear modulus
ν	The Poission's ratio
ξ	Dislocation line direction

$\underset{\sim}{\gamma}$	A sensor in a nonorthogonal coordinate system
κ	A constant
ρ	To remove the divergence of equation (2.18), it is postulated that two elements, of the dislocations, dl_1 and dl_2 do not interact when they are closer than distance ρ
ρ_d	Dislocation density
Σ	Denotes "summation"
$\underset{\sim}{\sigma}$	A stress tensor
$\sigma_{\alpha\beta}$	A stress tensor evaluated on a dislocation segment α due to the presence of a dislocation segment β
σ_{xz} and σ_{yz}	Stress tensors evaluated in x and y direction and perpendicular to z direction of external coordinate system
σ_{YZ}	A stress tensor evaluated in Y direction and perpendicular to Z direction of local coordinate system
$\underset{\sim}{\nabla}$	Gradient operator
$\tilde{\ }$	Denotes a first-order tensor
$\underset{\sim}{\ }$	Denotes a second-order tensor
(...)	Crystal lattice plane

LIST OF TABLES

LIST OF FIGURES

Chapter I

INTRODUCTION

A more complete and realistic understanding of the stress-deformation relations pertaining to polycrystalline solids remains a major objective of the mechanics of deformable bodies. Classical continuum mechanics and its extensions of high order, try to describe these relations by utilizing mathematical models based on the observations of the material in bulk and employing the simple assumption that the material is locally homogeneous. This classical approach is a macroscopic description of the material behaviour which ignores the non-deterministic influence of the microstructure of real materials and consequently is unable to include the properties of this microstructure within its mathematical formulation. These theories have been accepted as an approximation to the response of materials, but they fail, to a certain extent, to close the gap between their theoretical predictions and existing experimental evidences.

To overcome the limitations of continuum mechanical theories, Axelrad [1-3] and Axelrad and Provan [4-6] have formulated a theory within which they accept polycrystalline materials as composed of real crystals. In this theory, the mechanical response of a polycrystal system is first formulated at a microstructural level by considering that the relevant quantities, characterizing the material system at this level, such as crystal orientation, size, position and shape of crystals, are random by nature. A transition is then obtained to the macrolevel by the use of certain concepts derived from statistical mechanics and the mathematical theory of probability.

This way of solution has two main objectives; first, to obtain a microscopic stress distribution leading to the predictions of local phenomenon such as the initiation and development of cracks and, secondly, to relate the observable macroscopic response behaviour of the polycrystalline system to the microstructural characteristics of such a system.

The aim of the present study is to furnish the probabilistic micromechanics theory with a method of determining the microstress distribution inside a single crystal. In this thesis, the dislocation segments embedded inside the single crystal are considered the main mechanism for obtaining the necessary knowledge to describe the microstress distribution in this crystal system.

In order to clarify this approach, a brief review of the development of dislocation theory is discussed next, while the micromechanical concepts for the case of polycrystalline solid is given in appendix I of this thesis.

I.1 The Development of Dislocation Theory

Crystalline solids deform by means of translational slip in a particular crystallographic plane (slip plane) along a particular crystallographic direction (slip direction) within that plane. The idea of slip seems to suggest that planes of atoms slide as rigid bodies across each other. However, this would mean that the shear stress on the slip plane is uniformly distributed and that the atoms in the slip plane can move simultaneously. Thus the material in this slip plane becomes amorphous as all the coherence between the atoms

on either side of the plane is destroyed. It is hard to accept that the shear stress on the slip plane can be uniformly distributed particularly in the presence of thermal vibrations of atoms themselves. Furthermore, the production of an amorphous layer is analogous to the process of melting, where crystallinity is lost, which involves energies much higher than that observed during the slip process.

Obreimov and Shubnikov [7], who analyzed the plastic deformation of NaCl in crystals in polarized light, showed that slip develops progressively. After this it became clear that translational slip cannot be reduced to simultaneous slipping of crystalline blocks and must necessarily be a consecutive slip. The concept of consecutive slip succeeded replacing the simultaneous slip idea and the same final result is achieved, but the consecutive slip generates a certain intermediate stage where there is discontinuity within the slip band with the lattice in register on either side. This discontinuity is a boundary separating the slipped and unslipped areas of the crystal and it is identified as a dislocation line.

The mathematical theory of dislocations in a elastic continuum was first systematically studied by Voltera [8] and Weingarten [9]. After a preliminary work by Prandtl [10] and Dehlinger [11], dislocations were applied to the explanation of the plastic deformation of a single crystal by Orowan, Polanyi and Taylor, independently. They considered the dislocations as imperfections in crystals and explained why the observed yield stresses of crystals are much lower than the theoretical values calculated from atomic theory assuming the perfect lattice state. Orowan [12] showed that the boundary of

a limited region forms a closed ring of dislocations if this region of one atomic plane slips along its neighbouring plane for a distance equal the parameter of the transition of the lattice. Further slip can extend along the slip plane by gradual widening of the regions of local slip which is equivalent to the displacement of the dislocation in the slip plane. Polanyi [13] investigated the edge dislocation, fig. 1.1, and noted that the displacement of the dislocation leads to slip by an amount equal to the parameter of the lattice. He attempted to calculate the stress necessary for the displacement of dislocations. Taylor [14] considered the atomic plane next to the dislocation as not remaining straight but continues to bend around the edge of the extra half plane which forms the dislocation line. He showed that translational slip for a length equal to the parameter of the lattice can occur due to the motion of positive, as well as negative, edge dislocations, fig. 1.2. The concept of non-straight dislocation and screw dislocation, fig. 1.3, was introduced by Burgers [15] who expressed also the elastic field caused by a dislocation loop by a surface integral of a known function over the slip surface bounded by the loop, using the analogy of Vortex lines in the theory of hydrodynamics.

The attention after that was paid to the effect of crystal structure on the dislocation properties. Examples of the results achieved in this way were the introduction of partial dislocations, by Heidenreich and Schockley [16] and by Frank [17], the concept of dislocation splitting and the recognition of the importance of the stacking fault energies. Seeger's theory of work hardening due to

dislocation accumulation in the crystal appeared as a result of the work of Mott [19], mechanical and x-ray studies and the investigations of slip line pattern by optical and electron microscopy. Peach and Koehler [20] transformed the Burgers surface integral into a line integral and defined the force acting on a line element of dislocations.

Turning our attention to attempts to describe the overall response of a crystalline material, Nye [21] introduced the density tensor of dislocations which was utilized later by Kondo [22], Bilby [23], and Kröner [24], independently. They found that the density tensor of dislocations can be written as the rotation of plastic distortion. Kröner [25] developed the theory of a continuous distribution of dislocations in connection with the stress function of elasticity. The relation between the incompability of strains and the Burgers vector due to a continuous distribution of stationary dislocations have been studied by Moriguchi and Kondo [26]. Mura [27-32] commenced his theory of continuous distribution of moving dislocations by deriving the deformation due to a single dislocation, then he extended this expression to the deformation field due to a continuous distribution of dislocations. From his theory, Mura derived Von Mises yield criterion and the Prandtl-Reuss relation between stress and plastic strain rate for isotropic and anisotropic elasto-plastic material and he derived the velocity tensor and density tensor of continuous distributions of dislocations considering the dynamic case.

Eshelby contributed markedly in the development of the mathematical theory of dislocations. He found the solution of an oscillating screw dislocation [33], moving dislocations [34], and dislocations in anisotropic media [35].

Probabilistic approaches include those by Nilson, Lagneborg and Sandstrom [36], who measured the mobile dislocation density. They considered that the increase in the stress inside the crystalline material is a direct measure of the effective stress where the average dislocation density is obtained from Orowan equation for plastic flow. Utilizing the concepts of micromechanics theory [1-6], which accepts the existence of imperfections inside the crystals within its mathematical formulations, Axelrad, Provan and el Helbawi [37] have developed an analytical model to evaluate the effect of internal dislocations in each crystal on the linear response of elastic heterogeneous solids (see appendix II).

Thus it can easily be realized, from this review, that the study of the mechanical properties of crystalline bodies is reduced essentially to the study of the defect structure of dislocations and the factors controlling their generation and dynamics.

Particular to the approach taken in this thesis, the analysis of the distributions of stress inside the crystal, stress on and due to isolated or determinately positioned dislocation have generally been investigated by Nabarro [38], Indenbom [39] and Li [40]. However, in real crystals, the dislocations are positioned quite randomly so that the local density and the positioning of dislocations change in a random manner from one volume of the crystal to another. Such

a nonuniformity inevitably leads to the nonuniformity of the stress field inside the crystal which in turn can exert a considerable influence on the motion and the pinning of dislocations, on the interaction of dislocations with impurities and point defects, on the deformation and development of cracks and on other processes which determine the mechanical properties of a crystalline system.

In this present study a theoretical-experimental work has been carried out to determine the internal stress distribution in parallel glide planes inside a single crystal. Utilizing a line-tension model, a modified expression to describe the stress field acting on a dislocation line in terms of the geometrical parameters of this dislocation is obtained. In this theoretical part, not only is the self-energy of a dislocation line assumed to change under the effect of stress field, but also the increase in energy due to interactions between this dislocation line and an infinite number of surrounded dislocations is considered. This part has been discussed in the subsequent Chapter 2 of this thesis.

An x-ray diffraction microradiography technique, known as the Lang Scanning Method, is used to obtain a dislocation distribution pattern under the effect of external and internal stress fields within glide planes {220} inside a Silicon single crystal. This technique is described in detail in Chapter 4 after a survey for the methods used to observe dislocations inside materials is presented in Chapter 3.

From the geometrical parameters measured from the experimentally-obtained pattern, the stress field acting on each dislocation in this pattern is calculated using the theoretical expression derived in Chapter

2. This leads to the description of the stress distribution inside a single crystal which is the ultimate aim of this present study. These results are discussed in Chapter 5 whilst the conclusions that may be drawn from this study as well as future research considerations are dealt with in Chapter 6.

CHAPTER II

DISLOCATION GEOMETRY AND ITS RELATED MICROSTRESS

II.1 Introduction

In a new unstrained and well-annealed single crystal, the dislocation density is typically 10^6 cm/c.c. These dislocations tend to arrange themselves in a low energy configuration, rather than being distributed at random. Such an arrangement would be aided by thermal fluctuations and so would occur readily at the higher temperatures encountered during and immediately after crystallization. A section of this configuration is shown in fig. 2.1. It consists of a three dimensional network of dislocation segments intersecting at various nodes. These configurations are called Frank networks and are relatively stable states in regard to both their own internal interactions and the effect of external stress.

Upon application of a stress to a newly formed crystal, one of the first events to occur is that any free dislocations not involved in a network begin to move and either glide out of the crystal or are stopped by the network. At some higher stress, Frank-Read sources begin to operate and produce a series of concentric loops as shown in fig. 2.2. In this figure a straight part AB of a dislocation line lies in a slip plane (the plane of the diagram) and its ends are pinned down by either intersection nodes or any other obstacle. This dislocation segment is forced to bow out in a circular shape, to keep its low energy configuration, under the action of an external shear stress until eventually a position of instability is reached and a closed loop of dislocation is then formed around AB in the slip plane

together with another piece adjoining A and B from which the process can be repeated.

This operation can then be divided into a reversible process, stage 1 and 2 in fig. 2.2 and an irreversible one, after stage 2, which need higher stresses to bend the dislocation segment into an approximately half-circle before it can expand outwards.

In this chapter, the following assumptions are made;

1. Infinity strong point obstacles are arranged at random at each slip plane.
2. These points are kept fixed while the external stress is applied to the system.
3. The stress will cause any dislocation lying in a particular slip plane to move following the Frank-Read source mechanism within this particular plane.

Following these assumptions and treating the Frank-Read sources on the basis of the line-tension model, a relation between the micro-stress on and due to dislocation interactions and the geometrical parameters of this dislocation is derived based on work of Jøssang, Lothe and Skylslad [41], Foreman [42] Blin [43] and DeWit and Koehler [44].

II.2 Interaction of Dislocations with an Applied Stress in an Anisotropic Crystal

In fig. 2.3, a dislocation line, pinned at its two end points A and B, is assumed to be lying entirely in its own glide plane which is taken to be X-Y plane with the Y-axis parallel to the Burgers vector direction. A parameter n is chosen along the dislocation

segment in such a way that it increases in the positive sense of the dislocation, i.e. $\eta = 0$ at A and $\eta = 1$ corresponds to B. Any general point $X(\eta)$, $Y(\eta)$ on the segment AB can be described by $\theta(\eta)$, the angle between the tangent at this point and the direction ℓ on the dislocation line

Upon applying an external shear stress, the dislocation line will bow out passing through the pinning points and stability occurs when the total self energy of the dislocation line is in balance with the externally applied force

The work done, W_E^d, on the dislocation segment is equal to the integral of the dislocation segment's self energy and has the form,[45]

$$W_E^d = \int_A^B E(\theta)\, ds \qquad (2.1)$$

where s is the arc length along the dislocation segment and $E(\theta)$ is described as the energy per unit length which is assumed to depend on θ at η Under any virtual change, the point η is displaced by an amount $\delta r(\eta) = (\delta X(\eta), \delta Y(\eta))$. Then, the work done on the dislocation segment due to this virtual displacement can be described as:

$$\delta W_f^d = \int_A^B \underset{\sim}{f}(\eta) \cdot \delta \underset{\sim}{r}(\eta)\, ds \qquad (2.2)$$

where:

$$\underset{\sim}{f}(\eta) = (\underset{\sim}{b} \cdot \underset{\approx}{\sigma}) \times \underset{\sim}{t} \qquad (2.3)$$

is given by Peach and Koehler [20] as the force per unit length on the dislocation line due to an external stress $\underset{\approx}{\sigma}$. However $\underset{\approx}{\sigma}$ can include the effects of other dislocations. In expression (2.3), $\underset{\sim}{t}$ is a unit vector tangent to AB at η and $\underset{\sim}{b}$ is the burgers vector

$\sim$ denotes a first-order tensor and $\simeq$ denotes a second-order tensor. The climb motion is assumed to be ignored and only the forces causing the glide effect will be considered, i.e., only the forces acting in the X-Y plane. Examination of equation (2.3) shows that only the σ_{YZ} component of $\underline{\underline{\sigma}}$ causes a force in the X-Y plane. Then,

$$f_{YZ}(\eta) = b\sigma_{YZ}(\sin\theta(\eta)\ , -\cos\theta(\eta)\ ,\ 0) \qquad (2.4)$$

Equation (2.1) after a virtual movement for the dislocation segment, under the effect of external stress, becomes:

$$\delta W_E^d = \delta \int_A^B E(\theta)\, ds \qquad (2.5)$$

Under the condition of continuity on the dislocation segment, expression (2.5) may be written in the form:

$$\delta W_E^d = \int_A^B \delta(E(\theta)\, ds) \qquad (2.6)$$

where:
$$ds = (X'^2(\eta) + Y'^2(\eta))^{\frac{1}{2}}\, d\eta \qquad (2.7)$$

Substituting equation (2.7) into equation (2.6) one gets;

$$\delta W_E^d = \int_0^1 \delta\,(E(\theta)\,(X'^2(\eta) + Y'^2(\eta))^{\frac{1}{2}}\, d\eta)$$

$$= \int_0^1 (E'(\theta)\,\delta\theta(\eta)\,(X'^2(\eta) + Y'^2(\eta))^{\frac{1}{2}} +$$

$$E(\theta)\ \delta\ (X'^2(\eta) + Y'^2(\eta))^{\frac{1}{2}})d\eta \qquad (2.8)$$

where E', X' and Y' are the 1st derivatives of these values.

Integrating by parts and using the fact that δX and δY vanish at $\eta = 0$ and 1, since the end-points are pinned, we obtain,

$$\delta W_L^d = \int_0^1 (E''(\theta) + E(\theta))(\sin\theta.\delta X - \cos\theta.\delta Y)\frac{d\theta}{d\eta}\, d\eta \qquad (2.9)$$

In equations (2.2) and (2.9) it is realized that the variation $(\delta X, \delta Y)$ is an arbitrary function of η, and hence it is possible to set the integrals equal to zero to obtain

$$f(t) \cdot \delta\underset{\sim}{r}(t) = [E(\theta) + E''(\theta)]\,[\sin\theta.\delta X - \cos\theta.\delta Y]\frac{d\theta}{ds} \qquad (2.10)$$

Substituting equation (2.4) into (2.10), gives the condition

$$b\,\sigma_{YZ} = [E(\theta) + E''(\theta)]\frac{d\theta}{ds} \qquad (2.11)$$

Thus, under a uniform shear stress σ_{YZ}, according to equation (2.11), the dislocation line would be approximately a circular arc of radius R and expression (2.11) becomes;

$$b\,\sigma_{YZ} = (E(\theta) + E''(\theta))\frac{1}{R} \qquad (2.12)$$

It should be noticed that σ_{YZ} in equation (2.12) is regarded as both due to a external applied stress on the dislocation segment and an internal stress due to the dislocation's bow out against the surrounding dislocations. Then $E(\theta)$ in this equation must be taken as the self energy of the dislocation segment plus the energy increase caused by the bow out and equation (2.12) should be written as,

$$b\,\sigma_{YZ} = (E_s(\theta) + \Delta E(\theta) + E_s''(\theta) + \Delta E''(\theta))\frac{1}{R} \qquad (2.13)$$

where, in equation (2.13), $E_s(\theta)$ is the self energy of the dislocation line and $\Delta E(\theta)$ is the energy increase of this dislocation line due to bow out movement. Expressions for $E_s(\theta)$ and $\Delta E(\theta)$ are calculated in the following sections of this chapter.

II.3 The Self Energy of a Dislocation Line

In fig 2.4, if a loop 1 is created while loop 2 is present, the stresses originating from loop 2 do work - W_{12}, where W_{12} is the interaction energy between the two loops and has the form;

$$W_{12} = \int_{A_1} dA_{1\beta}\ b_{1\alpha}\ \sigma_{2\alpha\beta} \qquad \alpha,\beta = 1,2 \qquad (2.14)$$

where A_1 is the area surrounded by the dislocation loop, $b_{1\alpha}$ are the components of the Burgers vector and $\sigma_{2\alpha\beta}$ is the self stress of a curved dislocation. It has been calculated by Peach and Koehler [20] and takes the form,

$$\sigma_{\alpha\beta} = \frac{-\mu}{8\pi} \oint_C \epsilon_{ilm} b_m \frac{\partial}{\partial X_i} \nabla^2 R\ dX_\beta - \frac{\mu}{8\pi} \oint_C \epsilon_{im\beta} b_m \frac{\partial}{\partial X_i} \nabla^2 R\ dX_\alpha -$$

$$\frac{\mu}{4\pi(1-\nu)} \oint_C \epsilon_{ilmk} b_m \left(\frac{\partial^3 R}{\partial X_i \partial X_\alpha \partial X_\beta} - \delta_{\alpha\beta} \frac{\partial}{\partial X_i} \nabla^2 R\right) dX_k \qquad (2.15)$$

where $\nabla^2 = \frac{\partial^2}{\partial X_l^2}$ $\quad l = 1,2,3$

μ is the shear modulus of the treated material, ν is the Poision ratio and $R = \hat{r} - r$ where $\hat{r}$ and r are the distances between the two dislocation loops and an arbitrary origin.

Substituting Equation (2.15) in (2.14) and using the Stokes' theorem

$$\int_A \left(\frac{\partial}{\partial X_j} dA_i - \frac{\partial \phi}{\partial X_i} dA_j\right) = \epsilon_{ijk} \oint_C \phi\ dX_k$$

where, in terms of the orthagonal unit vectors, the Einstein permutation operator is given by, [46]

$$\epsilon_{ijk} = e_i \cdot (e_j \times e_k)$$

Then equation (2.14) yields:

$$W_1 = -\frac{\mu}{2\pi} \oint_{C_1} \oint_{C_2} \frac{(b_1 \times b_2) \cdot (dl_1 \times dl_2)}{R} +$$

$$\frac{\mu}{4\pi} \oint_{C_1} \oint_{C_2} \frac{(b_1 \cdot dl_1)\ (b_2 \cdot dl_2)}{R} +$$

$$\frac{\mu}{4\pi(1-\nu)} \oint_{C_1} \oint_{C_2} (b_1 \times dl_1) \cdot \underset{\sim}{T} \cdot (b_2 \times dl_2) \qquad (2.16)$$

where $\underset{\sim}{T} : T_{ij} = \frac{\partial^2 R}{\partial X_i\ X_j}$; $dl_\alpha = \xi_\alpha d\ell$ $\alpha = 1,2$ (2.17)

and where ξ is a unit vector in the direction of a dislocation loop whose length is ℓ.

Expression (2.16) was first obtained by Blin [43] and the details of its derivation are described in appendix III of this thesis while expression (2.15) which was obtained by Peach and Koehler [20], the details of its derivation are in appendix IV.

Each element dl_α of any dislocation loop is acted upon by a force caused by the stress originating from all other parts of the loop and the work done against all these forces is the work done to supply the self energy. Then, the self energy E_s is obtained in equation (2.16) one inserts $C_1 = C_2 = C$ and $b_1 = b_2 = b$ and then divides by 2, i.e.;

$$E_s = \frac{\mu}{8\pi} \oint_{C_1=C} \oint_{C_2=C} \frac{(b.dl_1)\ (b.dl_2)}{R} +$$

$$\frac{\mu}{8\pi(1-\nu)} \oint_{C_1=C} \oint_{C_2=C} (b \times dl_1) \cdot \underset{\sim}{T} \cdot (b \times dl_2) \qquad (2.18)$$

In equation (2.18), the self energy is regarded as the interaction energy between all segments of the loop. Since the integrations in equation (2.16) count the interaction between two given elements twice, then to calculate the self energy of one dislocation loop, the result must be divided by 2 as in equation (2.18).

The self energy of a dislocation line, as it is expressed in equation (2.18), diverges logarithmically. To remove this divergence, Hirth and Lothe [46] postulated that two elements, $d\underset{\sim}{l}_1$ and $d\underset{\sim}{l}_2$ do not interact when they are closer than some distance ρ. On basis of this convention the self energy of a straight-dislocation segment of any character is found by those two authors, to be;

$$E_s = \frac{\mu}{4\pi}\left[(\underset{\sim}{b}\cdot\underset{\sim}{\xi})^2 + \frac{(\underset{\sim}{b}\times\underset{\sim}{\xi})^2}{1-\nu}\right] L \ln\frac{L}{e\rho} \qquad (2.19)$$

where $\rho = \frac{b}{\alpha}$

while α, the dislocation core parameter, has been evaluated by Huntington [47] and Maradudin [48] using numerical computations and semi-empirical atomic force laws. α is found to take $\simeq 4$ as a rough average.

II.4 Interaction Energy Between Two Straight Dislocations

In fig. (2.5) two dislocation segments x_1-x_2 and y_1-y_2 lying in the same plane and oriented to each other are shown. A non-orthogonal coordinate system xyz is constructed consisting of two senses $\underset{\sim}{\xi}_1$ and $\underset{\sim}{\xi}_2$ and a third perpendicular unit vector $\underset{\sim}{e}_3$;

$$\text{where } \underset{\sim}{e}_3 = \frac{\underset{\sim}{\xi}_1 \times \underset{\sim}{\xi}_2}{|\underset{\sim}{\xi}_1 \times \underset{\sim}{\xi}_2|} \qquad (2.20)$$

In this coordinate system, suggested by Jøssang, Lothe and Skylstad [41], the interaction energy E_{12} between the two dislocation segments is given by equation (2.16) and takes the form;

$$E_{12} = \left[-\frac{\mu}{2\pi}\ (\underset{\sim}{b}_1 \times \underset{\sim}{b}_2)\ .\ (\underset{\sim}{\xi}_1 \times \underset{\sim}{\xi}_2) + \frac{\mu}{4\pi}\ (\underset{\sim}{b}_1\ .\ \underset{\sim}{\xi}_1)\ .\ (\underset{\sim}{b}_2\ .\ \underset{\sim}{\xi}_2)\right] \times$$

$$\int_{x_1}^{x_2} dx \int_{y_1}^{y_2} \frac{dy}{R} + \frac{\mu}{4\pi(1-\nu)}\ (\underset{\sim}{b}_1 \times \underset{\sim}{\xi}_1)\ .\underset{\sim}{T}.\ (\underset{\sim}{b}_2 \times \underset{\sim}{\xi}_2) \qquad (2.21)$$

where T, the tensor defined in (2.17), becomes:

$$\underset{\sim}{T} = \int_{x_1}^{x_2} dx \int_{y_1}^{y_2} dy \left[\underset{\sim}{\xi}_2\ \underset{\sim}{\xi}_1 \left(-\frac{\cos\theta}{\sin^4\theta}\ \frac{\partial^2}{\partial x^2} - \frac{1+\cos^2\theta}{\sin^4\theta}\ \frac{\partial^2}{\partial x \partial y} - \frac{\cos\theta}{\sin^4\theta}\ \frac{\partial^2}{\partial y^2} +\right.\right.$$

$$\underset{\sim}{e}_1\ \underset{\sim}{\xi}_1 \left(\frac{1}{\sin^2\theta}\ \frac{\partial}{\partial x} + \frac{\cos\theta}{\sin^2\theta}\ \frac{\partial}{\partial y}\right) +$$

$$\left.\left.\underset{\sim}{\xi}_2\ \underset{\sim}{e}_1 \left(-\frac{\cos\theta}{\sin^2\theta}\ \frac{\partial}{\partial x} - \frac{1}{\sin^2\theta}\ \frac{\partial}{\partial y}\right)\right] R(x,y) \qquad (2.22)$$

Here

$$R^2(x,y) = x^2 + y^2 - 2xy\cos\theta \qquad (2.23)$$

All the integrals in equations (2.21) and (2.22) can be calculated explicitly. For example;

$$\iint \frac{dx\,dy}{R} = \underset{\sim}{I}(x,y)$$

which is to be used in equations (2.20) and (2.21) in the form

$$\int_{x_1}^{x_2} \int_{y_1}^{y_2} \frac{dx\,dy}{R} = \underset{\sim}{I}(x_\alpha, y_\beta) \quad \alpha, \beta = 1,2 \qquad (2.24)$$

while $I(x,y) = x\ \ln\frac{R + y - x\cos\theta}{x} + y\ \ln\frac{R + x - y\cos\theta}{y}$

Utilizing equations (2.22) and (2.24), then equation (2.21) can be written in the form;

$$E_{12} = \frac{\mu}{4\pi}\left\{(\underset{\sim}{b}_1 \cdot \underset{\sim}{\xi}_1)(\underset{\sim}{b}_2 \cdot \underset{\sim}{\xi}_2) - 2[(\underset{\sim}{b}_1 \times \underset{\sim}{b}_2) \cdot (\underset{\sim}{\xi}_1 \times \underset{\sim}{\xi}_2)] + \frac{1}{1-\upsilon}[\underset{\sim}{b}_1 \cdot (\underset{\sim}{\xi}_1 \times \underset{\sim}{e}_3)][\underset{\sim}{b}_2 \cdot (\underset{\sim}{\xi}_2 \times \underset{\sim}{e}_3)]\right\} I(x_\alpha, y_\beta) + \frac{\mu}{4\pi(1-\upsilon)}[\underset{\sim}{b}_1 \cdot \underset{\sim}{e}_3)(\underset{\sim}{b}_2 \cdot \underset{\sim}{e}_3)] \times \left(R(x_\alpha, y_\beta) - \cos\theta\,[x_\alpha \ln t(x_\alpha, y_\beta) + y_\beta \ln s(x_\alpha, y_\beta)]\right) \quad (2.25)$$

where

$$\left.\begin{aligned} s &= y\cos\theta - \frac{x + R}{\cdot} \\ t &= x\cos\theta - y + R \end{aligned}\right\} \quad (2.26)$$

II.5 The Energy Increase Caused by the Bow Out

A segment AB in an infinite edge dislocation bowed out to ACB as shown in fig. 2.6. The energy increase caused by this bow out must be

$$\Delta E = \lim_{m \to \infty} \Delta E_m \quad (2.27)$$

Where ΔE_m is given in terms of the self energies, E_s, and interaction energies, ΔE_{int}, among the symmetrical arrangement shown in fig. 2.5. Then, ΔE_m can be constructed as;

$$\Delta E_m = 2E_s(AC) + 2E_{int}(AC,EA) - E_s(AB) + 2E_{int}(AC,BF) + E_{int}(AC,CB) - 2E_{int}(EA,AB) \quad (2.28)$$

where the self energy E_s can be calculated from equation (2.19) while all of the interaction energies needed are calculated from equation (2.25).

In this particular case, expression (2.25) becomes:

$$E_{12} = \left(\frac{\mu}{4\pi}\right)(\underset{\sim}{b}_1 \cdot \underset{\sim}{\ell}_1)(\underset{\sim}{b}_2 \cdot \underset{\sim}{\ell}_2) + \frac{\mu}{4\pi(1-\nu)}[(\underset{\sim}{b}_1 \cdot (\underset{\sim}{\ell}_1 \times \underset{\sim}{e}_3))][\underset{\sim}{b}_2 \cdot (\underset{\sim}{\ell}_2 \times \underset{\sim}{e}_3)]] \times$$

$$I(x_\alpha, y_\beta) \qquad (2.29)$$

Considering first the contribution:

$$\Delta E_1 = 2E_s(AC) + E_{int}(AC,CB) - E_s(AB) \qquad (2.30)$$

where;

$$E_s(AC) = \frac{\mu b^2}{4\pi}\left\{\cos^2(90-\theta) + \frac{\sin^2(90-\theta)}{1-\nu}\right\}\frac{L}{2\cos\theta}\ln\frac{L}{2e\rho\cos\theta}$$

$$= \frac{\mu b^2}{4\pi}\left\{\sin^2\theta + \frac{\cos^2\theta}{1-\nu}\right\}\frac{L}{2\cos\theta}\ln\frac{L}{2e\rho\cos\theta} \qquad (2.31)$$

and;

$$E_s(AB) = \frac{\mu b^2 L}{4\pi(1-\nu)}\ln\frac{L}{e\rho} \qquad (2.32)$$

From equations (2.24) and (2.29), the interaction energy can be written as,

$$E_{int}(AC,CB) = \frac{\mu b^2}{4\pi}\left[\sin\theta - \frac{\cos^2\theta}{1-\nu}\right]\frac{L}{\cos\theta}\ln\frac{1+\cos\theta}{\cos\theta} \qquad (2.33)$$

Expanding equation (2.33) in a Taylor series about $\theta = 0$ and taking the limit as $\theta \to 0$, one obtains,

$$\Delta E_1 = \frac{\mu b^2 L\theta^2}{8\pi}\left(\frac{1-2\nu}{1-\nu}\ln\frac{L}{4e\rho} + \frac{3}{2} - 2\ln 2\right) \qquad (2.34)$$

In the limit $m \to \infty$, the remaining terms

$$\Delta E_2 = 2E_{int}(AC,EA) + 2E_{int}(AC,BF) - 2E_{int}(EA,AB)$$

are similarly calculated to yield

$$\Delta E_2 = \frac{\mu b^2 L\theta^2}{8\pi}(-2 + 2\ln 2) \qquad (2.35)$$

The total energy increase due to bow out given by equation (2.28) is then,

$$\Delta E = \frac{\mu b^2 L\theta^2}{8\pi(1-\nu)} \left((1-2\nu) \ln\frac{L}{4e\rho} - 0.5\right) \qquad (2.36)$$

II.6 The General Equation

For the case of an edge dislocation, AB in fig. 2.3, following the Frank-Read source mechanism through its advance in the slip plane under the effect of an externally applied stress and internal interaction stress, the situation can be summarized as follows:

I - The relation between the total energy of this dislocation line and the total applied stress is described as:

$$b\,\sigma_{YZ} = (E_s(\theta) + \Delta E(\theta) + E_s''(\theta) + \Delta E_s''(\theta))\,\frac{1}{R} \qquad (2.13)$$

II - The self energy of this dislocation line, AC + CB in fig. 2.6, is described in equation (2.19) as,

$$E_s(\theta) = \frac{\mu}{4\pi}\left[(\underline{b}\cdot\underline{\xi})^2 + \frac{(\underline{b}\times\underline{\xi})^2}{1-\nu}\right] L \ln\frac{L}{e\rho}$$

which can be written as;

$$E_s(\theta) = \frac{2\mu b^2}{4\pi}\left[\cos^2(90-\theta) + \frac{\sin^2(90-\theta)}{1-\nu}\right]\frac{L}{2\cos\theta} \ln\frac{L}{2e\rho\cos\theta}$$

$$= \frac{\mu b^2}{4\pi}\left[\sin^2\theta + \frac{\cos^2\theta}{1-\nu}\right]\frac{L}{\cos\theta} \ln\frac{L}{2e\rho\cos\theta} \qquad (2.37)$$

III - The energy increase due to bow out mechanism is given in equation (2.36) and it is:

$$\Delta E(\theta) = \frac{\mu b^2 L\theta^2}{8\pi(1-\nu)} \left((1-2\nu) \ln\frac{L}{4e\rho} - 0.5\right)$$

Now, by direct substitution from equations (2.36) and (2.37) into equation (2.13), the general form of solution is obtained as:

$$\sigma_{YZ} = \frac{\mu b}{4\pi(1-\nu)}\left[(\sec^3\theta + \sec\theta\tan^2\theta - \nu\cos\theta)(1-\nu)\ln(c\sec\theta) + \right.$$

$$\left(\frac{\theta^2}{2} + 1\right)(1-2\nu) \ln\frac{c}{2} - 0.5) +$$

$$\left.(1-2\nu)\sec\theta\tan^2\theta - \nu\tan\theta\sin\theta + \sec^3\theta\right]\frac{1}{R} \qquad (2.38)$$

where

$$c = \frac{L}{2e\rho}$$

Chapter III

THE OBSERVATION OF DISLOCATIONS IN CRYSTALS

III.1 Decoration Techniques

Hedges and Mitchell [49] were the first to observe the dislocations within crystals. They found that particles of photolytic silver, separated along the dislocation lines of low angle sub-boundaries within crystals of silver chloride or silver bromide, could be seen with normal bright field illumination. The silver halide crystals provided a realistic model for studying the probable behaviour of dislocations in crystals of metals with face-centered-cubic structure. Networks of dislocations in crystals in Alkali Halides, made visible for dark field microscopic examination by the separation of calloidal particles, have been studied by Amelinckx DeKeyser and co-workers [50].

In 1956, Dash [51] developed a method for decorating dislocations in single crystal plates of silicon. Silicon deforms plastically at temperatures above 1000 °C. Thus thin plates can be prepared by sectioning and polishing at room temperature. The points of intersection of dislocations with the surface can be made visible by the deformation of etch pits which can be observed in an infrared transmission microscope. With his method, Dash made the first observation of the Frank-Read source in Crystals. Bartlett and Mitchell [52] used gold to decorate the materials. In their method the crystals are exposed to light at room temperature and this causes nuclei to form along the dislocation lines throughout the thickness

of crystal. The nuclei are made visible by the precipitation of gold.

Many theoretically predicted dislocation phenomena have been observed experimentally in crystals in which the dislocations were made visible by decoration methods. These methods, however, suffered from a number of disadvantages. Configurations of dislocations induced by plastic deformation are modified by thermally activated climb or glide processes during heat treatment. Also, it is not possible to observe the motion of dislocations or even two successive positions of an array of dislocations during plastic formation. Finally, these decoration techniques spoil the crystals in such a way that no further physical investigations can be made. Therefore, these decoration methods have limited use in practice.

III.2 Transmission Electron Microscope

The transmission Electron microscopy of thin foils devised by Bollman [53] and Hirsch and Whelan [54] made it possible to observe the distribution of dislocations for any material which is stable in an electron beam and can be produced in the form of thin sections. This method depends on the diffraction contrast arising from the interactions of the electron beam with the displaced atoms in the strain fields around the dislocation.

Although electron microscopy has great advantages, one being that it is a high power nondestructive method (magnifications up to 100,000 are attainable), the use of thin foils approximately 10^3 A° thick is a serious limitation of the method. This is probably not of great importance if the static distribution is the target of the

study - provided that the distribution itself is not affected by the method used for the preparation of such foils - however, if the dynamical behaviour of dislocations is under investigation, the method of foil preparation may have serious consequences.

III.3 Infrared Technique

In 1975, at Siemen's Munich Laboratory, Heinrich Grienauer and his associates [55] devised a nondestructive infrared film method to detect dislocations and other crystal structure defects. The key item in this method is a laser that emits linearly polarized infrared light at a wavelength of 1.1 microns onto the crystal under study. A microscope enlarges the view of a section of the crystal for examination. An analyzer absorbs the transmitted light that has not had its plane of polarization rotated. An infrared TV camera converts the IR picture at the transmitted light into video signals for display on a monitor. In examining a crystal specimen, the analyzer is adjusted so that it absorbs the portion of the light that passes through the crystal without deviating from its plane of polarization so that the flowless crystal areas show up dark on the monitor. Zones with defects in the lattice structure cause the polarization plane to rotate and show up on the monitor as light spots against a dark background.

III.4 X-Ray Technique

Independently in several laboratories, it was discovered that individual dislocations could be observed by the x-ray diffraction technique. This technique is based upon the theory of x-ray diffraction

by perfect crystals. From point-to-point variations in the direction and/or the intensities of the diffracted x-ray, the defect structure of the crystal may be examined.

The methods of Gunier and Tennevin [56], Schulz [57] and Weissmann [58] are methods that mainly measure the local variations of the diffracted beam. These methods are useful for the detection of gross orientation. Intensity mapping methods are concerned with individual defects, such as dislocations, which can be treated as local perturbations within the perfect crystal. These methods can be classified according to their geometrical arrangements as follows:

(1) The Back Berg-Barrett method. The diffracted beam leaves the same side of the crystal through which the incident beam enters. This method yields a projection of the dislocations structure at and near a crystal surface. Newkirk [59] used this method which had also been used by Bonse and Kappler [60] but with strict collimation of the incident beam by prior reflection from a monochromator crystal.

(2) The Transmission Berg-Barrett method. This is a thin crystal transmission method, in Laue geometry, in which the diffracted beam and the transmitted beam leave the same side of the crystal. Utilizing this technique, Lang [61,62] presented his methods "Section Topograph" and "Projection Topograph" where the images of individual dislocations were first recorded. The transmission Berg-Barrett method was used and developed by Webb. [63]

(3) Anomalous Transmission or Borrmann method. This is a thick crystal transmission method in which the diffracted and transmitted beam leave the same side of the crystal and both beams are used. This technique has been applied with success by Borrmann and co-workers [64], Barth and Hosemann [65], Gerold and Meier [66] and Authier [67]

Selection from among these three methods, as they have been described and shown in fig. 3.1 and table 3.1, depends on the perfection, x-ray absorption coefficient, thickness and size of the crystal to be studied. In all of the methods discussed above, a special x-ray film must be used to record a maximum resolution for the topograph images. These film plates must be carefully processed to obtain maximum contrast.

While it is not the intent of this thesis to present x-ray theory in detail, the interpretation of contrast is of paramount importance in using x-ray topographical techniques, so a considerable amount of discussion is necessary. However, for detailed theories, Zachariasen [68], Battermann and Cole [69], James [70], Hart [71], Meieran [72], Penning and Polder [73], Penning [74] and Authier [75] should be consulted.

In the next section, the dynamical theory will be discussed briefly, followed by a discussion of the possible mechanism by which dislocations can produce contrast.

III.5 The X-Ray Dynamical Theory of Contrast of Dislocation Images

When an x-ray impinges on a crystal, the alternating electric field of the x-ray sets the electrons inside the crystal into forced vibration. The scattered wavelet is the result of the acceleration

and deceleration of the vibrating dipoles and is coherent with the exciting field in polarization, frequency, phase and amplitude.

As shown in fig. 3.2, two main directions of polarization can be distinguished. The first is the σ-polarization, which occurs if the scattered wavelet is emitted in a direction perpendicular to the electric field strength of the incident field. The other polarization direction is the π-polarization which occurs if emission takes place in a direction perpendicular to the magnetic field strength at the exciting field. If the wavelet is emitted in an arbitrary direction, the incident field may be decomposed into two parts, each corresponding to one of the main polarization directions.

Diffraction is a constructive interference that occurs when the difference in the distance travelled by two identical diffracted waves is equal to an integral number of wavelengths, so that the two waves are in phase. The total path difference between the two rays, shown in fig. 3.3, is $2\ d_{hkl}\ \sin\theta_o$ and can be formulated as:

$$n\lambda = 2\ d_{hkl}\ \sin\theta_o \qquad (3.1)$$

This relation is known as Bragg's law and it states the essential condition which must be satisfied if diffraction is to occur. In equation(3.1),λ is the wavelength of the characteristic radiation from the x-ray target material, d is the interplanar spacing for the tested specimen, θ_o the Bragg angle, is half the angle between the incident and diffracted beam and n is the order of reflection and it may take any integral value consistent with $\sin\theta_o$ not exceeding unity.

There are two general theories which may be used to account for the intensities observed in x-ray diffraction studies. The kinematical theory treats the scattering from each volume in the sample as being independent of that of other volume elements, except for incoherent power losses in reaching and leaving that particular volume element. The other theory, called the dynamical theory, takes into account all wave interactions within the crystalline particle. The difference between these two general theories will be made clear in the following discussion.

Consider an x-ray wave of vacuum value vector $\underset{\sim}{\kappa}_o$ ($|\underset{\sim}{\kappa}_o| = \frac{1}{\lambda}$) falling on a crystal set exactly at the Bragg angle θ_β for diffraction from a set of planes (hkl) with interplanar spacing d_{hkl}. The origin of this wave vector is the point L, fig. 3.4, and has an end point at the origin O of the reciprocal lattice. According to the geometrical theory of x-ray diffraction there will be a diffracted beam in the direction LH with wave vector $\underset{\sim}{\kappa}_H$ ($|\underset{\sim}{\kappa}_H| = \frac{1}{\lambda}$) if the reciprocal lattice point H at the end of the reciprocal lattice vector $\underset{\sim}{g}_{hkl} = OH$ ($|\underset{\sim}{g}_{hkl}| = \frac{2\sin\theta_\beta}{\lambda} \quad \frac{1}{d_{hkl}}$) lies on the surface of a sphere of radius $|\underset{\sim}{\kappa}_o|$ and center L. This sphere is called the Ewald sphere. In this geometrical approach no account is taken of the interactions between the direct beam and the diffracted beam. The calculated intensities corresponding to the above are known as the kinematical theory of x-ray diffraction.

In fig. 3.4, since Bragg's law is satisfied for reflection from (hkl) planes, the diffracted beam is in correct orientation for diffraction back into the incident beam direction by the (hkl) planes and interferes with the incident beam.

The interaction of the waves in the transmitted beam direction and the diffracted beam direction is the basis of the dynamical theory of x-ray diffraction. The problem of multiple interactions was treated by Darwin [76], Borie [77] and Ewald [78]. The most generalized approach was taken by Von Laue [79]. Von Laue considered the crystal to be made up of a periodic continuous distribution of scattering material and the dynamical conditions were determined by requiring the crystal waves to satisfy Bragg's law and Maxwell's equation in a medium of periodically varying complex dielectric constant. The solution of the resultant dynamical equation gives allowable wave vectors in the crystals, and the properties of these vectors determine scattered intensities.

For the case of Laue Transmission, shown in fig. 3.5 and for the σ-polarization state, the dynamical equivalent to the geometrical theory as given by Batterman and Cole is shown in fig. 3.6.

The solution of the dynamical equation for each state of polarization consists of two hyperbolic sheets in reciprocal space, centered on Q, which are the two branches of the dispersion surface. One branch, the α-branch, gives the locus of the wave points of wave vector $\underset{\sim}{\kappa}_{\alpha}$ longer than $\underset{\sim}{\kappa}_{o}$ and the other branch, the β-branch, gives the locus of wave vectors $\underset{\sim}{\kappa}_{\beta}$ shorter than $\underset{\sim}{\kappa}$. Each wave vector has a component in the incident beam direction $\underset{\sim}{\kappa}_{o\alpha}$ and $\underset{\sim}{\kappa}_{o\beta}$ and a component in the diffracted beam direction $\underset{\sim}{\kappa}_{H\alpha}$ and $\underset{\sim}{\kappa}_{H\beta}$. The α branch waves are 180° out of phase from the β branch.

A perfect single crystal will only diffract dynamically where the two branches of the primary wave $\underset{\sim}{\kappa}_{o}$ and the two branches of the diffracted wave $\underset{\sim}{\kappa}_{H}$ are still coherently bounded to each other. However a defect in the crystal may severely bend the lattice planes surrounding

it and this distorted region can diffract x-ray intensities from the wings of the incident beam, fig. 3.7. This excess diffracted intensity will give rise to the kinematical images where the coupling of $\underset{\sim}{K}_0$ and $\underset{\sim}{K}_H$ is destroyed because of large lattice distortion. In addition to the dynamical image diffracted from perfect areas and kinematical images diffracted from distorted areas around the defect, there will be an intermediate dynamical image of the defect. This image arises from the areas of the strain field which are not reversely distorted as the kinematical region itself and this intermediate image is equivalent to interbranch scattering or transfer of energy from one branch to the other. The intermediate dynamical image may or may not be superimposed on the direct image.

Fig. 3.8 shows three situations each with a narrow beam of characteristic radiation incident at I on the x-ray entrance surface of the specimen and radiation leaving the specimen over the region HT on the exit surface. The angle HIT=2θ, and the incident beam has typically a divergence of 1′ or 2′ of arc in the plane of the diagram. Fig. 3.8a represents the diffraction from a perfect crystal. In fig. 3.8b, a dislocation line normal to the plane of the diagram lies within the triangle IHT. The area of dislocation is divided to the outer zone of coherent scattering and inner zone of incoherent scattering. In fig. 3.8c, the incident beam cuts through the center of the dislocation. The inner zone of the dislocation can reflect a considerable fraction of the energy within the angular range of the incident beam and it produces an intense diffracted beam which overshadows the other rays travelling in the triangle IHT. The intense,

sharper image is the "direct image" and the diffuse, weaker image arising from the outer zone is the "dynamical image". In the projection topographical technique for high contrast and good topograph resolution, a direct image, strongly compared with the dynamical image is desirable.

Chapter IV

THE EXPERIMENTAL INVESTIGATION

IV.1 The Geometry of Topographical Technique and Image Resolution

The experimental work in this present study has been done utilizing a transmission Lang technique for which the horizontal geometry is schematically shown in fig. 4.1. A divergent beam of x-rays is emitted from an x-ray focal spot of height h and width w. As x-rays cannot be focused by lenses, parallel beams can be obtained by allowing a very small portion of the emitted radiation to pass through a set of slits L, at a distance L from the source. The collimated (parallel) beam of x-ray is diffracted by the crystal planes that have crystallographic directions inclined at Bragg angle θ_β. An x-ray counter, set at twice the Bragg angle, is used to align the crystal for maximum diffracted intensity.

The directly transmitted x-ray beam is intercepted by a metal shield while the diffracted beam is passed through a slit L_2 in the shield and falls on a special photographic plate. The diffraction image produced on the plate represents that part of the crystal which the beam traverses. Since L_1 is generally small, only a narrow portion of the crystal is imaged at one time, and the crystal and film must be scanned through the x-ray beam in a directions. shown in fig. 4.1.

The resolution of the images obtained by Lang Topographical technique is in general different in vertical and horizontal direction In the vertical direction, which is the direction parallel to the long

axis of the collimating slit L_1, the geometrical resolution is given by

$$v = \frac{xh}{L} \tag{4.1}$$

where x is the distance between the sample and film, h is the x-ray focus height and L is the collimator length. The distance x is limited by the need to avoid the undiffracted beam. The geometrical resolution of the image is determined by

$$z = \frac{x\Delta\theta_{1-2}}{\sin(\alpha \pm \theta)} \tag{4.2}$$

where $\alpha = 90 \pm \theta_\beta$, x is the specimen - film distance and the difference in diffraction angle, $\Delta\theta_{1-2}$, between the κ_{α_1} and κ_{α_2} doublet is: [80]

$$\Delta\theta_{1-2} = \frac{\Delta\lambda}{2\, d_{hkl} \cos\theta_\beta} \tag{4.3}$$

where $\Delta\lambda$ is the separation of the $\kappa_{\alpha_1} - \kappa_{\alpha_2}$ and d_{hkl} is the spacing of the crystal planes (hkl) used for diffraction.

In the present work, the dimensions of the x-ray focal spot is 500μ x 500μ, the specimen used is a Silicon single crystal and the crystal planes used for diffraction arc (220). With reference to table 4.1, one can calculate the image resolutions in this particular case:

Vertical Resolution $V = \frac{xh}{L}$

$$= \frac{5 \text{ mm} \times 0.5 \text{ mm}}{840} 10^3$$

$$= 2.97619 \text{ micron}$$

from (4-2) and (4-3), the Horizontal resolution is:

$$Z = \frac{x\Delta\lambda}{2\, d_{hkl} \sin(\alpha \pm \theta_\beta) \cos\theta_\beta} \tag{4.4}$$

$$= \frac{5\,(0.7135 - 0.7093)}{2\,(1.9199) \sin(90-21.27) \cos 21.27} 10^3$$

$$= \frac{5\,(42)\,(10^{-4})}{3.334492} 10^3$$

$$= 6.297810 \text{ micron}$$

With reference to fig. 4.2, following Okkerse and Penning [81] the distance, SD, between κ_{α_1} and κ_{α_2} images can be calculated to indicate to what degree it effects the resolution. This distance on film is,

$$\delta D = \frac{\chi \delta\theta}{\cos^2\theta} \qquad (4\text{-}5)$$

since $$\lambda = 2d \sin\theta \qquad (4\text{-}6)$$

then $$\delta D = \frac{\chi \sin\theta}{\cos^2\theta} \frac{\delta\lambda}{\lambda} \qquad (4\text{-}7)$$

The maximum value SD_m between the images occurs when the crystal - film distance is at its minimum value χ_m

$$\chi_m = \frac{w}{2 \sin\theta} \qquad (4\text{-}8)$$

where w is the x-ray focal spot width.

In the present study, w = 500μ and with reference to table 4.1, for (220) reflection in Silicon one can calculate δD_m

$$\delta D_m = \frac{w}{2\cos^2\theta} \frac{\delta\lambda}{\lambda}$$

$$= \frac{(0.5)\ 10^3}{2\cos^2(21.27)} \frac{.42}{.7093}$$

$$= 1.7045$$

which is of considerable consequence.

The Lang camera used in this experimental part of this thesis is shown in fig. 4.5a, 4.5b and 4.5c. It consists of an adjustable width incoming beam slit (3), a high precision slide assembly (5), a slide drive mechanism consisting of a reversible variable speed dc motor (6) and a set of adjustable position limit switch (2), a beam-stop slit (7) whose position and opening can be adjusted - by (8) -

and a light tight but x-ray transparent film holder (9) that allows transmittance of the intensity monitoring beam even with the film in place.

The sample (12), a single crystal of silicon, is mounted in a stress apparatus fig. 4.5c, which has been made to fit with the rest of the camera and allows a tensile load to be easily applied to the specimen through the use of an accurately measured lever. The load at the far end of the lever is transferred to the specimen axis, scaled up by the value $\frac{b}{a}$ where b and a are the lever's dimensions as shown in fig. 4.5c. The sample is positioned to diffract incoming x-rays into an x-ray counter (1), Scintillation counter, used for alignment purposes and set at the predetermined angle, $2\theta_\beta$, for the reflection chosen.

The beam stop slits are positioned to allow the entire diffracted beam to pass while stopping the direct beam, these slits are as close to the sample as is experimentally possible. In this particular experimental work, the distance is 3mm.

The scan speed and scan length are then set by means of the motor control and limit switches. The x-ray film is positioned as close as possible to the back of the beam stop slits and is aligned normal to the diffracted beam as shown in fig. 4.1.

IV.2 Silicon Crystals; Description and Cleaning

Silicon is an appropriate material to use to study the diffraction phenomena associated with dislocations. Its low absorption does not require the use of very thin samples while through the use of a single crystal of silicon, a wide range of dislocation densities

can be obtained.

Silicon belongs to the cubic system and has a diamond structure. This is characterized by each atom being symmetrically surrounded by four equally spaced neighbours. Fig. 4.3 shows an isometric and a planar view of the position of the atoms with respect to the crystal axes x, y and z. Fig. 4.3 can be extended as shown in fig. 4.4 to show two face centered cubes combined to form a diamond lattice.

The preferred growth habit for silicon is Octahedra, i.e., bounded by the family of {111} planes.

The silicon crystals used in the present study have faces on the {111} planes and diffraction planes on the {220} planes.

It is important to know that the ultimate result of any method utilizing silicon slices depends heavily upon the initial cleaning of the slice.

The following method [82] provides a technique for the cleaning of silicon slices. Although the method outlined is long and involves many steps, each individual step is simple. If the procedure is followed methodically, the results are good.

1. Slices are placed in 1, 1, 2 Trichloroethylene at 75 °C for 450 ± 150 seconds.
2. After all visible organic contaminants have been removed, slices are placed into 2 - propanal or methanol for 300 ± 30 seconds.
3. Slices are rinsed in flowing water which should be distilled and/or de-ionized.
4. Slices are immersed in boiling Hydrogen peroxide for 300 ± 30 seconds.
5. Step number 3 to be repeated.

6. Slices are immersed in Hydrofluoric acid for 5 + 0.5 minutes such that slices are covered.
7. Slices are rinsed thoroughly in water at 90°c.
8. The polished surfaces of the slices are examined by eye to determine if they are hydrophobic. If they are, the inspection should be done under bright illumination with the unaided eye to determine whether there is any visible particulate matter. If a specimen passes both examinations, it is considered to be clean.

IV.3 Processing of Ilford Nuclear Plates

Ilford nuclear plates are used in this study to record the dislocation images. The following processing procedure has been found to give good results for the development of 2" x 2" Ilford L4 nuclear plates with 50μ emulsion.

1. Developer is 1:2 diluted 0-19 at 0°C for up to 30 minutes without agitation. The plates have to be checked after 10 minutes to determine if they are overexposed.
2. Stop bath is 1% glacial acetic acid. It is used for 0°c for 5-10 minutes depending on the thickness of nuclear emulsion.
3. Fixer is Kodak rapid fix with 100% extra hardener added. The fixing solution is initially at 0°c and warms up to room temperature during the fixing time which could be one hour.
4. Washing is done using a methanal ultrasonic bath for 5 minutes to eliminate dust from the emulsion.
5. The plates are washed up in running water for two hours and then are left to dry.

CHAPTER V

MICROSTRESS DISTRIBUTIONS IN A SINGLE CRYSTAL

In this chapter the analytic results of this thesis are combined with the experimental observations in order to determine the microstress distributions in a Silicon single crystal. As a result of the theoretical study in Chapter 2, the stress field acting on a dislocation line is described in equation (2.38). The important variables governing this equation are the dislocation segment's length, L, the radius of its curvature, R, and θ, the angle between the dislocation direction and the X-axis of its local coordinates ($\theta = \sin^{-1}\frac{L}{2R}$). These geometrical parameters are evaluated from the dislocation pattern obtained experimentally as described in Chapter 4 and shown in fig. 5.1.

V.1 The Observation and Histograms of the Dislocation Lengths, L, and their Radii of Curvature, R.

The work that has been done in this thesis is based on the idea of bow out under stress of pinned segments of loop as illustrated in fig. 2.2. The configurations of the dislocation segment, as is discussed in Chapter 2, depend on a balance between forces associated with applied stress, line self energy and interactions with other segments. Aside from these considerations, the dislocation behaviour can be described in terms of the strength of the pinning points. In the present study, the pinning points A and B in fig. 2.3 are assumed to withstand the bow-out of the dislocation segment under the effect of a stress field acting within the elastic region of the tested material. Thus, the distance between A and B will stay fixed while the radius of the curvature is decreased due to the bow-out mechanism.

This independence between the two variables L and R is important in handling the analysis process of the stress distributions which are, due to the nature of equation (2.38), functions of these two random variables.

The values of L and R for each dislocation are measured from fig. 5.1 using computer program described in Appendix (V) and the values are tabulated in tables 5.1 and 5.2. Their corresponding histograms are shown in figs. 5.2 and 5.3, respectively.

V.2 Microstress Distributions

The values of L, R and θ for each measured dislocation, which are indicated in fig. 5.1, are inserted in equation (2.38) and the corresponding microstresses are evaluated using computer program described in Appendix (V).

As discussed in Chapter 2, the microstress values, σ_{YZ}, are acting in the Y-direction of the local coordinate system XYZ. A transformation is needed to correlate these local stresses with the material (external) coordinate system xyz shown in fig. 2.3. This transformation is achieved using Γ_{ij}, a second order orientation tensor, which can be expressed as:

$$\Gamma_{ij} = \begin{pmatrix} \cos\beta & \sin\beta & 0 \\ -\sin\beta & \cos\beta & 0 \\ 0 & 0 & 1 \end{pmatrix} \qquad (5.1)$$

where β is the angle between Y-axis in the local coordinate system and y-axis in the external coordinate system.

Consequently, the microstresses can be calculated as:

$$\sigma = \begin{pmatrix} 0 & \sigma_{YZ} & 0 \\ \sigma_{YZ} & 0 & 0 \\ 0 & 0 & 0 \end{pmatrix} \cdot \Gamma_{ij} \qquad (5.2)$$

Utilizing equation (5.2), the microstresses acting on every dislocation segment indicated in fig. 5.1 are evaluated. The results are tabulated in table 5.4 and the corresponding histograms are shown in figs. 5.4 and 5.5.

These histograms, as a result of the combination between the theoretical and experimental study of this thesis, form the basis for the determination of continuous microstress distributions in the case of uniaxially stressed specimens. This is one of primary goals of micromechanics theory [1-6].

V.3 Possible Gaussian Interpretation

Strunin [83, 84] investigated the probability distribution for the values of the components of the internal-stress tensor produced by randomly positioned linear dislocations in a crystal. The histogram obtained from his investigation is fitted to a normal distribution curve.

This leads to the strong assumption that adding an external stress distributions (due to externally applied load) to the internal stress distributions (due to the presence of dislocations and their interactions) within the range of the elastic regime of the tested material, will result in a total stress distribution which is normally distributed.

Provan and Axelrad [85], in their application of probabilistic micromechanics to actual polycrystalline solids, in the form of pure copper and aluminum, predicted and utilized the idea that the microstress distributions are of Gaussian form. Following the concepts of these two approaches and realizing that for a random-vector gaussian process $\underset{\sim}{x}$, the mean $\mu_{\underset{\sim}{x}}$ and the variance $V_{\underset{\sim}{x}}$ are given by;

$$\mu_{\underset{\sim}{x}} = \lim_{n\to\infty} \frac{1}{n} \sum_{i=1}^{n} \underset{\sim}{x}_i \tag{5.3}$$

and

$$V_{\underset{\sim}{x}} = \lim_{n\to\infty} \left[\frac{1}{n} \sum_{i=1}^{n} (\underset{\sim}{x}_i - \mu_{\underset{\sim}{x}})^2\right]^{\frac{1}{2}} \tag{5.4}$$

Then, within the limitation of the present experimental work - 47 dislocation segments have been investigated - we may fit the histograms obtained in figs. (5.4) and (5.5) to the gaussian form under assumption that the mean and the variance, described in relations (5.3) and (5.4), can be accepted as;

$$\mu_{\sigma_{yz}} = \lim_{n\to\infty} \sum \sigma_{yz} \approx \frac{1}{47} \sum_{n=1}^{47} (\sigma_{yz})_n \tag{5.5}$$

and

$$V_{\sigma_{yz}} = \lim_{n\to\infty} \left[\frac{1}{n} \sum_{i=1}^{n} ((\sigma_{yz})_i - \mu_{\sigma_{yz}})^2\right]^{\frac{1}{2}}$$

$$\approx \left[\frac{1}{47} \sum_{i=1}^{47} ((\sigma_{yz})_i - \mu_{\sigma_{yz}})^2\right]^{\frac{1}{2}} \tag{5.6}$$

where $\mu_{\sigma_{yz}}$ and $V_{\sigma_{yz}}$ are the mean and the variance, respectively,

for the suggested gaussian process of the stress variable σ_{yz}.

Carrying out this assumption, the histograms representing the microstresses, in the x-direction and the y-direction of the external coordinate system, are fitted to gaussian distributions. The results are shown in figs. 5.4 and 5.5.

Following the same fitting process, the histograms of the lengths and the radii of the dislocation segments shown in figs. 5.2 and 5.3 are fitted to gaussian distributions. The results are also shown in figs. 5.2 and 5.3.

V.4 Discussion of Results

The results obtained in the last three sections of this chapter lead to the following observations.

1. In fig. 5.2, the histogram representing the lengths of the dislocation segments, the values of L vary from zero to 0.006 μm. At the same time, the lengths distribute themselves, approximately equally, around the mean value of the lengths 0.0028 μm.

2. In fig. 5.3, the histogram representing the radii of the dislocation segments, the values of R vary from zero to 0.010 μm. This histogram shows a peak corresponding to dislocation segments that have bowed out critically near the mean value of the radii, 0.0036 μm.

3. The histograms representing the lengths and the radii of the dislocation segments are similar to those obtained by Mughrabi [86].

4. Studying the histograms in figs. 5.4 and 5.5, the microstresses in the x-direction and the y-direction of the external coordinate

system xyz, it is found that the high stress values are affected mainly by critical values of the radius, while length changes, which lie in a narrow range compare to that of the radii, do not critically effect the values of the stresses.

5. Inserting the mean values of L, R, and θ in equation (2.38), the mean values of stress are calculated and the results are compared to those obtained experimentally as follows.

Micro-stresses	$\mu_\sigma = \sigma(\mu_R, \mu_L, \mu_\theta)$	μ_σ = Equation (5.4)
σ_{xz}	19.219	21
σ_{yz}	33.779	42

These results show that in the x-direction of the external coordinate system, the direction of application of the external load of 20 kg/cm^2, the mean value of the microstresses can be evaluated through a knowledge of the means of L, R, and θ.

Chapter VI

CONCLUDING REMARKS

VI.1 Summary and Conclusions

Since the main aim of this thesis has been to provide a method to determine the microstress distributions in crystals, the following conclusions of the investigations can be stated,

i) From the independent work of Jøssang, Lothe and Skylslad [41], Foreman [42], Blin [43] and de Wit and Koehler [44] and treating the Frank-Read source on the basis of the line tension model, a theoretical relation between the microstresses on the dislocation segment and the geometrical parameters of this dislocation is derived. In this derivation the microstresses due to dislocation interactions are considered.

ii) The X-ray topographical technique, Lang method, provides an accurate pattern of the dislocation individuals - in a selected specimen - under the effect of an external load and within the range of the elastic behaviour of the tested material. From this pattern the geometrical parameters of these dislocation individuals can be easily measured.

iii) The combination of this theoretical and experimental study is able, as is described and analyzed in chapters 2, 4, and 5, to provide enough information to determine continuous distributions of microstresses inside single crystals.

VI.2 Proposal for Future Research

On basis of the presented work in this thesis, it is suggested

that the following items should be considered for future research.

i) The main purpose of this thesis is to introduce a method to determine the stress distributions inside single crystals, so the information obtained from the small area of the tested specimen which has been examined and analyzed was enough to test the validity of the introduced method. In any future research, large areas should be examined and analyzed, in the same way as it has been done in Chapter 5, in order to get enough information to test the validity of the gaussian distribution assumption. Furthermore, from the general expression of stresses, expressions for the mean value and the variance can be determined using the well known basic relations of normal distributions.

ii) In the present work, only one stress tensor component acting on the dislocation line and parallel to the glide plane is considered. Also, in the derivation of the equation pertaining to the equilibrium of microstresses using an energy argument, the energy dissipation due to the dislocation movement has been neglected in order to remain within an elastic analysis. This study should be extended in future to include all the stress tensor components which are working on the dislocation line in a glide plane taken as randomly oriented. The energy dissipation factor should also be taken into consideration in any future analytical formulation so that plastic or creep descriptions can be formulated.

iii) The author believes that the knowledge obtained from the microstress distributions in a crystalline system is a key to future analytic formulations developed in conjunction with nondestructive fatigue testing and stress microanalysis. Furthermore, the necessary knowledge to describe the irreversible behaviour response of crystalline materials will be mainly obtained through the study of its dynamic dislocation patterns. This suggests that future research should be carried out by more advanced experimental techniques, such as an IR technique, which are able to show the dislocation patterns, in practically tested specimens, while their dynamic movement is irreversible.

LIST OF REFERENCES

1. AXELRAD, D.R. — "Micromechanics of Solids" Graduate Seminars, McGill University, (1968)

2. AXELRAD, D.R. — "Rheology of Structured Media" Archwn Mech. Stosowanej, 23, 131, (1971)

3. AXELRAD, D.R. — "Introduction to the Probabilistic Micromechanics of Solids" Lectures delivered at the institution for Mechanics, University of Bochum - Qerenburg, West Germany, (1974)

4. AXELRAD, D.R. PROVAN, J.W. — "Probabilistic Micromechanics of Solids" Polish Academy of Science, Jablonna, (September, 1972)

5. AXELRAD, D.R. PROVAN, J.W. — "Microrheology of Crystalline Media" Rheol. Acta., 12, 177, (1973)

6. AXELRAD, D.R. PROVAN, J.W. — "Deformation Theory of Elastic Polycrystalline Materials" Ach., Mech. Stos., 25, 811, (1973)

7. OBREIMOV, I.V. SHUBRIKOV, L.V. — "Investigation of Plastic Deformation in Rock Salt Crystals by Optical Methods" Zhur. Russ. Fiz. Khim. Obsh. 58, 817, (1962)

8. VOLTERRA, V. — "L'Equilibre des Corps Elastiques Mulplement Connexes" Annls. Scient. Ecol. Norm. Sup. Paris, III, 24, 401, (1967)

9. WEINGARTEN — "Sulle Superficie di Discontinuita-Nella Teoria Della Elasticita dei Corpi Solidi" Atti. Accad. Nax. Lincei, Rend., Cl. Sci. fis. mat. natur. V. 10/1, 57, (1901)

10. PRANDTL, L. — "Ein Gedankenmodele zur Kinetischen Theorie der festen Korper" (Haupt anfsatze) Z. Angew. Math. Mech. (ZAMM) 8, 85, (1928)

11. DEHLINGER, U. "Zur Theorie der Umwandlung von Metallischen Mischphasen" Ann. der Physik, 20, 646, (1934)

12. ORWAN, E. "Zur Kristall Plastizitat" Z. Phys., 89, 605, (1934)

13. POLANYI, M. "Uber eine Art Gitterstorung, die einen Kristall Plastich Machen Konnen" Z. Phys., 89, 660, (1934)

14. TAYLOR, G.I. "The Mechanism of Plastic Deformation of Crystals" Proc. Roy. Soc., A, 145, 362, (1934)

15. BURGERS, J.M. "Some Considerations of the Field of Stress Connected with Dislocations in a Regular Crystal Lattice" Proc. Kon. Nederl. Akad. Wetensch., 42, 293, 378, (1939)

16. HEIDENRICH, R.D. SHOCKLEY, W. "Study of Slip in Aluminum Crystals by Electron Microscope and Electron Diffraction Method" Rep. Conf. on Strength of Solids, The Physical Soc., London, 57, (1948)

17. FRANK, F.C. "On the Equation of Motion of Crystal Dislocations" Proc. Phys. Soc., 62A, 131, (1949)

18. SEEGER, A. "Dislocations and Mechanical Properties of Crystals" J. Wiley and Sons, Inc., N.Y., (1967), p. 243

19. MOTT, N.F. "A Theory of Work Hardening of Metal Crystals" Phil. Mag. 43, 1151, (1952)

20. PEACH, M.O. KOEHLER, J.S. "The Forces Exerted on Dislocations and the Stress Fields Produced by Them" Phys. Rev., 80, 436, (1950)

21. NYE, J.F. "Some Geometrical Relations in Dislocated Crystals" Acta Met., 1, 153, (1953)

22. KONDO, K. "On the Geometrical and Physical Foundations of the Theory of Yielding" Proc. 2., Japan Nat. Congr. Appl. Mech., 2, 41, (1947)

23. BILBY, B.A. BULLOUGH, R. SMITH, E. "Continuous Distributions of Dislocations: A New Application of the Methods of Non-Riemannian Geometry" Proc. Roy. Soc. (London), A, 231, 263, (1955)

24. KRÖNER, E. "Der Fundamentale Zusammenhang zwischen Versetzungsdichte und Spannungsfunktionen" Z. Phys., 142, 463, (1955)

25. KRÖNER, E. "Kontinuums Theorie der Versetzungen und Eigenspannungen" Springer-Verlag, Berlin, (1958)

26. KONDO, K. "Memoirs of the Unifying Study of the Basic Problems in Engineering Sciences by Means of Geometry" Gakujatsu Bunken Fukyu-Kai, Tokyo, (1955)

27. MURA, T. "Continuous Distribution of Moving Dislocations" Phil. Mag. 8, 843, (1963)

28. MURA, T. "On Dynamic Problems of Continuous Distribution of Dislocations" Int. J. Engng. Sci. 1, 371, (1963)

29. MURA, T. "Continuous Distribution of Dislocations and the Mathematical Theory of Plasticity" Phys. Stat. Sol. 10, 447, (1965)

30. MURA, T. "Continuous Distribution of Dislocations and the Mathematical Theory of Plasticity II" Phys. Stat. Sol 11, 663, (1965)

31. MURA, T. "Continuum Theory of Plasticity and Dislocations" Int. J. Engng. Sci. 5, 341, (1967)

32. MURA, T.
"Continuum Theory of Dislocations and Plasticity"
Mechanics of Generalized Continua
IUTAM Symposium
Springer-Verlag, N.Y., 269, (1968)

33. ESHELBY, J.D.
"Dislocations As a Cause of Mechanical Damping in Metals"
Proc. Roy. Soc. (London), A, 197, (1947)

34. ESHELBY, J.D.
"Uniformly Moving Dislocations"
Proc. Phys. Soc., A, 62, (1949)

35. ESHELBY, J.D.
"Edge Dislocations in Anisotropic Materials"
Phil. Mag., 40, 903, (1949)

36. LAGNEBORG, R.
NILSON, S.
SANDSTROM, R.
"A Method to Determine the Mobile Dislocation Density in Low Carbon Steels"
Materials Center, Royal Institute of Technology, Stockholm, (1973)

37. AXELRAD, D.R.
PROVAN, J.W.
EL-HELBAWI, S.M.
"Dislocation Effects in Elastic Structured Solids"
Archivum Mechaniki Stosowanej, 25, 801, (1973)

38. NABARRO, F.R.N.
"The Mathematical Theory of Stationary Dislocations"
Adv. Phys., 1, 269, (1952)

39. INDENBOM, V.L.
"Some Problems in the Physics of Plasticity of Crystals"
Izd. AN SSSR, Moscow, (1960), p. 117

40. LI, J.C.M.
"Electron Microscopy and Strength of Crystals"
Wiley, (1963), p. 713

41. JØSSANG, T.
LOTHE, J.
SKYLSTAD, K.
"Explicit Expressions for the Energy of Dislocation Configuration Made Up of Piecewise Straight Segments"
Acta Meta. 13, 271, (1965)

42. FOREMAN, A.J.E.
"Dislocation Energies in Anisotropic Crystals"
Acta Meta. 3, 322, (1955)

43. BLIN, J. "Energie Mutuelle de Deux Dislocations" Acta Meta. 3, 199, (1955)

44. DEWIT, G.
KOEHLER, J.S. "Interaction of Dislocations With an Applied Stress in Anisotropic Crystals" Physical Rev., 116, 113, (1959)

45. LARDNER, R. "Mathematical Theory of Dislocations and Fracture" University of Toronto Press, (1974)

46. HIRTH, J.P.
LOTHE, J. "Theory of Dislocations" McGraw-Hill Book Co., N.Y., (1968)

47. HUNTINGTON, H.B.
DICKEY, J.E.
THOMSON, R. "Dislocation Energies in NaCL" Phys. Rev., 100, 117, (1955)

48. MARADUDIN, A. "Screw Dislocations and Discrete Elastic Theory" J. Phys. Chem. Solids, 9, 1, (1959)

49. HEDGES, J.M.
MITCHELL, J.W. "The Observation of Polyhedral Sub-Structures in Crystals of Silver Bromide" Phil. Mag., 44, 223, (1953)

50. DEKEYSER, W.
et al "Defects in Crystalline Solids" Physical Society, London, (1955), p. 134

51. DASH, W.J. "Copper Precipitation on Dislocations in Silicon" J. of Appl. Phys., 27, 1193, (1956)

52. BARTLETT, J.T.
MITCHELL, J.W. "The Decoration of Dislocations in Crystals of Silver Chloride with Gold" Phil. Mag., 3, 334, (1958)

53. BOLLMAN, W. "Interference Effects in the Electron Microscopy of Thin Crystal Foils" Phys. Rev. 103, 1588, (1956)

54. HIRSCH, P.B.
HORNE, R.W.
WHELAN, M.J. "Direct Observations of the Arrangement and Motion of Dislocation in Aluminum" Phil. Mag. 1, 677, (1956)

55. GRIENAUER, H. "I.R. Laser Shows Crystal Defects" Electronics, July 10, (1975)

56. GUINIER, A.
TENNEVIN, J. "Sur Deux Variantes de la Méthode de Laue et Leurs Applications" Acta Cryst., 2, 133, (1949)

57. SCHULZ, L.G. "Method of Using a Fine-Focus X-Ray Tube for Examining the Surface of Single Crystals" J. Metals, 6, 1082, (1954)

58. WEISSMANN, S. "Method for the Study of Lattice Inhomogeneities Combining X-Ray Microscopy and Diffraction Analysis" J. Appl. Phys., 27, 389, (1956)

59. NEWKIRK, J.B. "The Observation of Dislocations and Other Imperfections by X-Ray Extinction Contrast" Trans. AIME 215, 483, (1959)

60. BONSE, U. KAPPLER, A. "Rontgenographische Abbildung des Verzerrungsfeldes einzelner Versetzungen in Germanium Einkristallen" Z. Naturf. 13a, 348, (1958)

61. LANG, A.R. "A Method for the Examination of Crystal Sections Using Penetrating Characteristics X Radiation" Acta Meta., 5, 358, (1957)

62. LANG, A.R. "The Projection Topograph: A New Method in X-Ray Diffraction Microradiography" Acta Cryst., 12, 249, (1959)

63. WEBB, W.W. "Direct Observation of Imperfections in Crystals" Interscience, N.Y., (1962), p. 29

64. BORRMAN, G. HARTWIG, W. IRMLER, H. "Schatten Von Verselzungslinien im Rontgen - Diagramm" Z. Naturforsch, 13A, 2123, (1958)

65. BARTH, H. HOSEMANN, R. "Anwendung der Parallelstrahlen methode im Durchstrahlungsfall zur Prufung des Kristall Inneren mit Rontgen - Strahlen" Z. Naturforsch, 13a, 792, (1958)

66. GEROLD, V. MEIER, F. "Der rontgenographische Nachweis von Versetzungen in Germanium" Z. Physik, 155, 387, (1959)

67. AUTHIER, A. "Observation des Dislocations Dans le Silicum a l'Aide des Rayons X Dans le Cas de la Transmission Anormale" J. Phys. Radium, 21, 655, (1960)

68. ZACHARIASEN, W.H. "Theory of X-Ray Diffraction in Crystals" John Wiley & Sons, N.Y., (1945)

69. BATTERMAN, B.W. COLE, H. "Dynamical Diffraction of X-Rays by Perfect Crystals" Rev. Mod. Phys., 36, 681, (1964)

70. JAMES, R.W. "The Dynamical Theory of X-Ray Diffraction" Solid State Physics, 15, 53, (1963)

71. HART, M. "Dynamic X-Ray Diffraction in the Strain Fields of Individual Dislocations" Thesis, Bristol University, (1963)

72. MEIERAN, E.S. "The Application of X-Ray Topographical Techniques to the Study of Semiconductor Crystals and Devices" Fairchild Semiconductor, Technical Report No. 400, (April, 1969)

73. PENNING, P. POLDER, D. "Dynamical Theory for Simultaneous X-Ray Diffraction" Philips Res. Repts., 23, 1, (1968)

74. PENNING, P. "Theory of X-Ray Diffraction in Unstrained and Lightly Strained Perfect Crystals" Thesis, Technological University of Delft, (1966)

75. AUTHIER, A. "Contrast of Dislocation Images in X-Ray Transmission Topography" Adv. in X-Ray Anal. 10, 3, (1967)

76. DARWIN, C.G. "Theory of X-Ray Reflexion" Phil. Mag. 27, 315, (1914)

77. BORIE, B. "The Darwin Dynamical Theory of X-Ray Diffraction" Acta Cryst. 23, 210, (1967)

78. EWALD, P.P. "Zur Begrundung der Kristall Optik" Ann. der Physik, 49, 1, (1916)

79. LAUE, M.V. "Die Energiestromung bei Rontgenstrahl - Interferenzen in Kristallen" Acta Cryst. 5, 619, (1952)

80. YOSHIMATSU, R. — "Scanning Type of X-Ray Diffraction Microscopy" Rig aku - Denki Co. Ltd.

81. OKKERSE, B. PENNING, P. — "Anomalous Transmission of X-Rays in Highly Perfect Crystals" Philips Technical Review, 29, 114, (1968)

82. GITTLER, T.L. — "Recommended Method for Cleaning of Silicon Slices" ASTM, Bell Northern Laboratories, August 14, (1969)

83. STRUNIN, B.M. — "Internal Stress Distribution for a Random Positioning of Dislocations" Soviet Physics - Solid State, 9, 630, (1967)

84. STRUNIN, B.M. — "Probabilistic Description of the Internal Stress Field in the Case of a Random Distribution of Dislocations" Soviet Physics - Solid State, 13, 772, (1971)

85. PROVAN, J.W. AXELRAD, D.R. — "The Effective Elastic Response of Randomly Oriented Polycrystalline Solids in Tension" Symposium on Continuum Models of Discrete Systems, Polish Academy of Sciences, June 22nd - 28th, (1975)

86. MUGHRABI, H. — "Some Observations of Fatigue in Copper Single Crystals"

87. AXELRAD, D.R. KALOUSEK, J. — "Measurements of Microdeformations by X-Ray Holographic Diffractions" Experimental Mechanics in Research and Development, Ed. J.T. Pindera, SM Study No. 9, University of Waterloo, Ontario, Canada, (1973)

88. DEWIT, R. — "The Continuum Theory of Stationary Dislocations" Solid State Phys. 10, 249, (1960)

89. ENGBERG, G. LAGNEBORG, R. — "A Method to Measure the Dislocation Link Length Distribution in Dislocation Structures" The Royal Institute of Technology, S-100 44 Stockholm 70, Sweden

TABLES

Technique	Back reflection Berg-Barrett	Transmission Berg-Barrett	Anomalous Transmission-Borrmann
Reference	Newkirk[59] Bonse and Kappler[60]	Lang[61,62] Webb[63]	Borrmann et al[64]
Scheme	Back diffraction Bragg Case - diffracted beam leaves the same surface entered by the incident beam	Thin crystal transmission diffraction, Laue Case - diffracted beam leaves through same surface as transmitted beam	Thick crystal, Laue Case - anomalous transmission and diffraction
Best geometric resolution	1-5μ	1-5μ	1-5μ
Sensitivity to dislocation sense of deformation	No	Yes	Yes
Thickness of specimen contribution to topograph	≤ 5μ	0-2mm	1-5mm
Absorption criterion	$M_0 t > 1$	$M_0 t << 1$	$M_0 t >> 1$
Structure factor ratio	Unrestricted	Unrestricted	$F_0/F_H = 1$
Beam recorded	H only	H only	H and T superimposed
Emulsion placement	in H only avoiding I	in H only avoiding I	in H and T on back surface of specimen
Dislocation image width	1-5μ	1-10μ	up to 150μ
Upper limit of dislocation density (lines/cm²)	5×10^6	5×10^3	5×10^6

Table 3.1 DISTINGUISHING CHARACTERISTICS OF DIFFRACTION TOPOGRAPHY METHODS FOR MAPPING INDIVIDUAL DISLOCATIONS

THE LATTICE PARAMETER OF SILICON IS 5.4305 ANGSTROMS										
HKL	D	MO KA1	MO KA2	MO KB1	CU KA1	CU KA2	CU KB1	CR KA1	CR KA2	CR KB1
(WAVELENGTH)		0.7093	0.7135	0.6322	1.5405	1.5443	1.3922	2.2900	2.2940	2.0850
111	3.1353	12.98	13.05	11.56	28.42	28.49	25.63	42.81	42.89	38.81
220	1.9199	21.27	21.40	18.94	47.27	47.39	42.48	73.17	73.32	65.73
311	1.6373	25.00	25.15	22.24	56.08	56.23	50.28	88.68	88.88	79.[illegible]
400	1.3576	30.26	30.45	26.91	69.08	69.28	61.65	114.92	115.24	100.26
331	1.2458	33.05	33.25	29.37	76.32	76.55	67.89	133.49	133.96	113.53
422	1.1084	37.29	37.52	33.11	87.97	88.25	77.75	0.00	0.00	140.17
511	1.0451	39.64	39.89	35.18	94.89	95.20	83.47	0.00	0.00	171.80
333	1.0451	39.64	39.89	35.18	94.89	95.20	83.47	0.00	0.00	171.80
440	0.9599	43.33	43.60	38.42	106.64	107.02	92.89	0.00	0.00	0.00

TABLE 4.1

CRYSTALLOGRAPHIC ORIENTATIONS VS. DIFFRACTION ANGLES FOR SILICON AND SELECTED TARGETS

Dislocation's number as indicated in fig. 5.1	Dislocation length x 10^{-4} µm
1	48.85
2	36.94
3	38.06
4	13.74
5	40.10
6	18.32
7	19.24
8	14.66
9	32.07
10	30.69
11	18.32
12	23.82
13	21.99
14	17.41
15	21.99
16	20.62
17	33.90
18	27.49
19	18.32
20	45.39
21	45.39
22	30.23
23	21.99
24	55.89

Table 5.1 Lengths of Dislocation Segments Shown in fig. 5.1.

Dislocation's number as indicated in fig. 5.1	Dislocation length x 10^{-4} mm
25	29.32
26	43.98
27	55.43
28	48.56
29	50.48
30	23.82
31	42.65
32	19.01
33	10.99
34	28.40
35	8.704
36	46.27
37	27.49
38	17.41
39	20.62
40	48.19
41	21.07
42	10.99
43	16.28
44	8.662
45	9.621
46	13.74
47	14.66

(Continued) -Table 5.1 Lengths of Dislocation Segments in fig. 5.1.

Dislocation's number as indicated in fig. 5.1	Dislocation radius x 10^{-4} μm
1	44.87
2	36.65
3	36.65
4	9.391
5	32.57
6	13.74
7	14.66
8	13.05
9	37.23
10	24.74
11	16.53
12	21.16
13	21.99
14	22.68
15	34.59
16	21.12
17	78.34
18	33.86
19	15.58
20	67.43
21	90.54
22	33.78
23	23.49
24	74.72
25	25.59

Table 5.2 Radii of Dislocation Segments Shown in fig. 5.1.

Dislocation's number as indicated in fig. 5.1	Dislocation radius x 10^{-4} μm
26	81.04
27	74.05
28	39.03
29	90.83
30	46.05
31	90.66
32	20.28
33	13.74
34	21.99
35	9.391
36	61.97
37	49.47
38	16.49
39	40.31
40	69.67
41	34.36
42	7.788
43	20.86
44	14.83
45	8.475
46	17.18
47	7.788

(Continued) - Table 5.2 Radii of Dislocation Segments Shown in fig. 5.1

Dislocation number as indicated in fig. 5.1	Stress in x-direction kg/cm²	Stress in y-direction kg/cm²
1	21.121	38.103
2	45.096	57.720
3	48.264	66.429
4	90.009	193.025
5	19.060	58.662
6	101.984	109.364
7	70.368	100.496
8	65.812	46.082
9	15.834	31.075
10	53.391	44.800
11	11.255	63.830
12	10.060	57.053
13	39.752	54.714
14	52.787	84.477
15	7.944	27.703
16	23.175	46.699
17	6.718	15.827
18	23.255	23.255
19	65.566	100.791
20	15.655	12.231
21	4.798	11.303
22	12.323	33.857
23	19.667	38.598
24	4.274	14.906

Table 5.3 Microstress Values in x and y directions of the External Coordinate System.

Dislocation number as indicated in fig. 5.1	Stress in x-direction kg/cm²	Stress in y-direction kg/cm²
25	20.881	36.166
26	4.398	12.085
27	7.580	13.675
28	33.514	23.467
29	2.693	12.669
30	16.892	21.620
31	3.229	12.053
32	34.008	84.172
33	25.356	69.665
34	43.760	62.495
35	63.614	157.449
36	10.376	16.604
37	6.751	22.080
38	36.260	118.601
39	11.670	32.064
40	8.857	15.341
41	10.812	29.705
42	195.984	147.684
43	22.260	45.639
44	73.776	113.604
45	120.328	90.673
46	28.603	61.339
47	266.056	266.055

(Continued) - Table 5.3 Microstress Values in x and y directions of the External Coordinate System

FIGURES

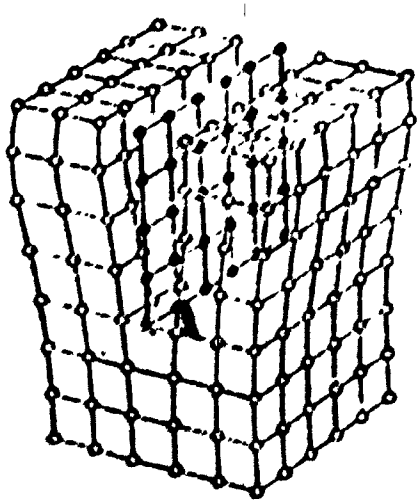

Figure 1.1 Atomic configuration surrounding an edge dislocation.

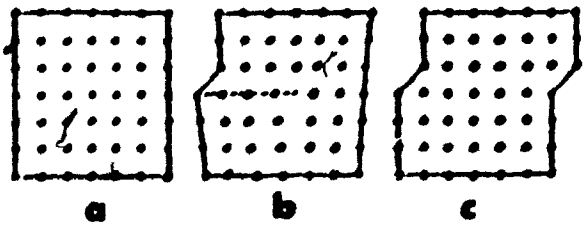

Positive Dislocation

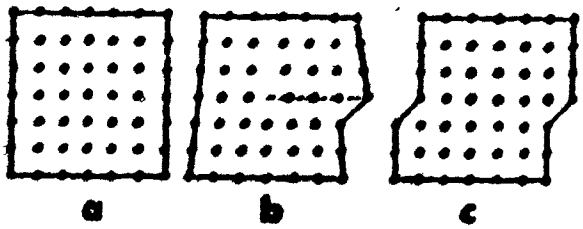

Negative Dislocation

Figure 1.2 Positions of atoms during the passage of a dislocation [After Taylor[14]].

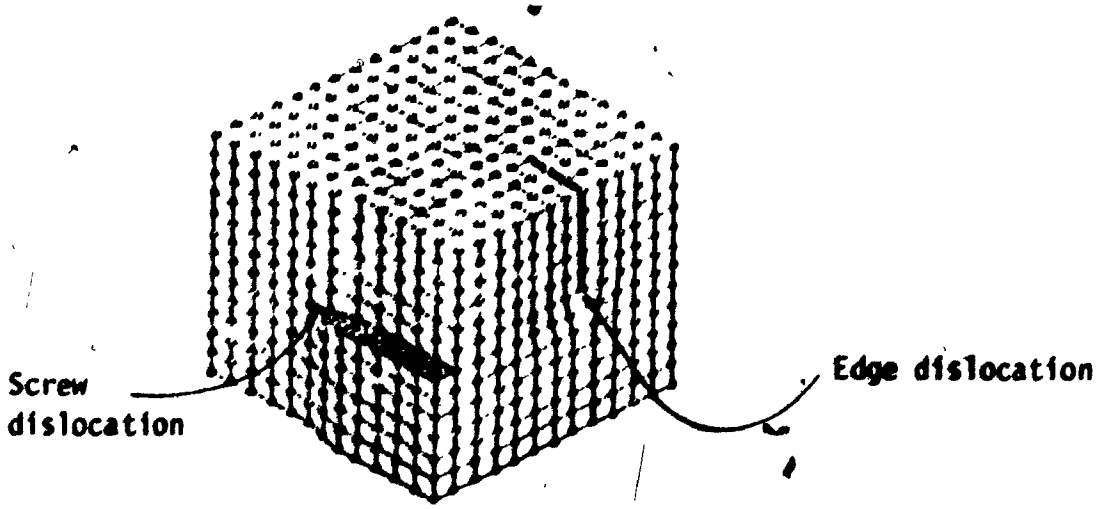

Figure 1.3 Screw dislocation and edge dislocation.

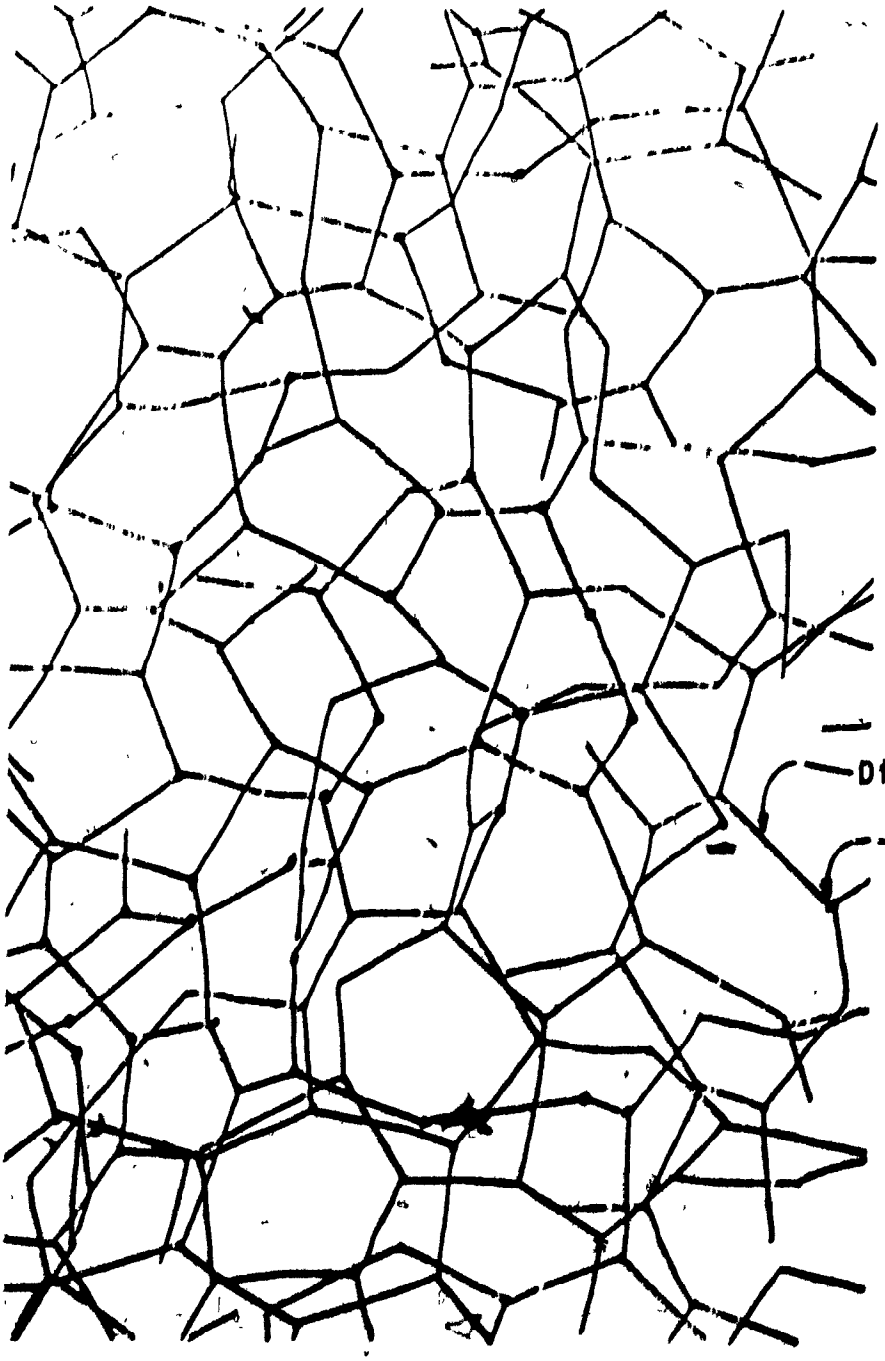

Figure 2.1 A model for a three dimensional dislocation configuration in a new and unstrained crystal (After Basinski and Lagneborg[80]).

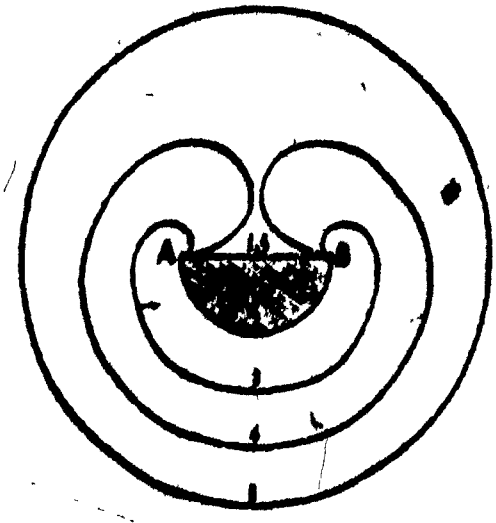

Figure 2.2 Frank-Read source mechanism
"Inside the shadow area the mechanism is reversible while outside the mechanism is irreversible"

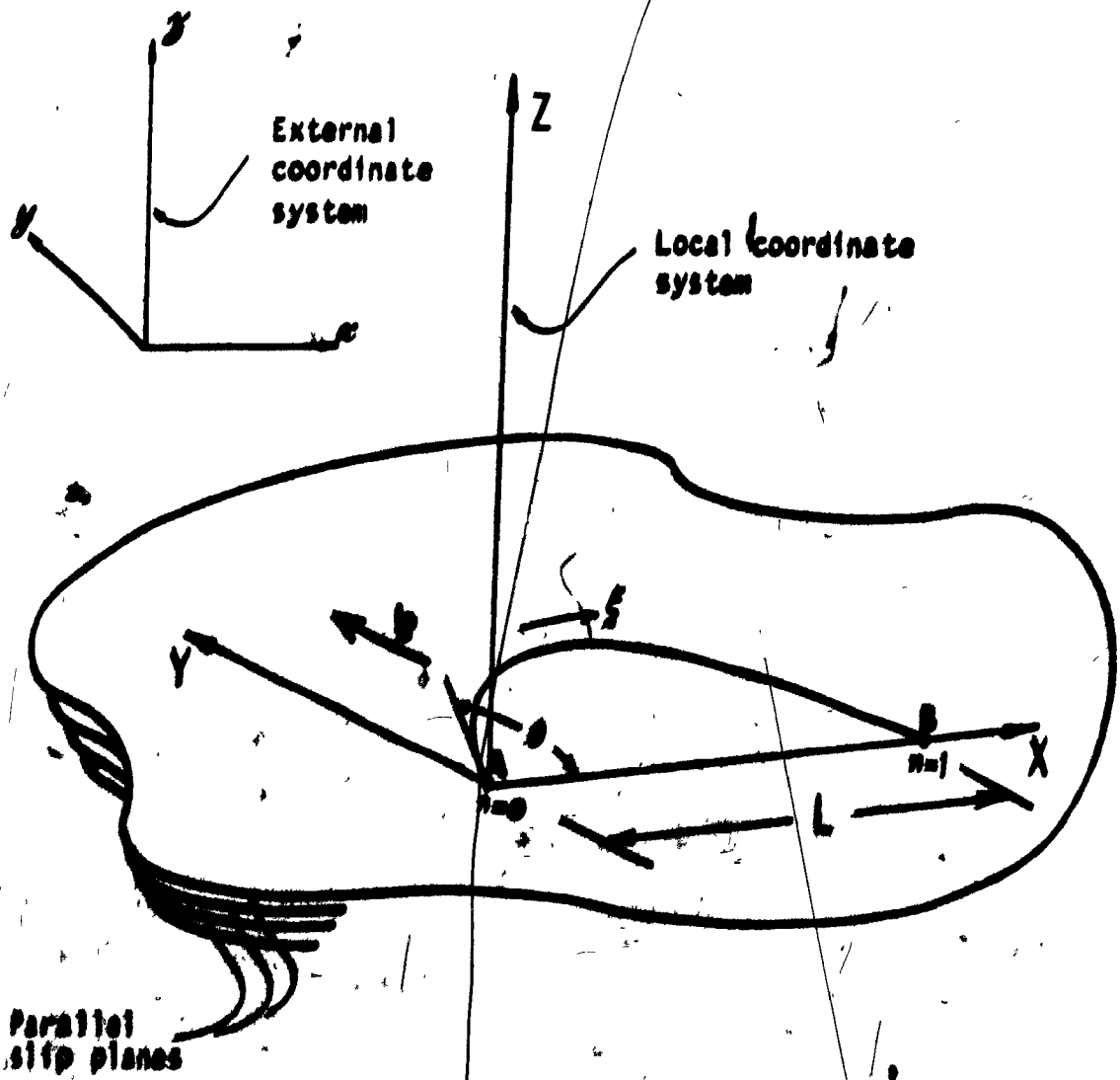

Figure 2.3. A dislocation's bow-out in a slip plane.

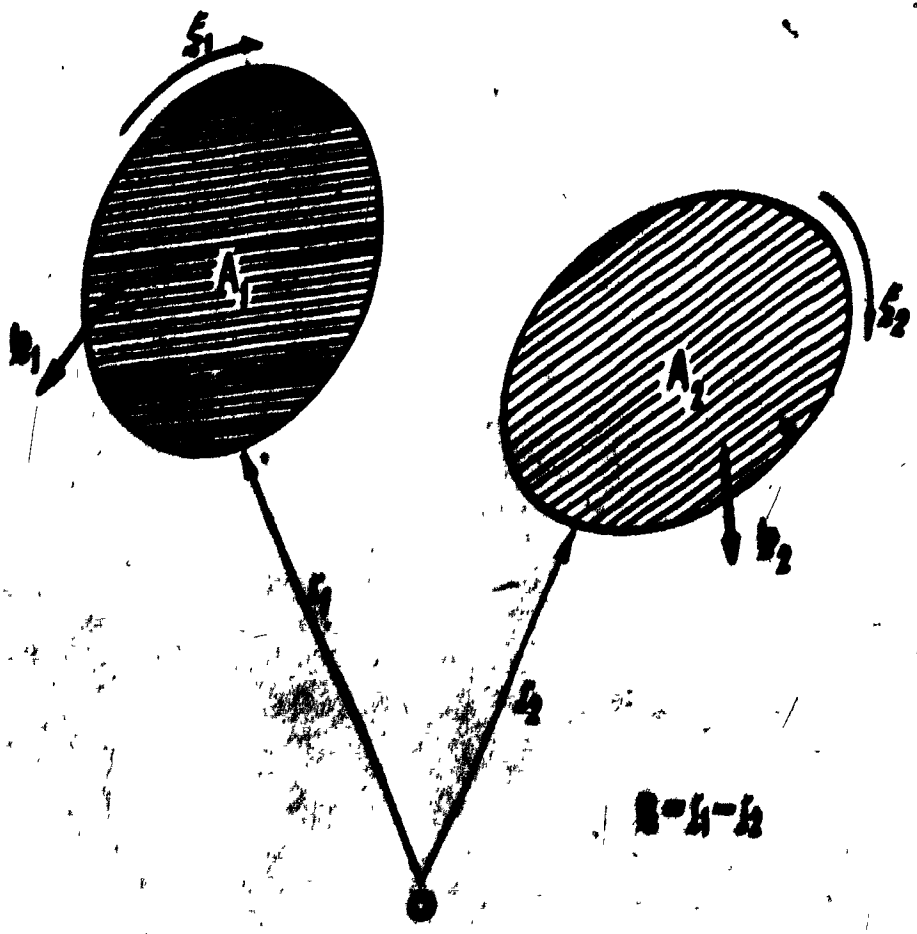

Figure 2.4 Two dislocation loops within the same elastic continuum (After Mirth and Lothe[46]).

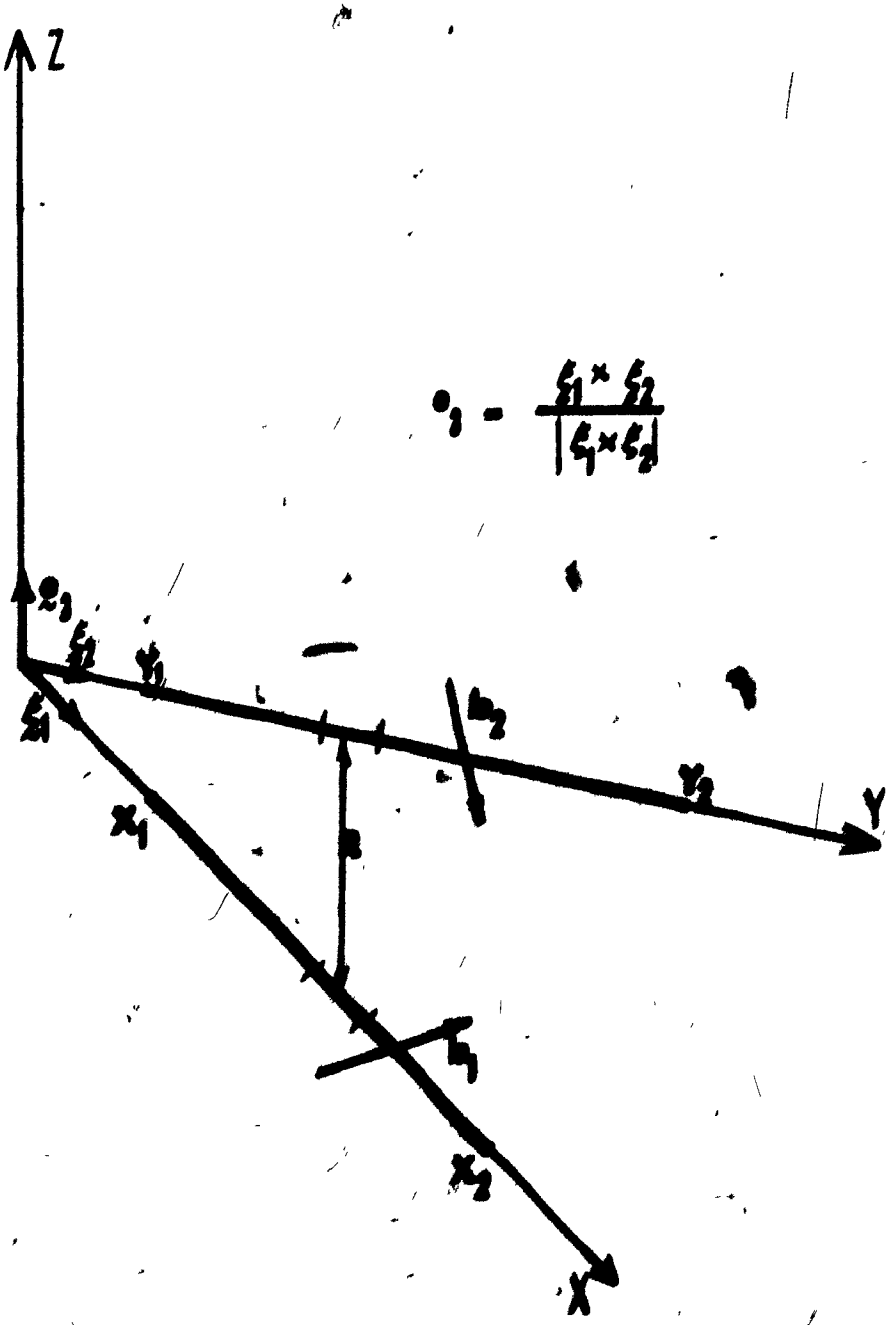

Figure 2.5 Coordinate system for interacted dislocation segments X_1X_2 and Y_1Y_2.

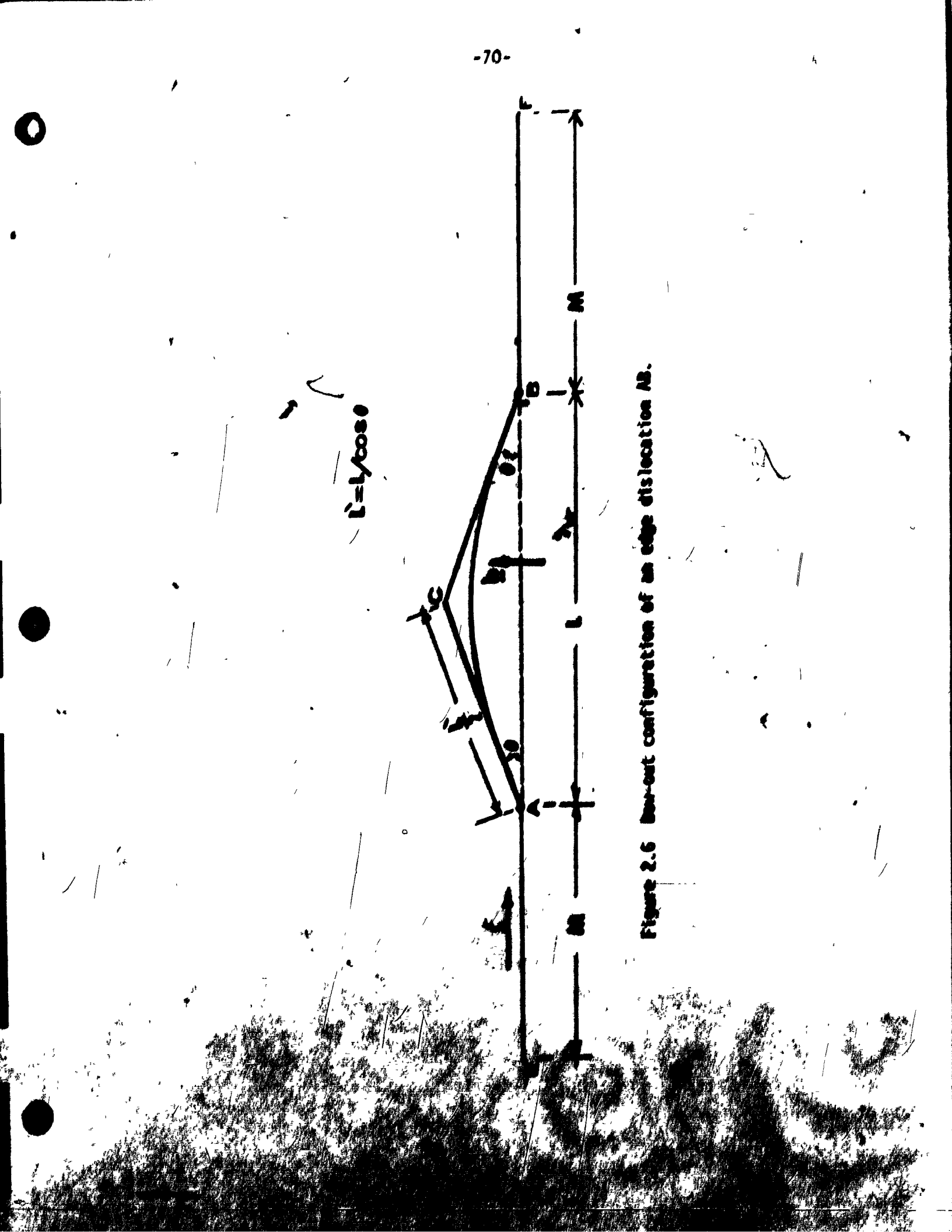

Figure 2.6 Aberrant configuration of an edge dislocation AB.

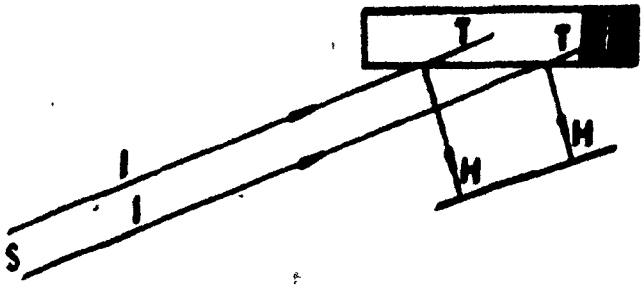

(a) Back-reflection Berg-Barrett method

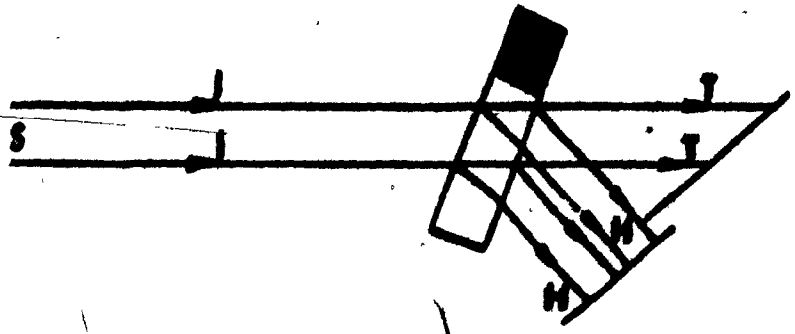

(b) Transmission Berg-Barrett method

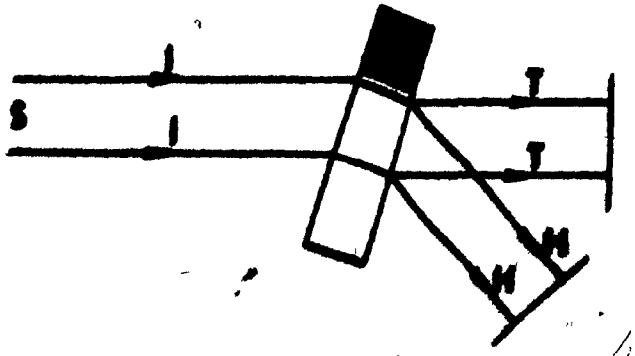

(c) Borrmann anomalous transmission method

Figure 2.1 Schemes for X-ray diffraction topography

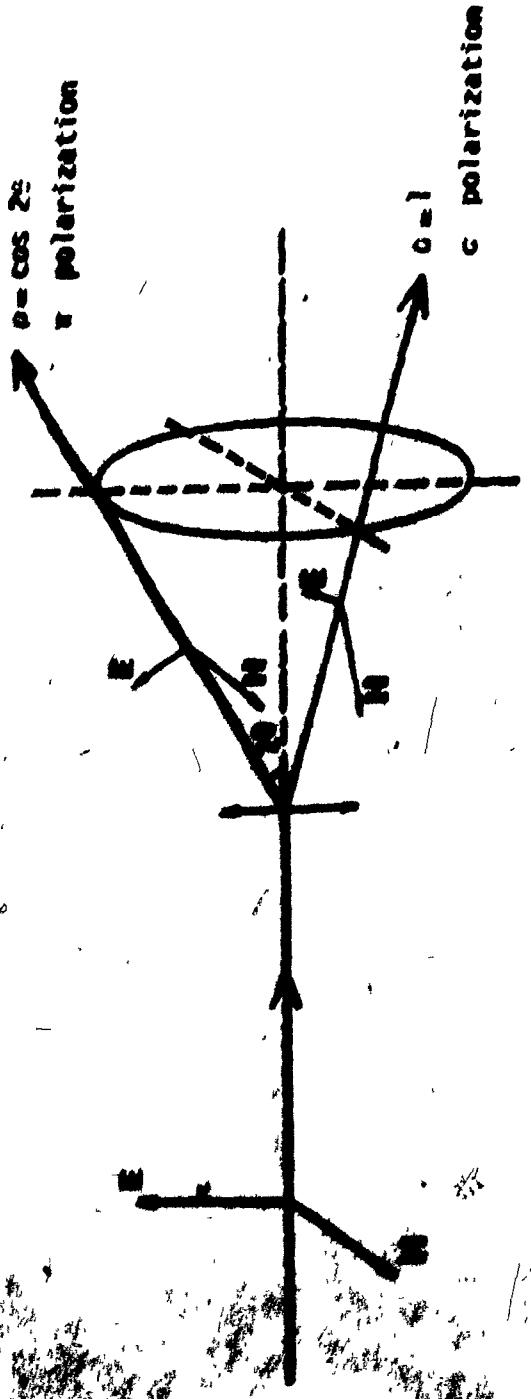

Figure 3.2 The two main directions of X-ray polarization.

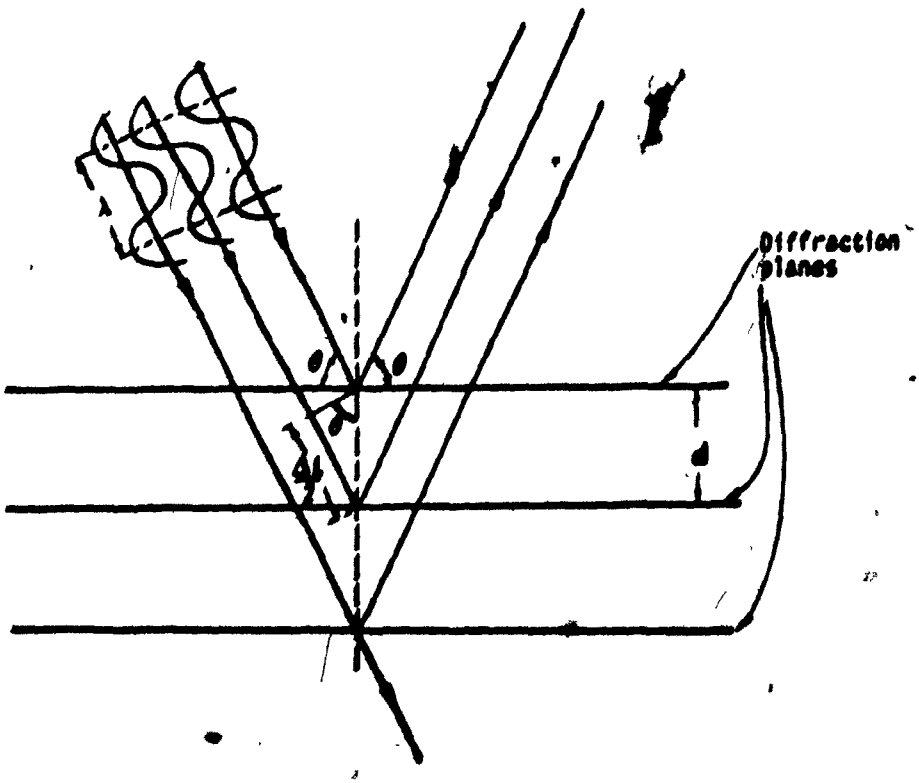

Figure 3.3 X-ray Bragg diffraction

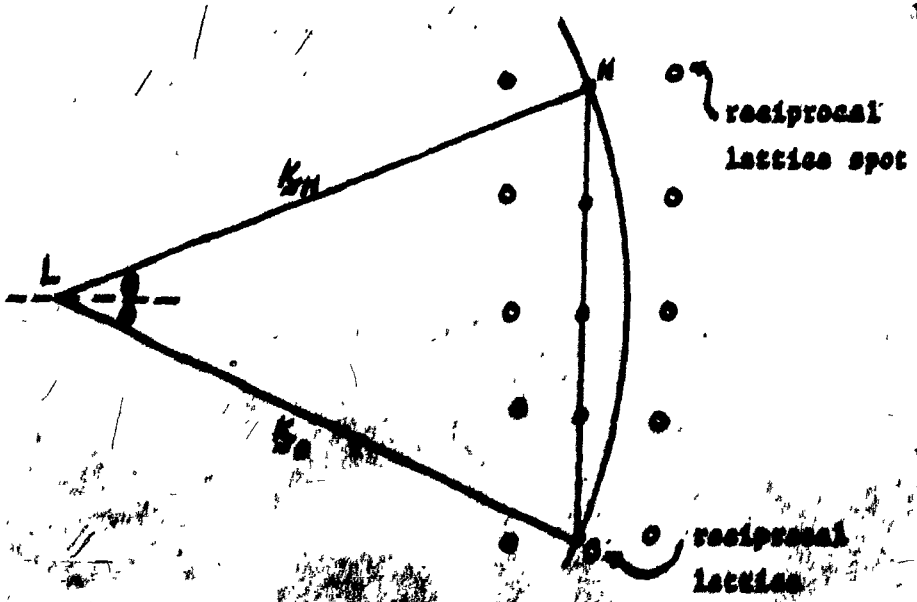

Figure 3.4

Ewald Sphere construction for the matrix lattice spots

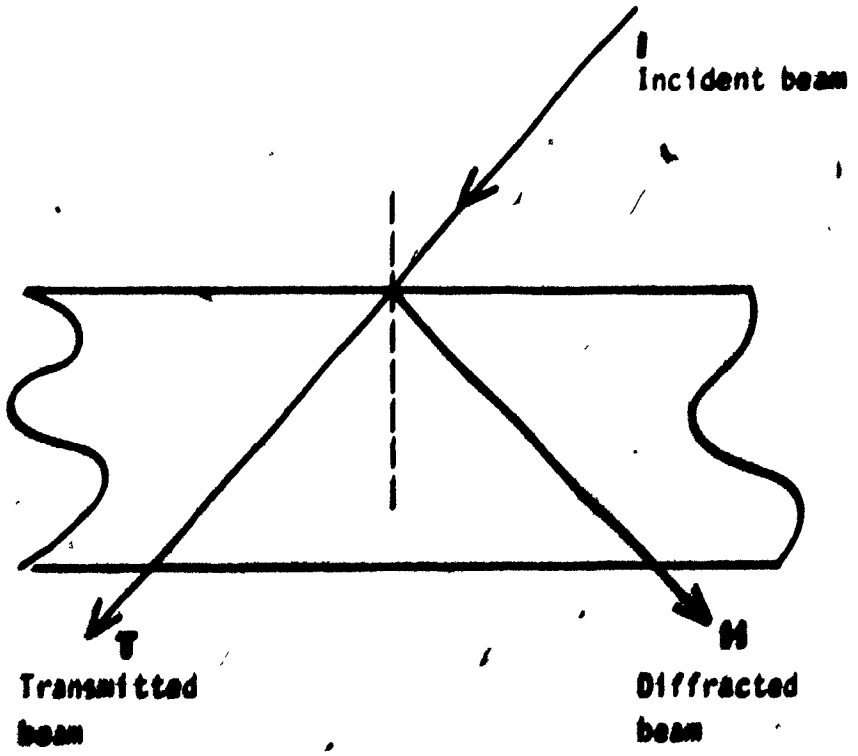

Figure 3.5 X-ray diffraction geometry of Laue case.

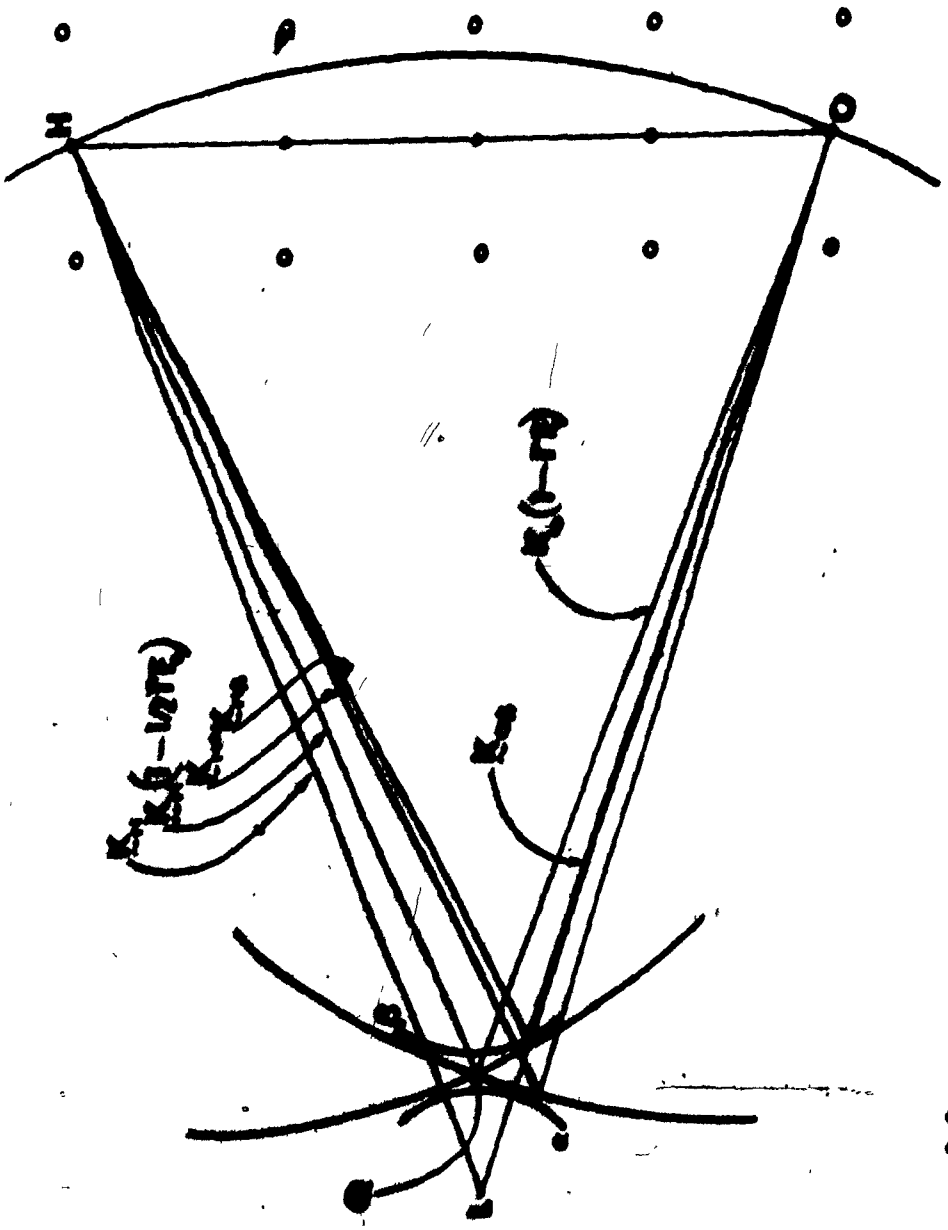

Figure 3.6
Ewald sphere construction for one active reciprocal lattice spot, dynamical diffraction, polarization state $\sigma = 1$. The distance QQ and $\overline{Q}\overline{Q}$ are greatly underexaggerated.

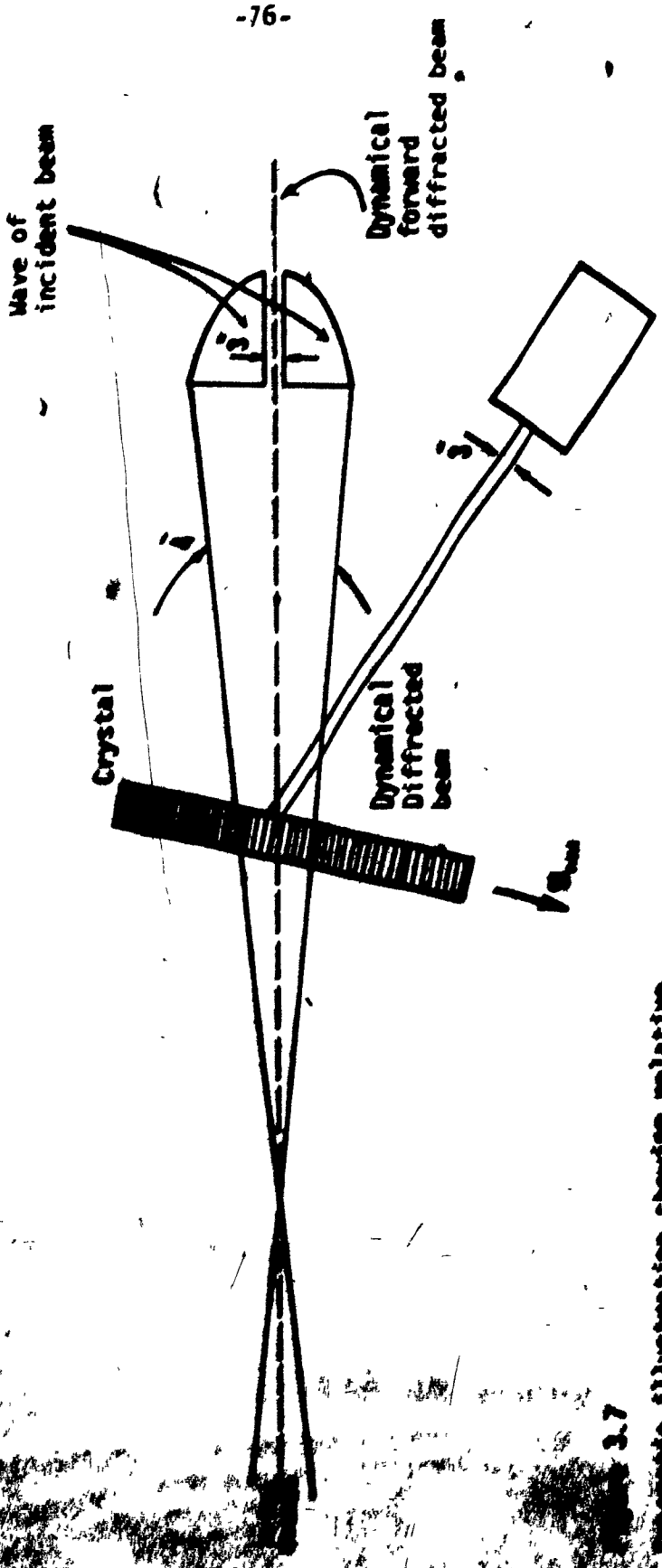

Fig. 3.7 Schematic illustration showing relative configuration of direct and dynamical portions of incident beam

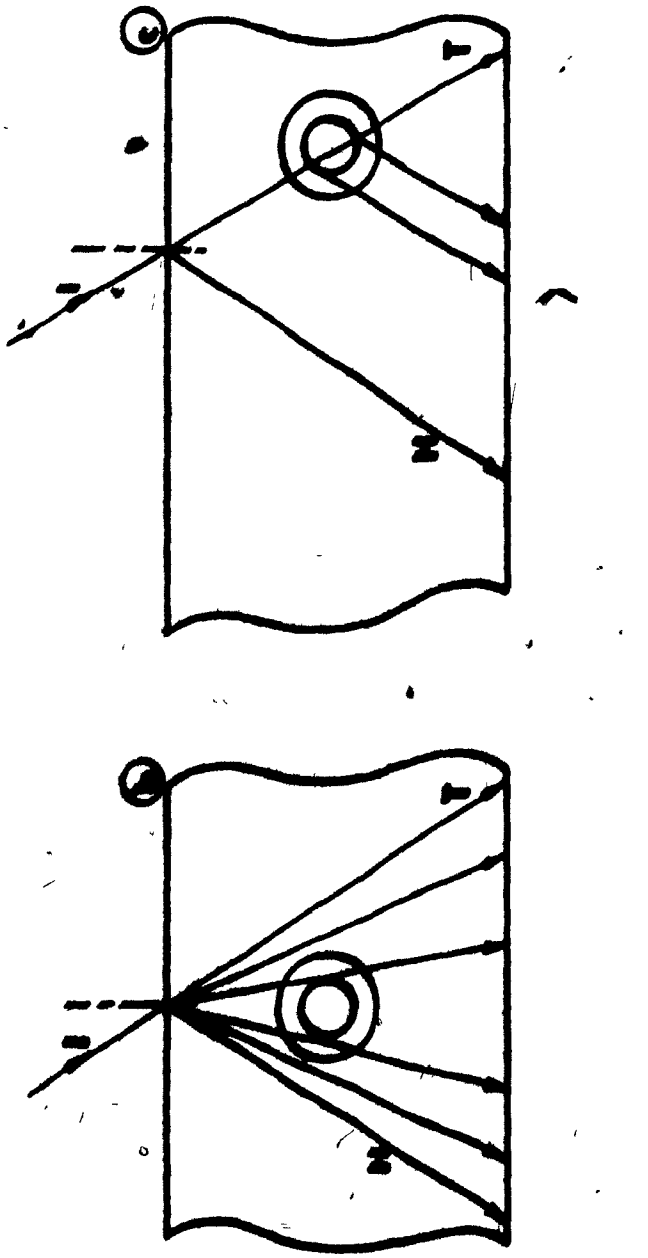

Figure 3.8 Geometry of dislocation image formation.

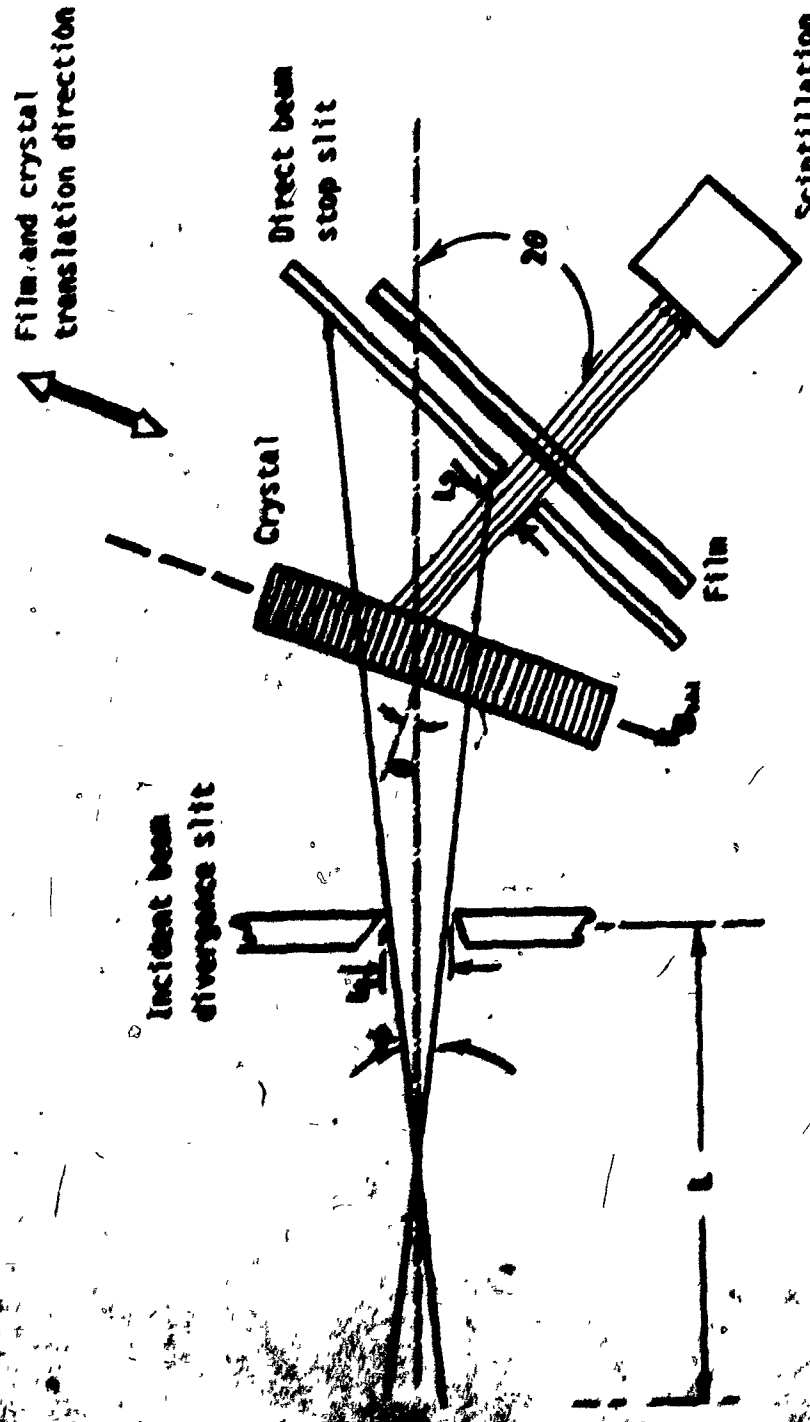

Figure 4.1 Scanning transmission Lang topograph geometry.

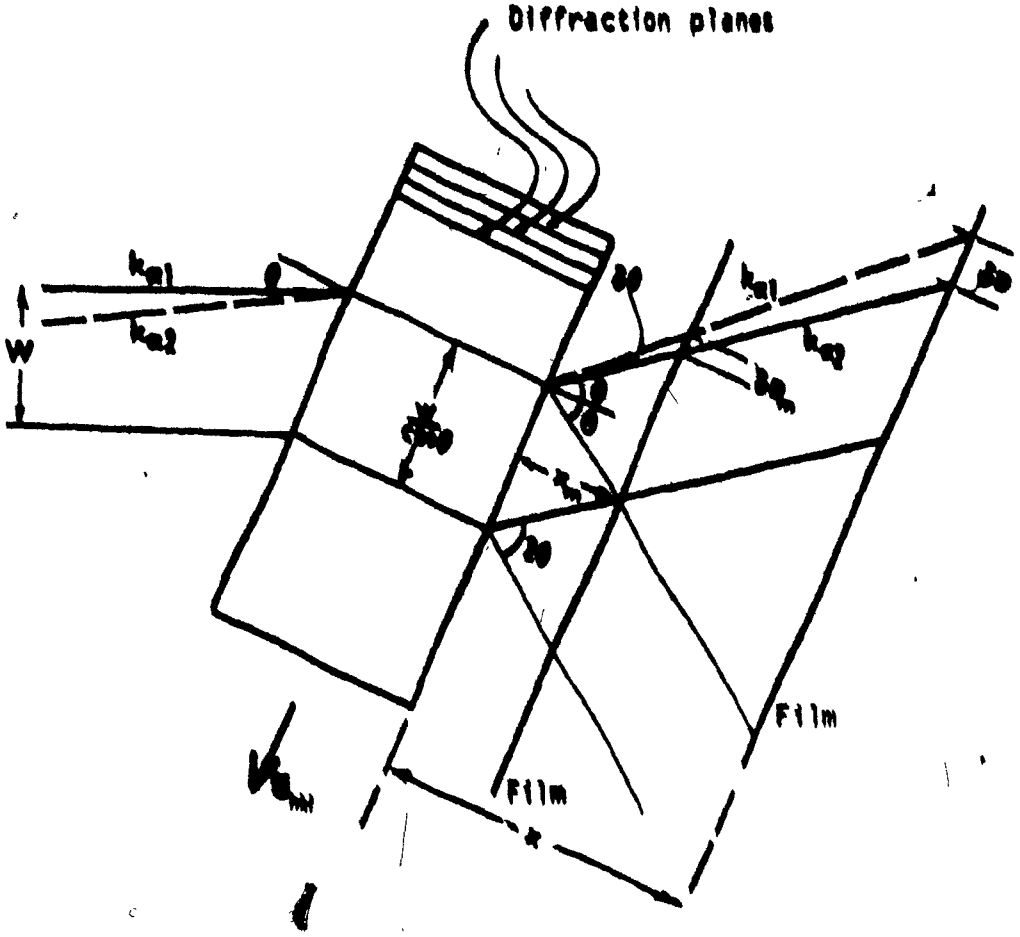

Figure 4.2 Diagram to illustrate calculations of the minimum distance δD_m of $M_0 k_{\alpha 1}$ and k_{m_1} images on the film (After Okkerse and Penning[81]).

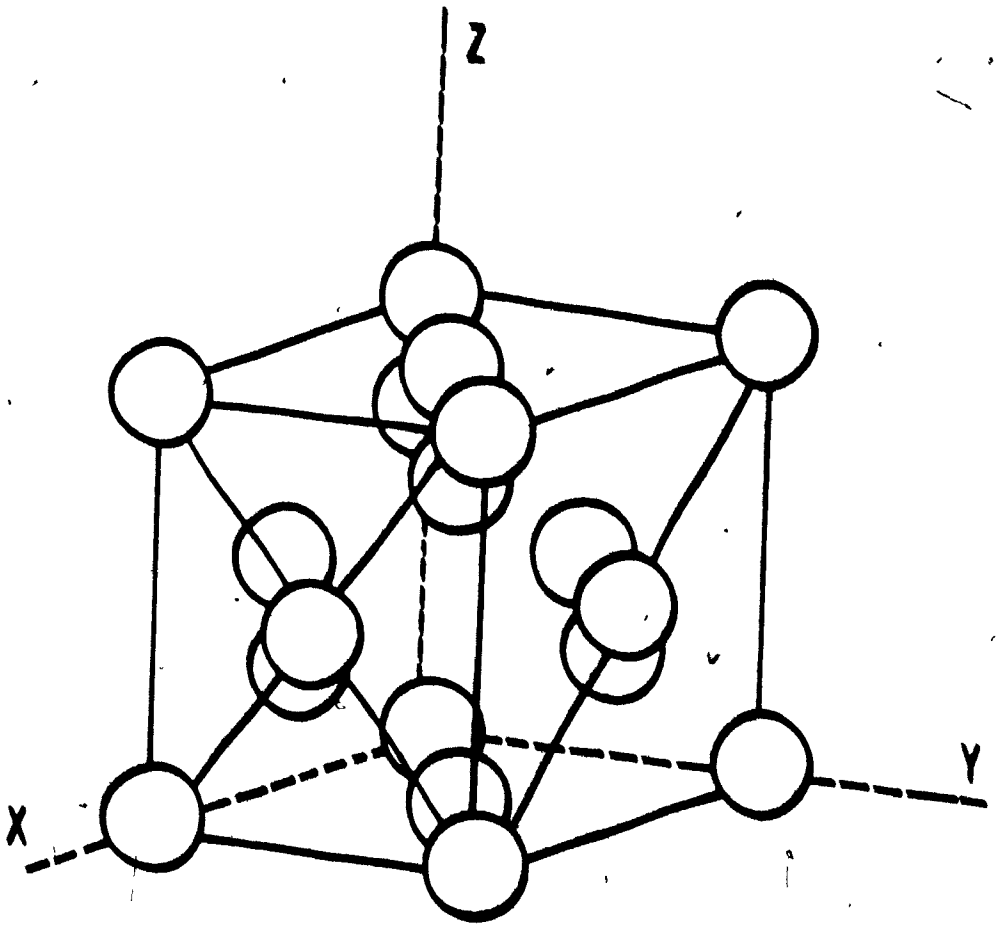

Figure 4.3 Diamond lattice

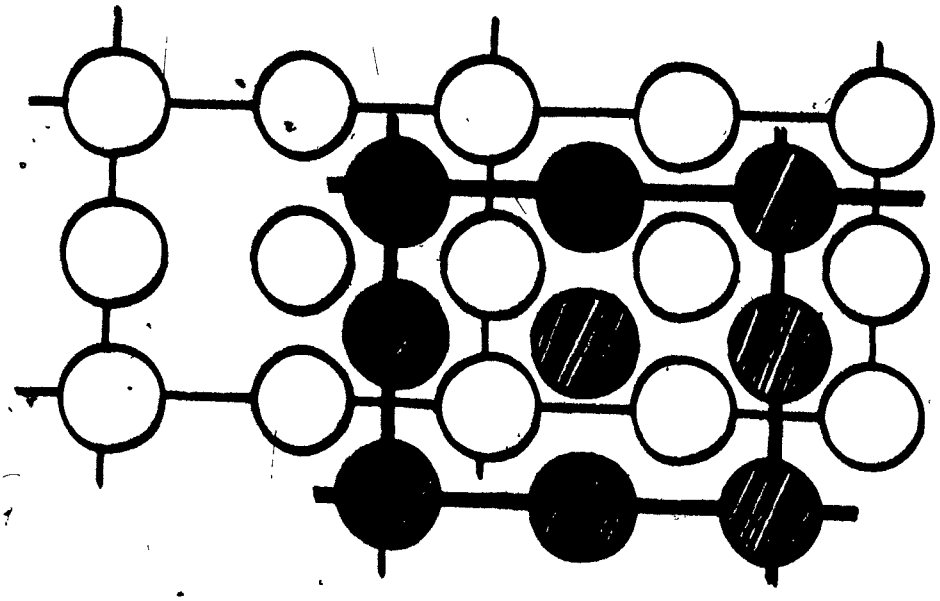

Figure 4.4 Two face centered cubes combined to form a diamond lattice.

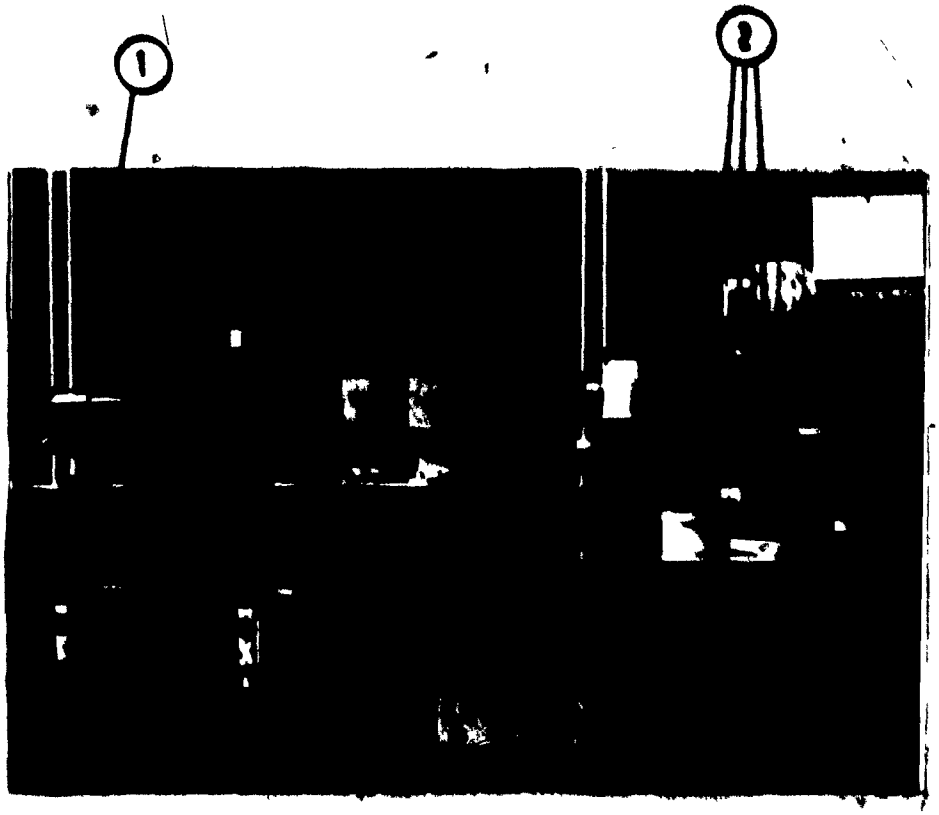

Figure 4.5a

X-ray Lens Camera-arrangement

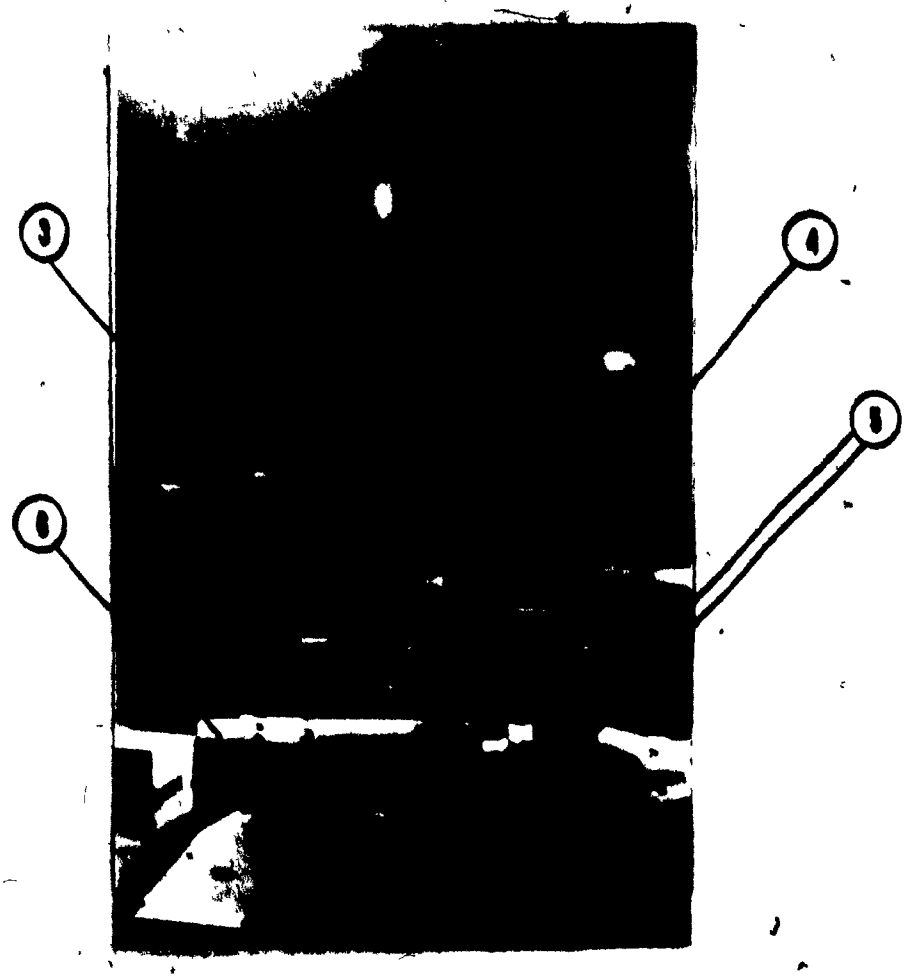

Figure 4.5b

Tensile apparatus and X-ray film positions.

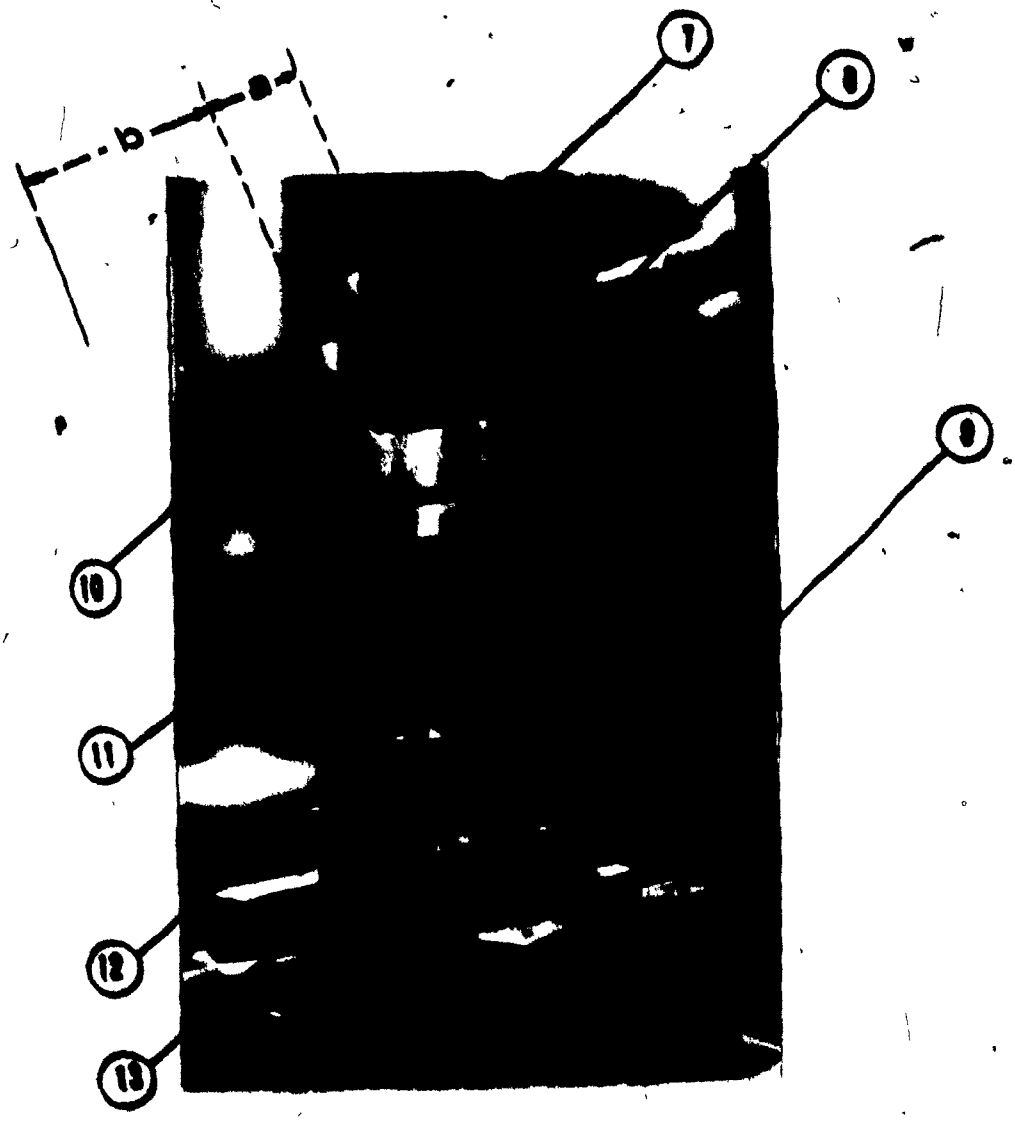

Figure 4.8c

Stress apparatus.

Figure 5.1

Dislocation pattern, 80x, obtained from Silicon single crystal (0.065 mm X 85 mm) using X-ray Lang Camera under external stress 20 kg/cm^2.

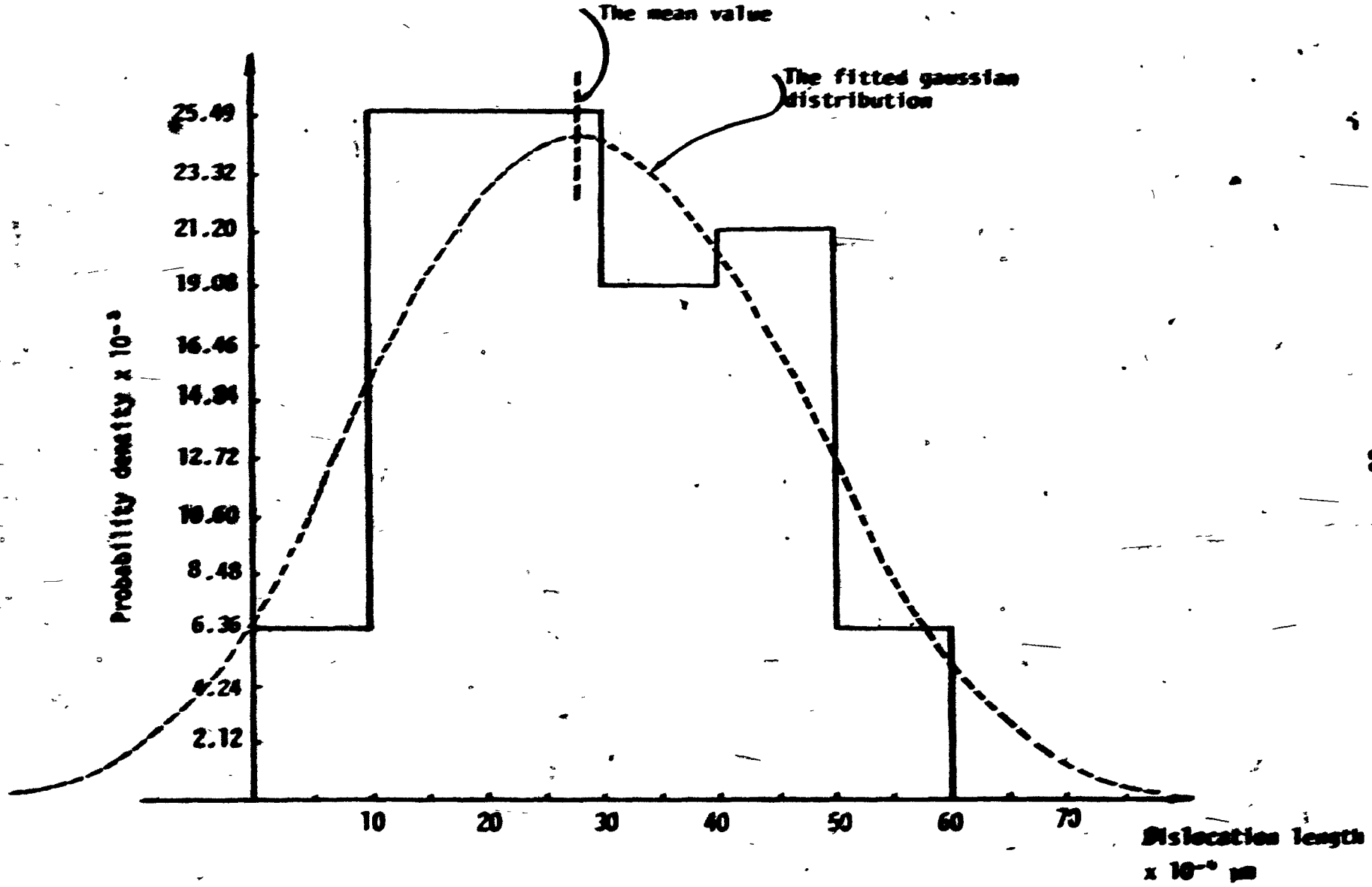

Figure 5.2 Histogram of the dislocation segment's lengths and its fitted gaussian distribution.

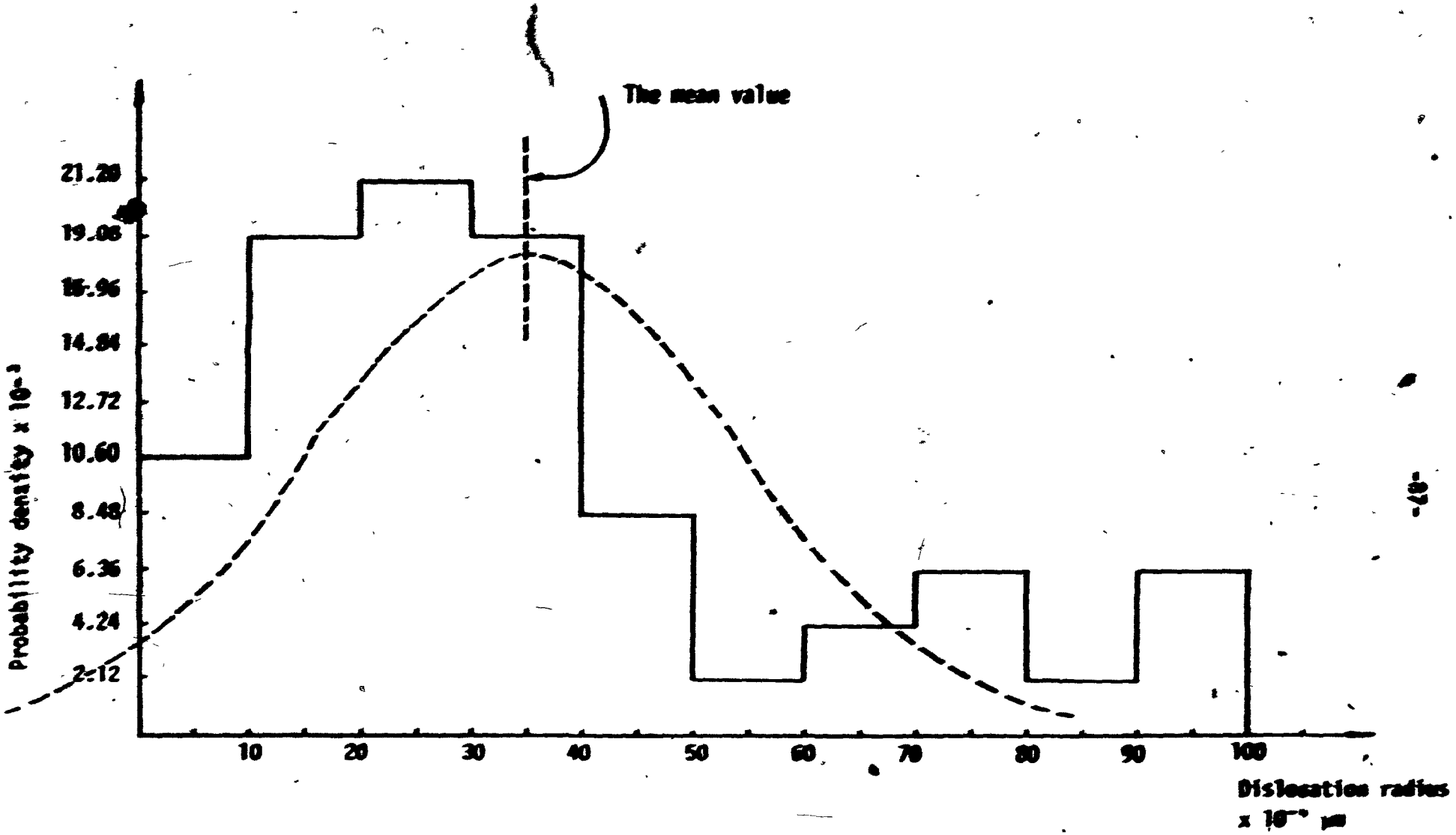

Figure 5.3 Histogram of the dislocation segment's radii and its fitted gaussian distribution.

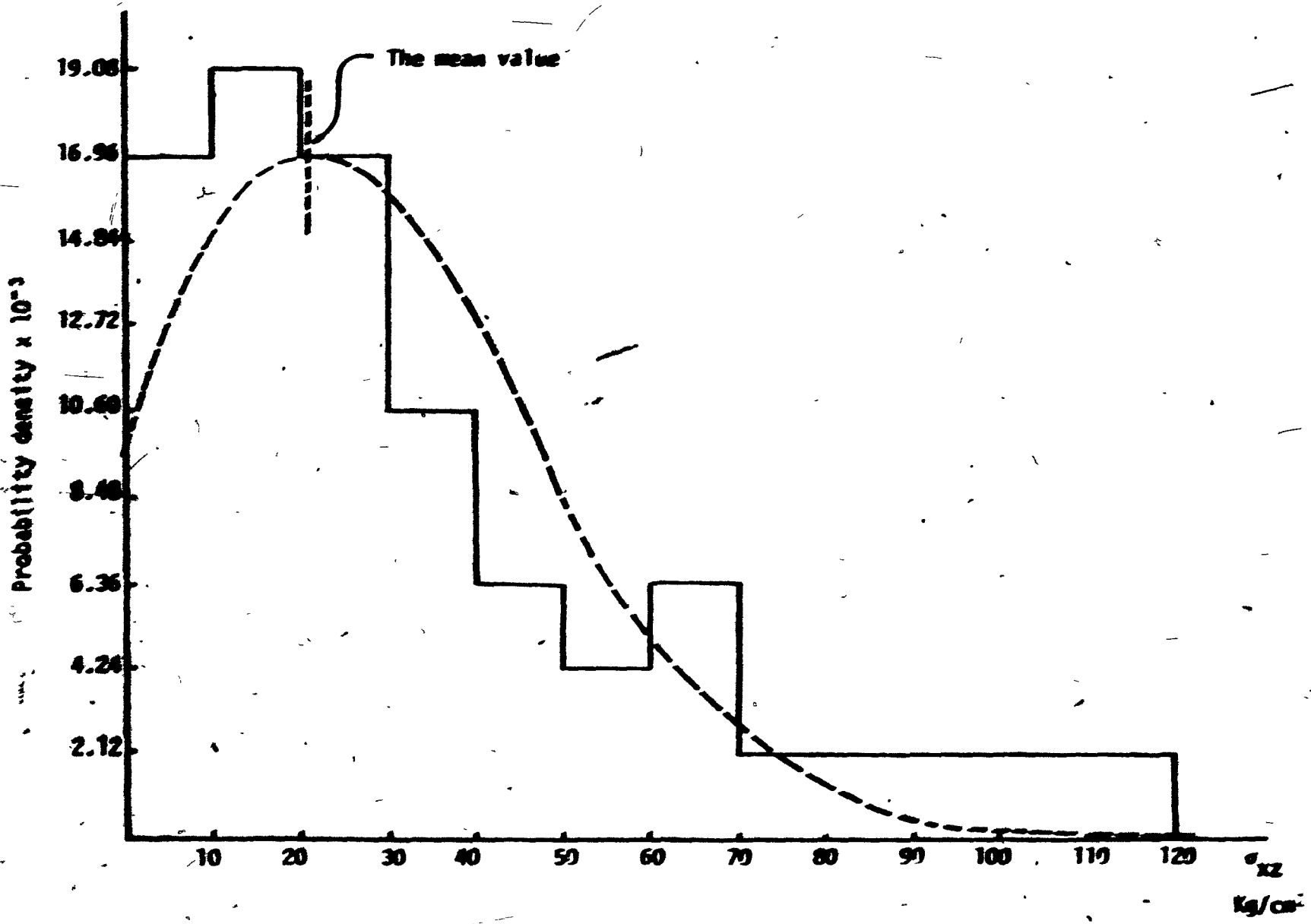

Figure 5.4 Histogram of microstresses σ_{xz} and its fitted gaussian distribution.

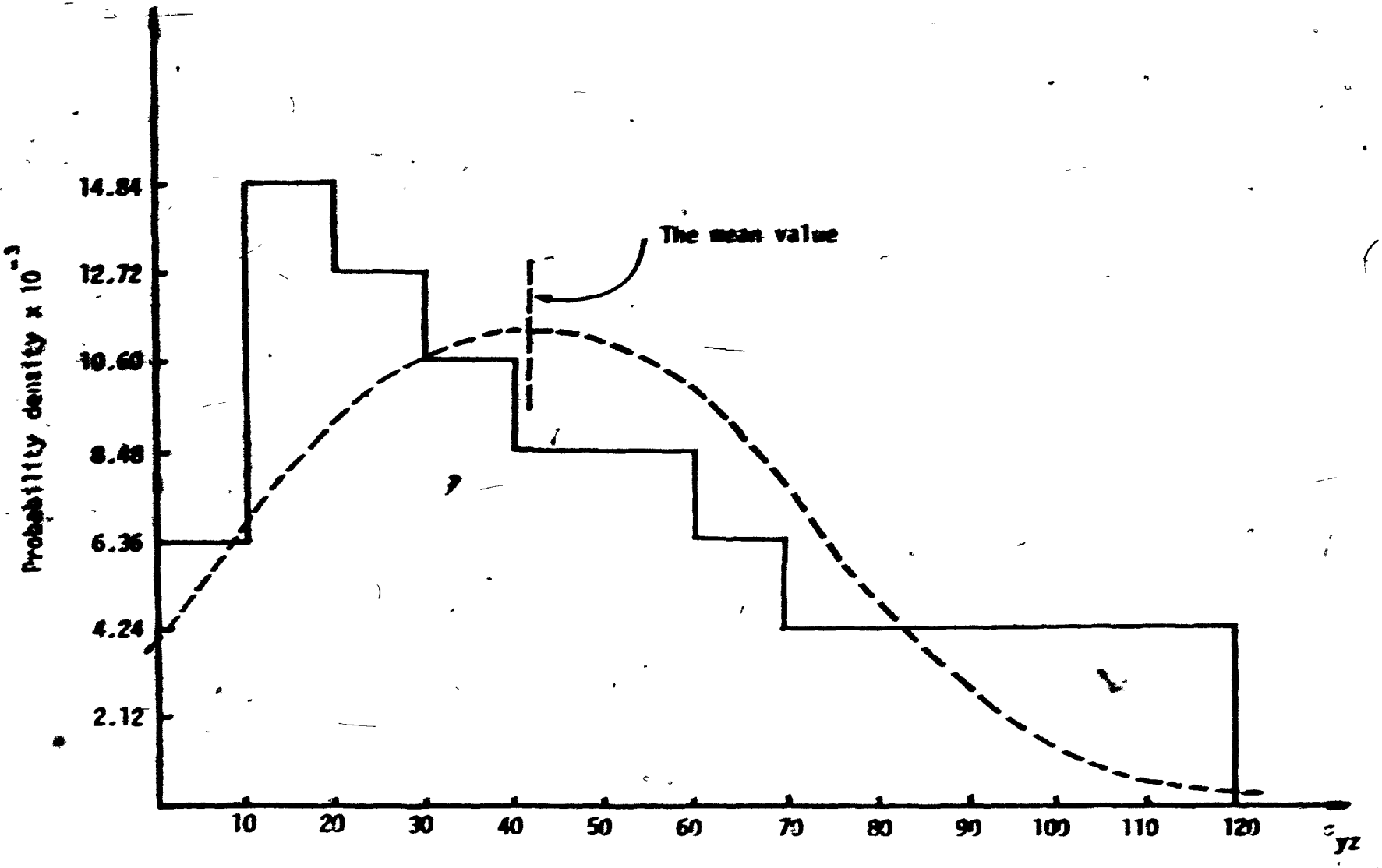

Figure 5.5 Histogram of microstresses σ_{yz} and its fitted gaussian distribution.

APPENDICES

APPENDIX I

BASIC CONCEPTS OF MICROMECHANICS

The first concept of theoretical micromechanics is the existence of three measuring scales for the description of the deformation of a structured medium. The largest region on which all the boundary conditions are assumed to be prescribed is known as the macrodomain, see fig. I-1. The smallest region of interest is referred to as the microelement and designated by its volume ${}^{\alpha}V$ and its surface ${}^{\alpha}S$. It is identified by the superscript α. This corresponds to one individual crystal in the polycrystalline solid. As a first approximation in the analysis of the material response, it is assumed that the constitutive relations of such elements are describable by continuum laws, whilst the stress and displacement fields are either random variables or stochastic processes depending on the medium and the boundary value problem under investigation. The mesodomain is an intermediary scale between the microdomain and the macrodomain and is such that it contains a large number, N, of microelements with $\alpha = 1, 2, \ldots, N$ and hence may be viewed upon analogously to the Gibbsian ensemble of statistical mechanics. Furthermore, a mesodomain is considered to be a physical domain in a macroregion for which the statistics of any random variable or stochastic process may safely be assumed to be spatially homogenous. All parameters relating to the microdomain, mesodomain and macrodomain are prefixed by "micro", "meso" and "macro" respectively.

The second concept of micromechanics involves the geometric description of the deformation kinematics of the microelements and

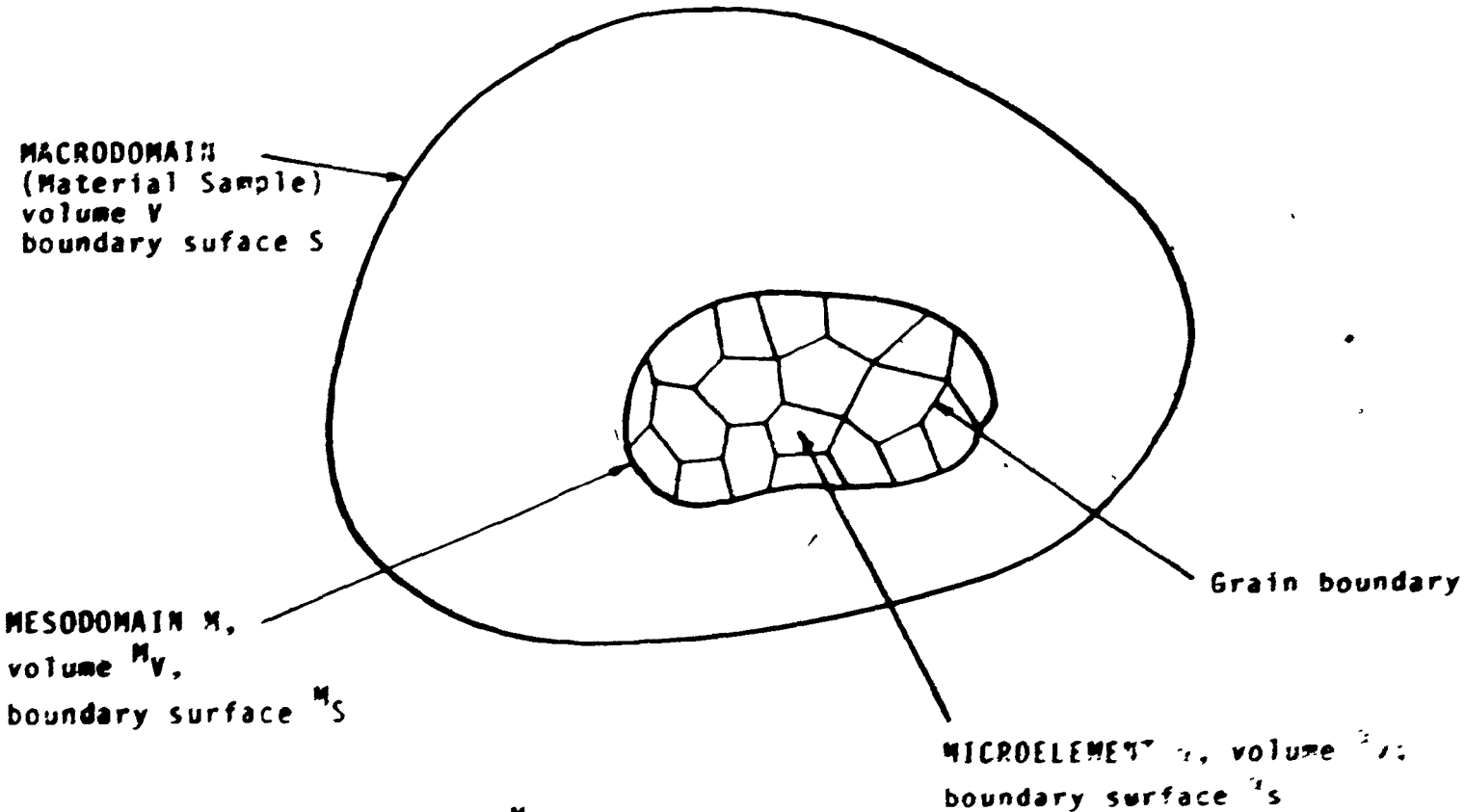

$$V = \bigcup_{M} {}^{M}V$$

$${}^{M_1}V \cap {}^{M_2}V = \emptyset \; ; \; M_1 \neq M_2$$

Figure I.1 Scheratic of a structured redium - The three measuring scales

grain boundaries. The displacement kinematics of the α^{th} crystal are idealized as shown in Fig. I-2, wherein the points interior to the crystal and on the grain boundary are distinguished. Thus, the position vector to any arbitrary point of the α^{th} crystal relative to a fixed Eulerian frame (X^1, X^2, X^3) can be expressed by:

$$^{\alpha}\underset{\sim}{X} = {}^{\alpha}\underset{\approx}{O}\ {}^{\alpha}\underset{\sim}{Y} + {}^{\alpha}\underset{\sim}{R}$$

or the indicial notation as: (I.1)

$$^{\alpha}X_I = {}^{\alpha}O_{IJ}\ {}^{\alpha}Y_J + {}^{\alpha}R_I$$

where $^{\alpha}\underset{\sim}{R}$ is the position vector to the centre of mass of the α^{th} crystal, $^{\alpha}\underset{\approx}{O}$ the orientation of the crystallographic axes of the microelement with respect to the fixed Cartesian frame and $^{\alpha}Y$ the position vector to the point relative to the crystallographic axes. Majuscules represent parameters in the undeformed configuration, while their corresponding minuscules represent their counterparts in the deformed configuration. Cartesian tensor notation is resorted to for clarity. Hence, during and at the end of a random deformation the position vector at $^{\alpha}\underset{\sim}{X}$ may be written as:

$$^{\alpha}\underset{\sim}{x} = {}^{\alpha}\underset{\approx}{o}\ {}^{\alpha}\underset{\sim}{y} + {}^{\alpha}\underset{\sim}{r}$$

or (I.2)

$$^{\alpha}x_i = {}^{\alpha}o_{ij}\ y_j + {}^{\alpha}r_i$$

For the subsequent analysis of grain boundary effects on the deformational behaviour of polycrystalline solid, the arbitrary points internal to the crystal, as indicated above, and the points at the grain boundary are distinguished. Hence, for a surface point (Fig. I.2) the relations (I.1) and (I.2) become:

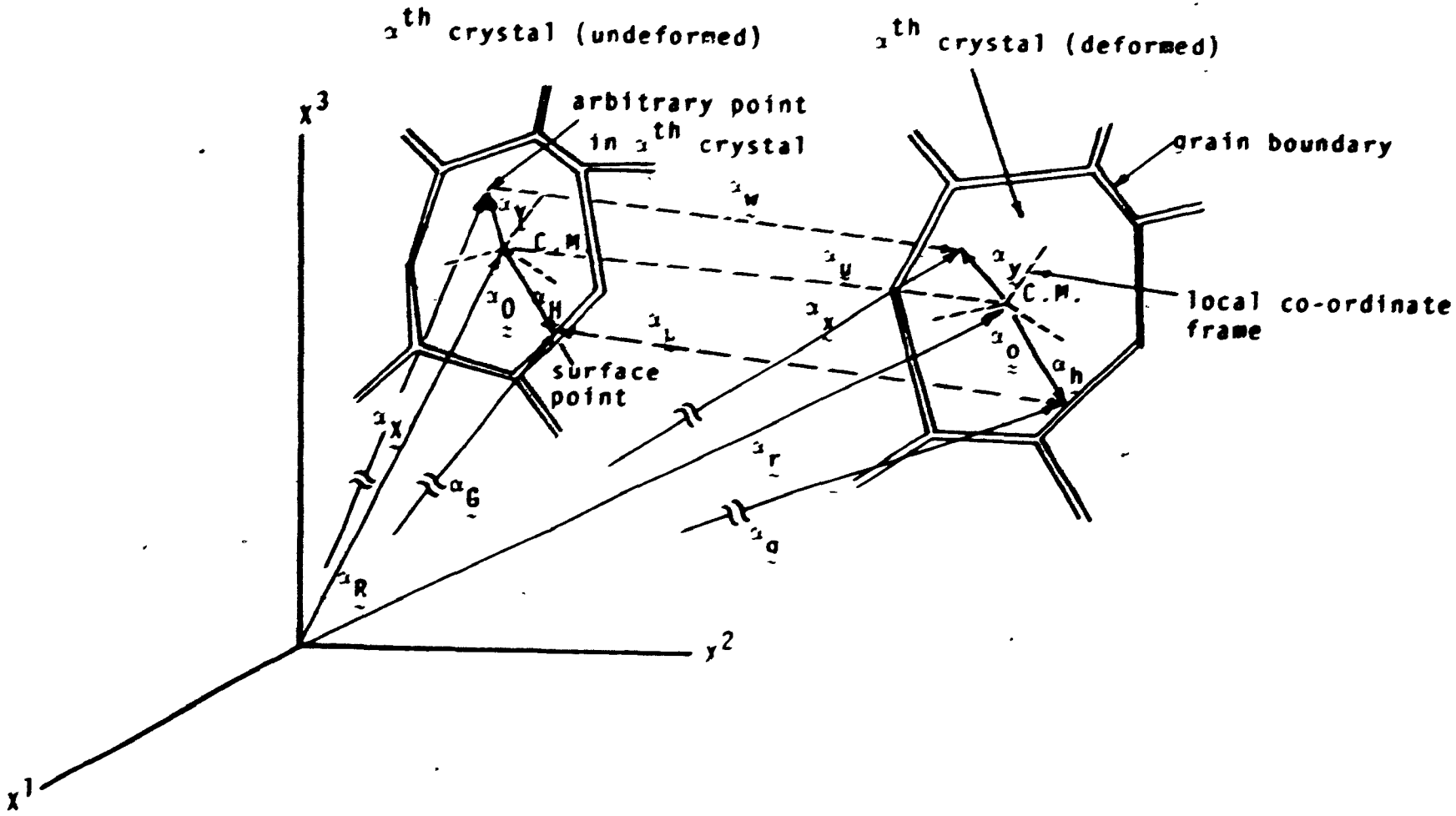

Figure I.2 Idealized model for dissplacement kinematics of α^{th} crystal

$$ {}^{t}\underset{\sim}{G} = {}^{t}\underset{\approx}{Q}\ {}^{t}\underset{\sim}{H} + {}^{t}\underset{\sim}{R} \; ; \quad {}^{t}\underset{\sim}{g} = {}^{t}\underset{\approx}{Q}\ {}^{t}\underset{\sim}{h} + {}^{t}\underset{\sim}{r} \tag{I.3} $$

where ${}^{t}G$, ${}^{t}H$ and ${}^{t}g$, ${}^{t}h$ are the position vectors of this point in the undeformed and deformed states, respectively. By means of the above relations the random deformation for the centre of mass of a grain will be given by:

$$ {}^{t}\underset{\sim}{u} = {}^{t}\underset{\sim}{r} - {}^{t}\underset{\sim}{R} \tag{I.4} $$

and for an arbitrary point inside the grain by:

$$ {}^{t}\underset{\sim}{w} = {}^{t}\underset{\sim}{x} - {}^{t}\underset{\sim}{X} = {}^{t}\underset{\approx}{Q}\ {}^{t}\underset{\sim}{y} - {}^{t}\underset{\approx}{Q}\ {}^{t}\underset{\sim}{Y} + {}^{t}\underset{\sim}{u} \tag{I.5} $$

Analogously, the deformation at the surface of the grain is given by:

$$ {}^{t}\underset{\sim}{v} = {}^{t}\underset{\sim}{g} - {}^{t}\underset{\sim}{G} = {}^{t}\underset{\approx}{Q}\ {}^{t}\underset{\sim}{h} - {}^{t}\underset{\approx}{Q}\ {}^{t}\underset{\sim}{H} + {}^{t}\underset{\sim}{u} \tag{I.6} $$

Hence the distance vector, $\underset{\sim}{\lambda}$, between the centre of mass of any contiguous grains α and β is:

$$ \underset{\sim}{\lambda} = {}^{t}\underset{\sim}{R} - {}^{t}\underset{\sim}{R} \tag{I.7} $$

and constitutes a significant correlation parameter as discussed later.

The idealized deformation kinematics of the grain boundary is as shown in Fig. I.3 with the relations defined relative to the surface co-ordinates (Fig.I-4)

$ {}^{t}\underset{\sim}{\zeta} : \ {}^{t}\underset{\sim}{\zeta}_j \quad (j = 1,2,3)$ given by:

$$ {}^{t}\underset{\sim}{\zeta}_1 = {}^{t}\underset{\sim}{n} \times {}^{\alpha\beta}\underset{\sim}{\lambda} \; ; \quad {}^{t}\underset{\sim}{\zeta}_2 = {}^{t}\underset{\sim}{n} \; ; \quad {}^{t}\underset{\sim}{\zeta}_3 = {}^{\alpha\beta}\underset{\sim}{\lambda} \tag{I.8} $$

In equation (I.8) ${}^{t}\underset{\sim}{n}$ is the normal vector to the boundary plane and ${}^{\alpha\beta}\underset{\sim}{\lambda}$ is the eigenvector about which a mismatch rotation of θ superimposes the local ${}^{\beta}\underset{\sim}{\gamma}$ axes on the ${}^{\alpha}\underset{\sim}{\gamma}$ axes (Fig.I.5). ${}^{\alpha\beta}\underset{\sim}{\Lambda}$, called

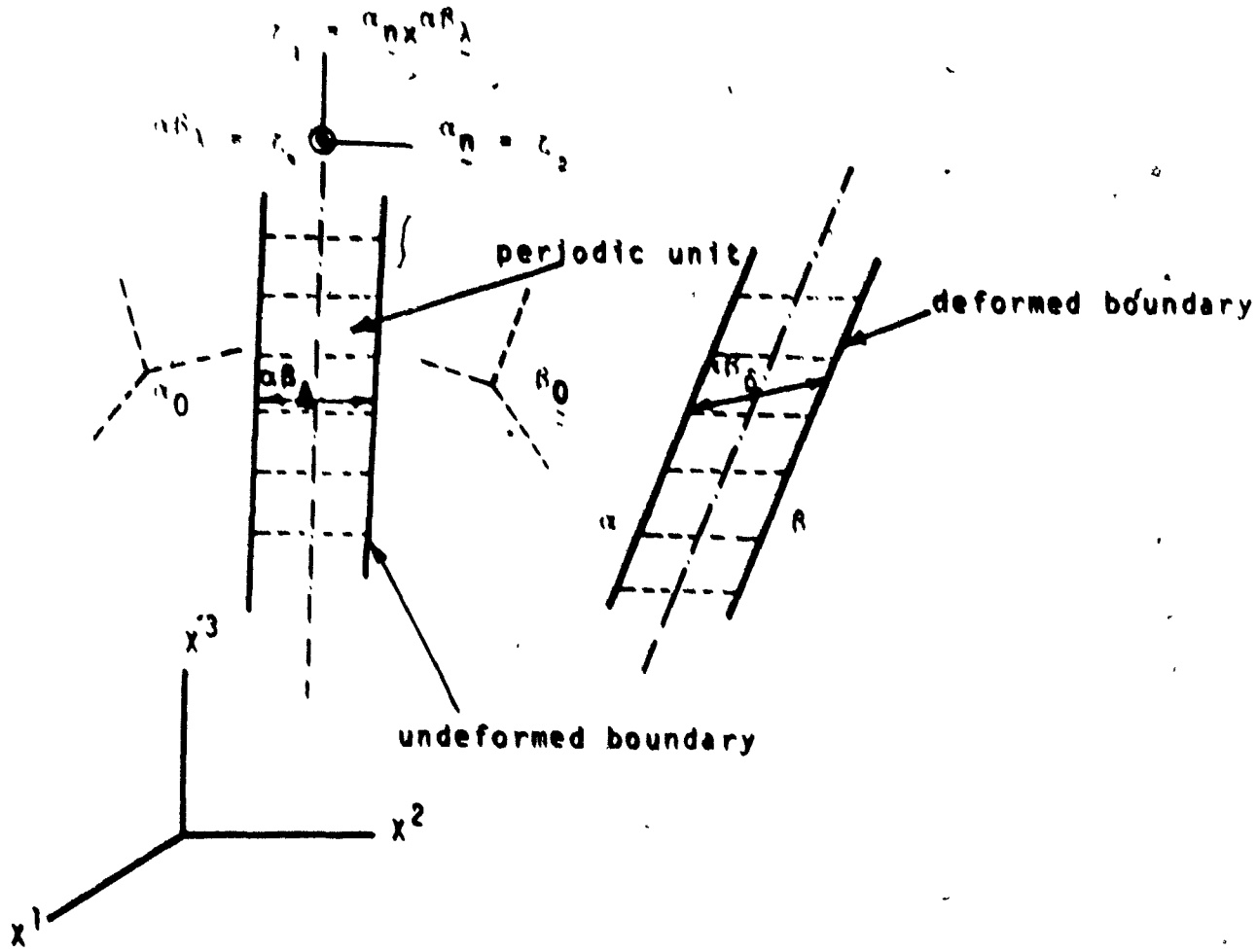

Figure I.3. Idealized grain boundary displacement kinematics

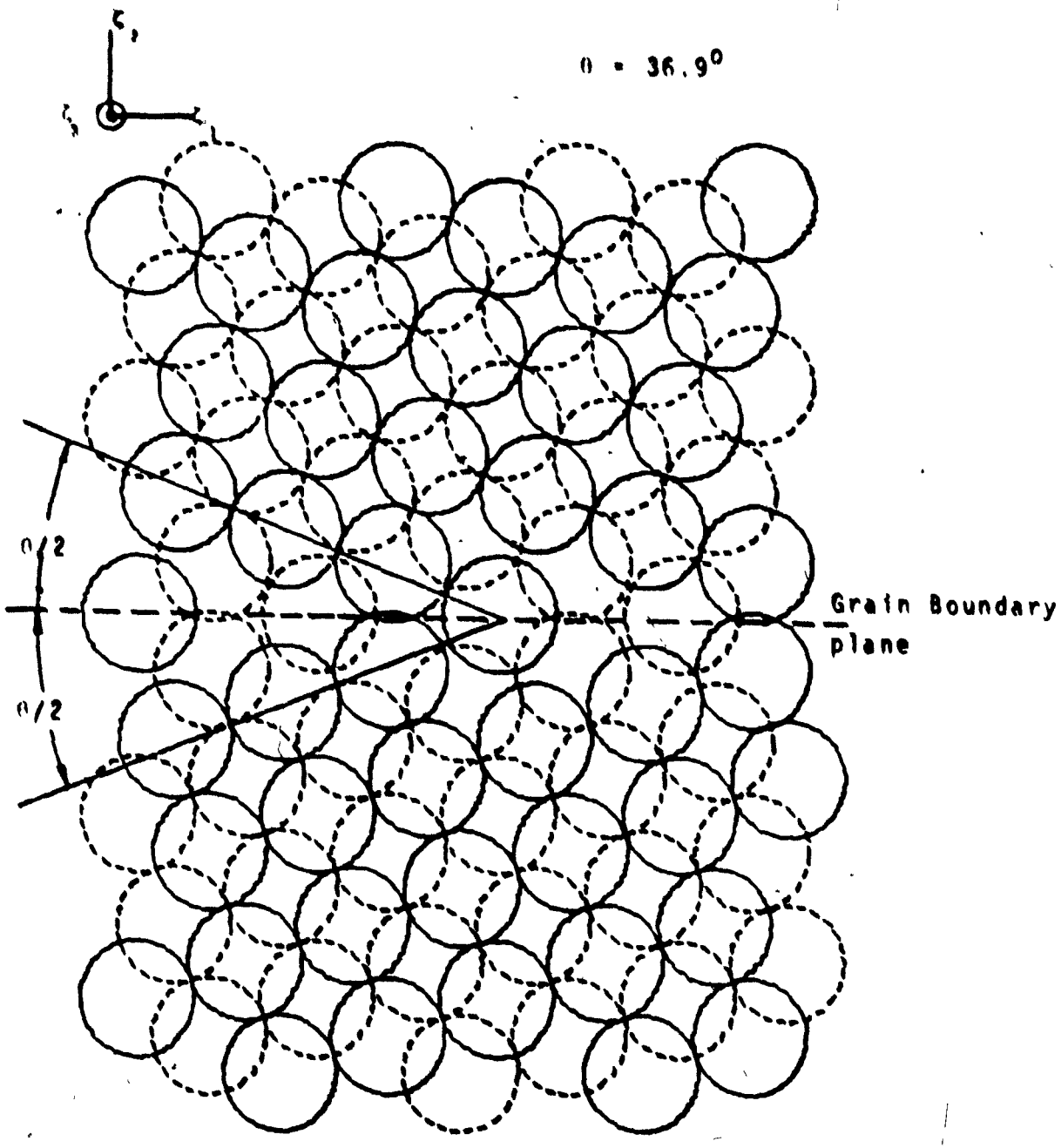

Figure I.4 Symmetric tilt copper boundary formed by a rotation of two crystals by 36.9° about $^{\alpha\beta}\lambda$ = [001] axis. Solid circles represent one (001) plane while dashed circles represent the other (001) plane. Solid line below the figure represents the periodicity along the ζ_1 direction.

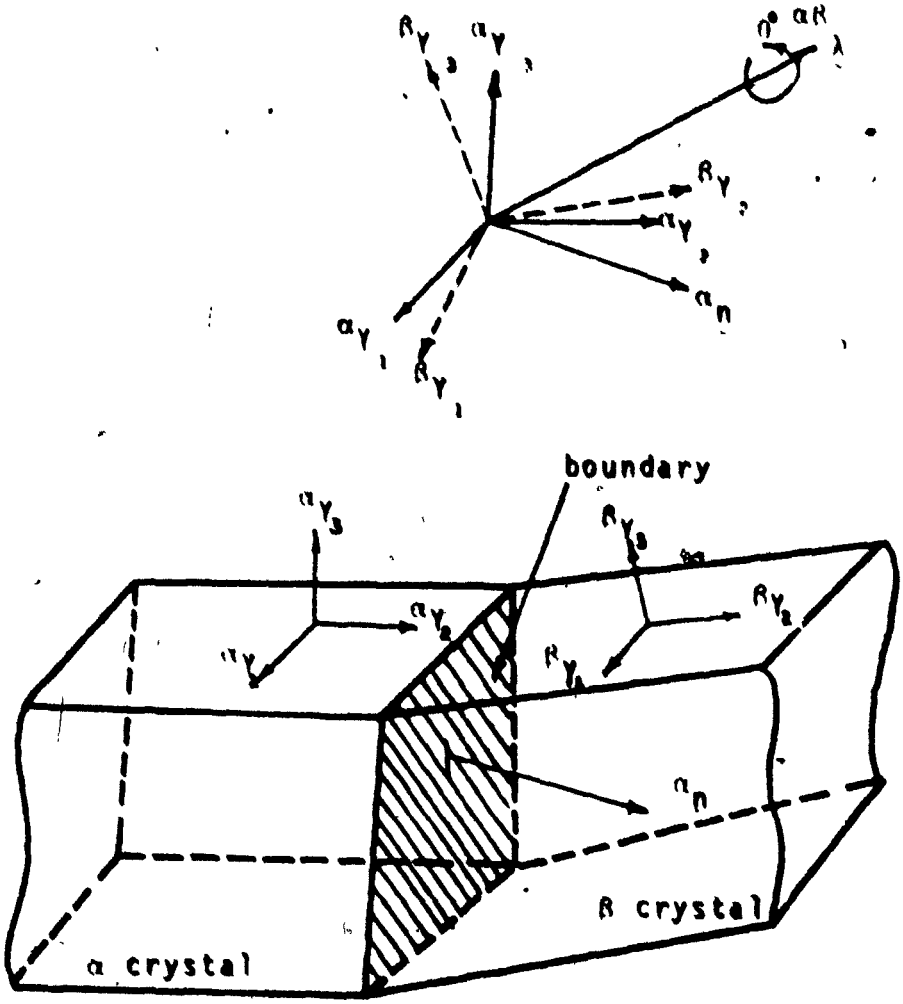

Figure I.5 ϕ General description of a bicrystal showing the five degrees of freedom

the "calculation zone", is the undeformed distance between the crystalline lattice of each adjacent crystal beyond which the conditions of the atoms are those of the perfect crystal lattice. It may be expressed as:

$$ {}^{\alpha\beta}\underset{\sim}{\Lambda} = {}^{\beta}\underset{\sim}{G} - {}^{\alpha}\underset{\sim}{G} = {}^{\beta}\underset{\approx}{0}\ {}^{\beta}\underset{\sim}{H} - {}^{\alpha}\underset{\approx}{0}\ {}^{\alpha}\underset{\sim}{H} + {}^{\beta}\underset{\sim}{R} - {}^{\alpha}\underset{\sim}{R} \qquad (I.9) $$

and in the deformed state, this distance becomes:

$$ {}^{\alpha\beta}\underset{\sim}{\delta} = {}^{\beta}\underset{\sim}{g} - {}^{\alpha}\underset{\sim}{g} = {}^{\beta}\underset{\approx}{0}\ {}^{\beta}\underset{\sim}{h} - {}^{\alpha}\underset{\approx}{0}\ {}^{\alpha}\underset{\sim}{h} + {}^{\beta}\underset{\sim}{r} - {}^{\alpha}\underset{\sim}{r} \qquad (I.10) $$

so that the stochastic relative displacement is:

$$ {}^{\alpha\beta}\underset{\sim}{d} = {}^{\alpha\beta}\underset{\sim}{\delta} - {}^{\alpha\beta}\underset{\sim}{\Lambda} \qquad (I.11) $$

The above geometric and physical parameters form the basic quantities utilized in the description of the response behaviour of crystalline solid. Given that each grain can be considered as an elastic continuum, conventional kinematic quantities such as "micro-strain" can readily be formulated. Thus for instance a "primitive strain measure" in terms of the microdeformation gradient will be as follows:

$$ {}^{\alpha}\underset{\approx}{F} = \frac{\partial {}^{\alpha}\underset{\sim}{Y}}{\partial {}^{\alpha}\underset{\sim}{Y}} \quad ; \quad {}^{\alpha}\underset{\approx}{f} = \frac{\partial {}^{\alpha}\underset{\sim}{Y}}{\partial {}^{\alpha}\underset{\sim}{y}} \qquad (I.12) $$

from which a micro-Langrangian or Eulerian strain can be defined as follows:

$$ 2\,{}^{\alpha}\underset{\approx}{E} = {}^{\alpha}\underset{\approx}{F}^{c} \cdot {}^{\alpha}\underset{\approx}{F} - \underset{\approx}{\delta} \quad ; \quad 2\,{}^{\alpha}\underset{\approx}{e} = \underset{\approx}{\delta} - {}^{\alpha}\underset{\approx}{f}^{c} \cdot {}^{\alpha}\underset{\approx}{f} \qquad (I.13) $$

where the superscript "c" on ${}^{\alpha}\underset{\approx}{F}$ or ${}^{\alpha}\underset{\approx}{f}$ indicates the dyadic conjugate and $\underset{\approx}{\delta}$ is the Kronecker Delta. The above forms are oversimplifications and overlook the influence of the grain boundaries and dislocations in the crystals. Incorporating such effects leads by necessity to

a more complex formulation of the response behaviour. Within the framework of micromechanics, taking into consideration these effects, the above kinematic parameters can be employed to define the linear "microstrains" within the crystal and at the grain boundary, respectively. These linear microstrains within the crystal and at the grain boundary calculation zone of two abutting crystals are expressed as follows:

$$ {}^{\alpha}\underset{\sim}{e} \; : \; {}^{\alpha}e_{ij} = \frac{1}{2} \left({}^{\alpha}w_{i,j} + {}^{\alpha}w_{j,i} \right) \qquad (I.14) $$

and:

$$ {}^{\alpha\beta}\underset{\sim}{e} \; : \; {}^{\alpha\beta}e_{ac} = \frac{1}{2} \left({}^{\alpha\beta}d_{a,c} + {}^{\alpha\beta}d_{c,a} \right) \qquad (I.15) $$

in which $\underset{\sim}{w}$ and $\underset{\sim}{d}$ are defined in (I.15) and (I.11), respectively. With the grain boundary surface co-ordinate system as defined in equation (I.8) the grain boundary displacements and strains become:

$$ {}^{\alpha\beta}\underset{\sim}{\Delta} = (0, \; \Delta, \; 0) \; ; \quad {}^{\alpha\beta}\underset{\sim}{\delta} = ({}^{\alpha\beta}d_1, \; {}^{\alpha\beta}d_2 + \Delta, \; {}^{\alpha\beta}d_3) $$

$$ {}^{\alpha\beta}\underset{\sim}{d} = ({}^{\alpha\beta}d_1, \; {}^{\alpha\beta}d_2, \; {}^{\alpha\beta}d_3) $$

$$ {}^{\alpha\beta}\underset{\sim}{e} = \frac{1}{2\Delta} \begin{pmatrix} 0 & {}^{\alpha\beta}d_1 & 0 \\ {}^{\alpha\beta}d_1 & 2\,{}^{\alpha\beta}d_2 & {}^{\alpha\beta}d_3 \\ 0 & {}^{\alpha\beta}d_3 & 0 \end{pmatrix} \qquad (I.16) $$

The third concept of the micromechanical theory involves the notion of a "material functional" or material operator which is

characteristic for a specific medium and which contains geometrical and thermomechanical parameters or functions of such parameters. The material functional takes the place of the familiar fourth-order material tensor relating the stress to the strain using a continuum model. It can be written as a characteristic energy functional in terms of the significant variables in the following manner:

$$\overset{M}{\mathcal{M}} = \overset{M}{\mathcal{M}}(\underset{\sim}{E}, \underset{\sim}{a}, \rho_d, \Psi, {}^{(1)}\underset{\approx}{0}, {}^{(1)}\underset{\sim}{0}, {}^{(1)}\nu ; T,t) \qquad (I.17)$$

where the full meaning of these parameters, characteristic for a polycrystalline solid are explained in ref. [1-6].

Finally the last concept of the micromechanical theory is that the theory is based on the mathematical theory of probability and statistical mechanics. This is inevitable due to the inherently random geometric and physical properties of a real material as pointed out earlier. The characteristic quantities involved in the analysis are therefore random variables or random functions of such variables and time. Hence the deformation process of the polycrystalline material is seen as a stochastic process. For the determination of the kinematic parameters and the material characteristics involved, mathematical expectations and second moments can be used. Some of the parameters are experimentally obtainable from crystallographic studies in the form of distributions. The Micromechanics theory hypothesised from the beginning that these distributions were Gaussian or nearly Gaussian, statistically homogenous and non-isotropic so that an approximation to a more rigorous correlation theory could be employed. Confirmation of the above hypothesis has been afforded by the experimental work of

Kalousek [87] involving combined holographic interferometry and X-ray diffraction studies of the distributions of the displacements and rotations of aluminium crystals embedded in an epoxy resin matrix under a tensile load.

APPENDIX II

THE EFFECT OF DISLOCATIONS ON THE LINEAR RESPONSE OF ELASTIC HETEROGENEOUS SOLIDS

For the simple case of the linear elastic response of polycrystalline solids taking into consideration the presence of mobile internal dislocations in the crystal, the stress ${}^{\alpha}\sigma_{ij}$, defined in the Cauchy sense, and internal strain ${}^{\alpha}e_{ij}$ (equation (I.14), relation for the α-th crystal has been approximated [37] in the following manner:

$$ {}^{\alpha}\sigma_{ij} = {}^{\alpha}D_{ijkl} \; {}^{\alpha}e_{kl} \tag{II.1} $$

$$ {}^{\alpha}D_{ijkl} = {}^{\alpha}E_{ijkl} + \eta \; {}^{\alpha}\Gamma_{ijkl} \tag{II.2} $$

in which ${}^{\alpha}D_{ijkl}$ is a fourth order tensor comprising of the elastic modulus E_{ijkl} of the single crystal and the dislocation effect $\eta \; {}^{\alpha}\Gamma_{ijkl}$.

$$ \underline{E} : E_{ijkl} = \frac{2G\nu}{(1-2\nu)} \delta_{ij}\delta_{kl} + 2G\delta_{ik}\delta_{jl} $$

$$ \eta = \frac{2}{3\pi} G (1-\nu) \ell^2 \alpha\rho_d \tag{II.3} $$

$$ {}^{\alpha}\underline{\Gamma} : {}^{\alpha}\Gamma_{ijkl} = {}^{\alpha}O_{3i} \; {}^{\alpha}O_{2j} \; {}^{\alpha}O_{3k} \; {}^{\alpha}O_{2l} $$

where G is the pure crystalline material's shear modulus, ν its Poisson's ratio, ℓ a characteristic length between pinning points of an edge dislocation acting on a slip plane, whose normal has direction cosines ${}^{\alpha}O_{3i}$, in the direction described by the cosines ${}^{\alpha}O_{2j}$, both with respect to the external coordinate frame, and finally where $\alpha\rho_d$ is the mobile

dislocation density. The quantity Γ is a fourth order tensor representing the orientation of the slip planes and direction of action of the inactivated Frank-Read sources.

The above random quantities were considered in terms of their first and second moments leading to the expression:

$$\langle \xi \rangle = \underline{E}\,\underline{\varepsilon} + n\underline{\Gamma}\langle \underline{e} \rangle + nV_{\Gamma e} \qquad (II.4)$$

where $\langle \xi \rangle$ is the mean stress and $\langle e \rangle$ the mean strain, whilst V represents the variance of the parameter indicated by the subscripts. $\underline{\lambda}$ being the distance between any two contiguous grains α and β (equation I.7)) is used as a correlation parameter to define the cross variance of the stress distribution $R_{\xi}(\underline{\lambda})$ and variance, V_{ξ} in terms of the corresponding statistics in the strain space so that:

$$\begin{aligned} R_{\xi}(\underline{\lambda}) = {} & (\underline{E} + n\langle \underline{\Gamma} \rangle)(\underline{E} + n\langle \underline{\Gamma} \rangle)^{T} R_{e}(\underline{\lambda}) \\ & n^{2} R_{\Gamma}(\underline{\lambda}) \langle \underline{e} \rangle \langle \underline{e} \rangle^{T} \\ & 2n(\underline{E} + n\langle \underline{\Gamma} \rangle) \langle \underline{e} \rangle^{T} R_{e\Gamma}(\underline{\lambda}) \\ & -n^{2} R_{e\Gamma}(\underline{\lambda}) R^{T}_{e\Gamma}(\underline{\lambda}) + 2n\underline{E}\, R_{ee\Gamma}(\underline{\lambda}) \\ & + n^{2}\langle \underline{e} \rangle R_{e\Gamma\Gamma}(\underline{\lambda}) + n^{2} R_{ee\Gamma\Gamma}(\underline{\lambda}) \end{aligned} \qquad (II.5)$$

and:

$$V_{\xi} = R_{\xi}(0) \qquad (II.6)$$

The above brief outline of the micromechanical theory as applied to a polycrystalline solid is seen to take into consideration the presence of dislocations internal to the crystal, which become mobile on application of a load.

This is formulated by the last two expressions in equation (II.4) which if the dislocation term is omitted leads to the familiar stress-strain relationship conventionally obtained from a continuum model.

APPENDIX III

ENERGY OF INTERACTION BETWEEN TWO DISLOCATION LOOPS

The interaction energy between two loops, fig 2.4, from equation (2.14) is,

$$W_1 = \int_{A_1} dA_{1\beta} \; b_{1\alpha} \; \sigma_{2\alpha\beta}$$

Substituting the value of $\sigma_{2\alpha\beta}$ from equation (2.15) into equation (2.14), one finds:

$$W_1 = -\frac{\mu}{8\pi} \int_{A_1} \int_{C} dA_{1\beta} \; dx_{2\beta} \; b_{1\alpha} \; b_{2m} \; \epsilon_{im\alpha} \; \frac{\partial}{\partial X_i} \; \nabla^2 R \; +$$

$$\frac{\mu}{8\pi} \int_{A_1} \int_{C} dA_{1\beta} \; dx_{2\alpha} \; b_{1\alpha} \; b_{2m} \; \epsilon_{im\beta} \; \frac{\partial}{\partial X_i} \; \nabla^2 R \; +$$

$$\frac{\mu}{4\pi(1-\nu)} \int_{A_1} \int_{C} dA_{1\beta} \; dx_{2\beta} \; b_{1\alpha} \; b_{2m} \; \epsilon_{imk} \; \frac{\partial^3 R}{\partial X_i \; \partial X_\alpha \; \partial X_\beta} \; -$$

$$\frac{\mu}{4\pi(1-\nu)} \int_{A_1} \int_{C} dA_{1\beta} \; dx_{2K} \; b_{1\alpha} \; b_{2m} \; \epsilon_{imk} \; \delta_{\alpha\beta} \; \frac{\partial}{\partial X_i} \; \nabla^2 R$$

(III.1)

By using Stokes' theorem and the relation;

$$(b_1 \times b_2) \cdot (dl_1 \times dl_2) = (b_1 \cdot dl_1)(b_2 \cdot dl_2) -$$

$$(b_2 \cdot dl_1)(b_1 \cdot dl_2)$$

for every part in equation (III.1), then it yields equation (2.16) where all the terms are described in section 3 of Chapter 2.

APPENDIX IV

SELF-STRESS OF A CURVED DISLOCATION

Consider a material of infinite extent and suppose that a closed loop C of Burgers vector $\underline{b}$ is created, fig. IV.1, some displacement $\underline{U}(r)$ at r will appear due to the creation of the dislocation. If a point force F acts at r while the dislocation is created, it does work;

$$W = F \quad U(r) = F_m U_m(r) \tag{IV.1}$$

where F_m and U_m are components of F and U respectively.

If the displacement relieve the point force, they decrease the energy of the mechanism producing the point force by an amount W, the interaction energy. Then the total energy contributed by the external mechanism producing the surface displacements and the point force equals the elastic energy of the self-stress field of the loop, then;

$$W = -\int_A dA_j \; b_i \; F_m \; \sigma_{ijm}(\bar{r} - r) \tag{IV.2}$$

Where $F_m \sigma_{ijm}(\bar{r} - r)$ is the stress σ_{ij} at $\bar{r}$ caused by the components F_m of a point force F at r. The b_i are the components of b, dA_j are the components of dA, etc.

Since the tensor green's function for the elastic displacement is

$$U_{ij}(r) = \frac{1}{8\pi\mu} \left(\delta_{ij} \; \nabla^2 r - \frac{\lambda + \mu}{\lambda + 2\mu} \; \frac{\partial^2}{\partial X_i \partial X_j}\right) \tag{IV.3}$$

Then equation (IV.2) can be written as:

$$W = -\int_A dA_j \; b_i \; C_{ijkl} \; \frac{\partial}{\partial X_l} \; F_m \; U_{mk}(\bar{r} - r) \tag{IV.4}$$

equating equations (IV.1) and (IV.5), one can get;

$$U_m(r) = -\int_A dA_j \; b_i \; C_{ijkl} \; \frac{\partial}{\partial X_l} \; U_{mk}(r' - r) \qquad (IV.5)$$

With the use of the fact that

$$C_{ijkl} = \mu (\delta_{ik} \; \delta_{jl} + \delta_{il} \; \delta_{jk}) + \lambda \; \delta_{ij} \; \delta_{kl} \qquad (IV.6)$$

Then, equation (IV.5) can be written, in a more extend form as;

$$U_m(r) = -\lambda \int_A dA_j \; b_j \; \frac{\partial U_{mk}}{\partial X_k} - \mu \int_A dA_j \; b_i \; \frac{\partial U_{mi}}{\partial X_j} -$$

$$\mu \int_A dA_j \; b_i \; \frac{\partial U_{mj}}{\partial X_i} \qquad (IV.7)$$

Since the stress can be expressed as,

$$\sigma_{\alpha\beta} = [\lambda \; \delta_{\alpha\beta} \; \delta_{m\ell} + \mu (\delta_{\alpha\ell} \; \delta_{\beta m} + \delta_{\alpha m} \; \delta_{\beta\ell}) \frac{dU_m}{\partial X_\ell}] \qquad (IV.8)$$

Then, from equations (IV.7) and (IV.8) and following the procedure of deWit [88], Peach and Koehler [20] derived equation (2.15) which enables one to determine the stress field of an arbitrarily curved dislocation by line integration.

APPENDIX V

(A)

```
C     THIS PROGRAM CALCULATES THE MEAN RADIUS OF CIRCULAR CURVATURE
C     OF A SERIES OF ARCS AND CALCULATES ALL RADII.  THE COMPUTATION
C     METHOD USED OBTAINS THE INTERSECTION COORDINATES OF THE TWO
C     PERPENDICULAR BISECTORS OF ADJACENT CHORDS OF THE ARC.  THESE
C     CHORDS ARE GIVEN AS THE COORDINATES OF 3 SUCCESSIVE POINTS ALONG
C     THE ARC.  ALL COMBINATIONS OF SUCCESSIVE CHORD PAIRS ARE USED
C     AND N-2 RADII ARE COMPUTED, WHERE N IS THE NUMBER OF POINTS ALONG
C     ANY GIVEN ARC.  THE AVERAGE OF THE N-2 RADII IS TAKEN AS THE MEAN
C     RADIUS OF AN GIVEN ARC.  UP TO 100 SEPARATE ARCS MAY BE
C     COMPUTED AND AN OVERALL MEAN RADIUS IS ALSO CALCULATED.  UP TO
C     10 POINTS FOR ANY GIVEN ARC MAY BE PRESENTED.
C     DATA FOR EACH ARC IS PRESENTED AS -
C     (A) A 1ST CARD WITH A LEFT JUSTIFIED I2 FIELD TO SPECIFY N
C     (B) 1 TO 4 CARDS.  THE 1ST WITH A LEFT JUSTIFIED 4F10 FIELD THE
C         4TH WITH A LEFT JUSTIFIED 4F10 FIELD, TO SPECIFY SUCCESSIVE
C         POINT COORDINATES ALONG THE ARC AS X(1) Y(1)     X(4) Y(4)
C         ON THE 1ST CARD AND X(5) Y(5) X(10) Y(10) ON THE 4TH.  IF
C         REQUIRED.
C     (C) THE PROGRAM IS TERMINATED IF MORE THAN 100 ARCS ARE
C         PRESENTED OR IF AN N PARAMETER IS SPECIFIED AS 2
C
C     (XM1 YM1)  (XM2 YM2)  MIDPOINT COORDINATES OF SUCCESSIVE ARC
C                           CHORDS
C     S1  S2                NEGATIVE SLOPES OF PERPENDICULAR BISECTORS
C                           OF SUCCESSIVE ARC CHORDS
C     B1  B2                Y-INTERCEPTS OF PERPENDICULAR BISECTORS OF
C                           SUCCESSIVE ARC CHORDS
C     (XC  YC)              COORDINATES OF THE CENTRE OF A CIRCLE
C                           LOCATED BY THE PERPENDICULAR BISECTORS
C     R(I)                  RADIUS COMPUTED ON THE BASIS OF 3
C                           SUCCESSIVE POINTS ALONG THE ARC
C     RM(I)                 AVERAGE OF ALL R(I) FOR ANY GIVEN ARC
C     RMN                   AVERAGE OF ALL RM(I) FOR ALL ARCS
C
      DIMENSION RM(100),X(10),Y(10),R(8)
      I=1
      READ(0,10)N
   10 FORMAT(I2)
      IF(N.GT.10) N=N-10
      IF(N.LT.3) GO TO 1000
      READ(0,20)(X(I),Y(I),I=1,N)
   20 FORMAT(8F10.0)
      INX=N-2
      RM(I)=0
      DO 100 I=1,INX
      XM1=(X(I+1)+X(I))/2
      YM1=(Y(I+1)+Y(I))/2
```

```
      XM1=(X(I+2)+X(I+1))/2
      YM1=(Y(I+2)+Y(I+1))/2
      S1=((X(I+1)-X(I))**2+(Y(I+1)-Y(I))**
      S2=((X(I+2)-X(I+1))**2+(Y(I+2)-Y(I+1))**
      D1=YM1+S1*XM1
      D2=YM2+S2*XM2
      XC=(D2-D1)/(S2-S1)
      YC=((D1+D2)*(S2-S1)+S2*S1*(XM2-XM1))/(
      R(I)=SQRT((X(I)-XC)**2+(Y(I)-YC)**2)+SQRT((X(I+1)-XC)**2+(Y(I+1
     *-YC)**2)+SQRT((X(I+2)-XC)**2+(Y(I+2)-YC)**2))/3
100   RM(I)=RM(I)+R(I)
      RM(I)=RM(I)/FLOAT(IMX)
      WRITE(12,*)(R(I),I=1,IMX)
50    FORMAT(10F10.2)
      WRITE(12,*)RM(I),N,I
      FORMAT(1H MEAN RADIUS =,F10.2,4H IN ,I2,4H DATA POINTS, TEST N
     *,I2)
      I=I+1
      IF(I.LT.100)GO TO 1000
      GO TO 2
1000  RMIN=0
      I=1
      DO 1100 I=1,N
1100  RMN=RMN+RM(I)
      RMN=RMN/FLOAT(N)
      WRITE(12,40)RMN
40    FORMAT(2H AVERAGE MEAN RADIUS =,F10.2)
      STOP
      END
```

Legibility of these documents may Reduce on Poor Microfilm Reproduction

APPENDIX V

(B)

```
*WATFIV MESABOOI GHONEM HAMDUDA
C          THIS PROGRAM IS TO CALCULATE THE MICROSTRESS VALUE
C          ACTING ON EVERY DISLOCATION SEGMENT BY INSERTING THE
C          VALUES OF THE DISLOCATION LENGTH ,ITS RADIUS AND THE
C          ANGLE BETWEEN THE TANGENT AND THE X-AXIS IN EQUATION
C          2-38 WAS BEEN DESCRIBED IN CHAPTER 2 OF THIS THISES.
      DIMENSION RI(50),RR(50),PHAY(50),SETA(50),STX(50),STY(50),E(50),
     *Z(50)    ,Z1(50)
      P=3.1416/180.
      PI=3.1416
      PR=0.216
      SHM=(4.14*10**.9716)*(10.**3)
      EX=2.718
      U=2.
      V=2.
      W=0.
      D=5.42
      R=(D/2.)*(((U**2.)+(V**2.)+(W**2.))**1./2.)
      XX=1.-2.*PR
      WRITE (6,4)
    4 FORMAT(1H1, 1X,10HISI ,NUM,      LENGTH       RADIUS       TANGENT
     *  ORIENTATION          STRESS          STRESS-X          STRESS-Y1)
      READ (5,1)(RI(I),RR(I),SETA(I),RE ,PHAY(I),I=1,47)
    1 FORMAT (5E4.2)
      DO 15 I=1,47
      RR(I)=RR(I)*3664R.0 /3.26
      RI(I)=RI(I)*3664R.0 /3.26
      C=(4.*PI(I))/(EX*R)
      E(I)=SETA(I)*P
      Z(I)=1./COS(E(I))
      Z1(I)=SIN(E(I))/COS(E(I))
      DA=((Z(I)**3)+Z(I)*(Z1(I)**2)-(PR/Z(I)))*((1.-PR)*ALOG((Z(I)))
      DB=(((E(I)**2)/2.)+1.)*(XX*ALOG(C/2.)-0.5)
      DC=XX*Z(I)*(Z1(I)**2)
      DD=-PR*Z1(I)*SIN(E(I))
      DE=Z(I)**3
      STRESS=((SHM*R)/(4.*PI*(1.-PR)))*(DA+DB+DC+DD+DE)    /RR(I)
      STX(I)=STRESS*SIN(PHAY(I)*P)
      STY(I)=STRESS*COS(PHAY(I)*P)
      WRITE (6,20)I,RI(I),RR(I),SETA(I),PHAY(I),STRESS,STX(I),STY(I)
   20 FORMAT (2X,I7,F12.4,5X,F12.4,5X,F7.3,5X,F12.3,4X,F12.4,5X,
     *F8.3 ,5X,F8.3 )
   15 CONTINUE
      STOP
      END
*DATA
```

Legibility of these subsections may leave much to be desired. Poor reproduction.